DESIGN, CONSTRUCTION AND PERFORMANCE TESTING

OF A FLUID-TO-FLUID HEAT-METER PROTOTYPE

by

FARID H. MIANDOAB

B.S., Kansas State University, 1981

———————————

A MASTER'S THESIS

submitted in partial fulfillment of the

requirements for the degree

MASTER OF SCIENCE

Department of Mechanical Engineering
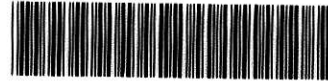
KANSAS STATE UNIVERSITY

Manhattan, Kansas

1983

Approved by:

B. Terry Beck
Major Professor

TABLE OF CONTENTS

Table of Contents (cont.)

Table of Contents (cont.)

LIST OF FIGURES

v

List of Figures (cont.)

FIGURE

LIST OF TABLES

CHAPTER I

INTRODUCTION

The basic purpose of this research was to design, construct and performance test a device to be referred to as a fluid-to-fluid heat-meter. The heat-meter is essentially a special-purpose type of heat exchanger. As shown in Figure 1.1, it is a laminated structure consisting of a thermally semi-conductive plate sandwiched between two metal slabs of high thermal conductivity such as aluminum. Flow channels are machined into each slab, allowing sufficient circulation of both primary and secondary fluids to maintain each slab at approximately a uniform temperature. When heat flows from the hot fluid to the cold fluid through the relatively thin semi-conductive plate, a measureable temperature difference is generated between the two slabs. This temperature difference is sensed by a thermopile embedded within the slabs and connected across the conductive plate. Once the device is calibrated, it provides a direct indication of the total heat transfer rate in terms of the voltage output of the thermopile.

1.1 Applications

The primary application of the heat-meter, for which it was basically developed, would be in controlling and accurately measuring the heat transfer rate from air spaces cooled or heated by fluid circulation.

In Figure 1.2, the arrangement for such an application is shown. Heat gained by circulating the primary fluid in the space to be cooled, is conducted through the semi-conductive plate to the secondary fluid. Then the calibrated measure of the heat transfer rate between fluids would be deter-

1

2

Primary Circuit

Thermopile
Output

Thermopile Section

Bolt Hole

Thermopile Plate

Flow Channel

Secondary Circuit

Cover Plate

Gasket

Semi-Conductive
Plate

Insulation

Primary Slab

Secondary Slab
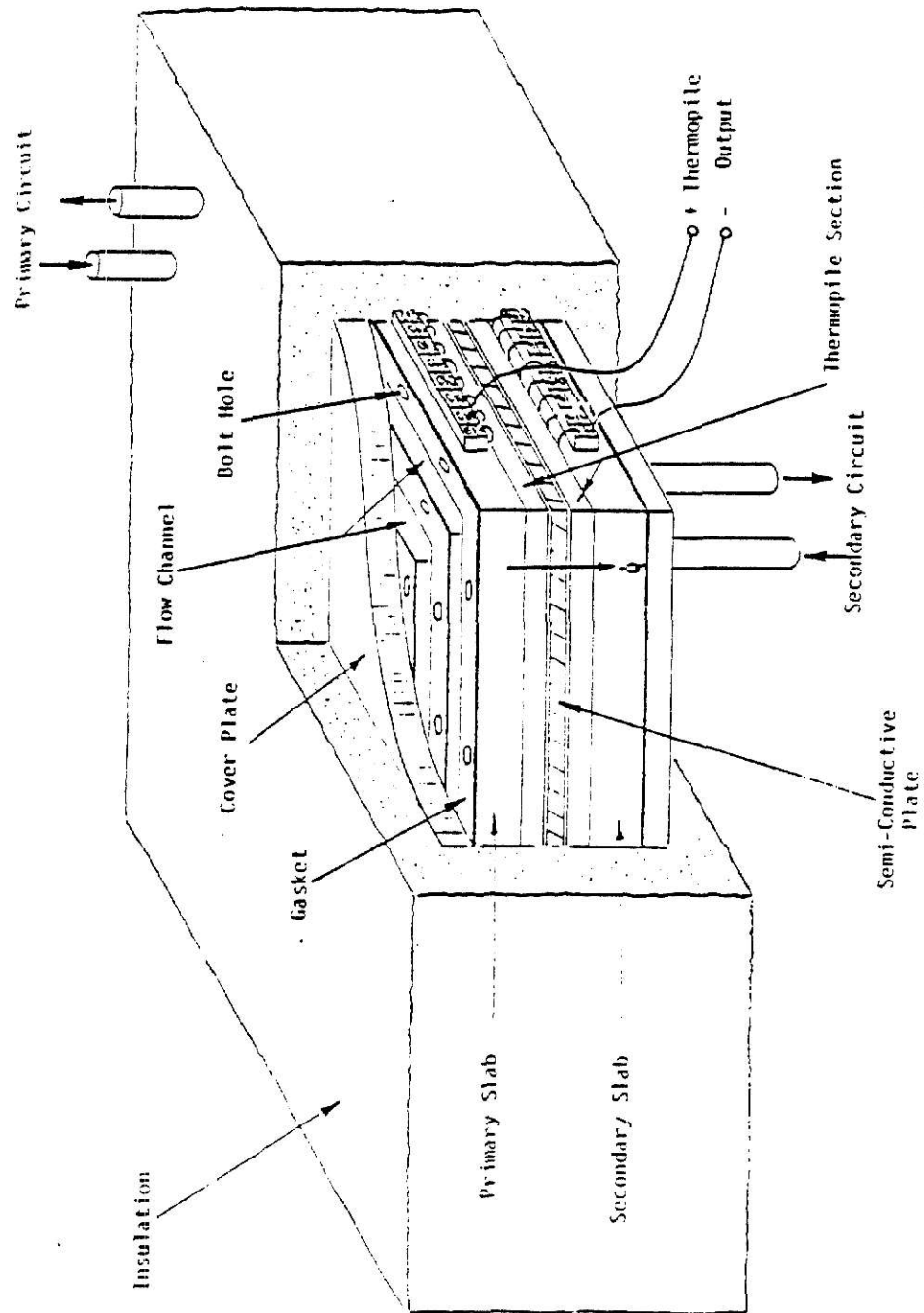
Figure 1.1 - Schematic diagram of fluid-to-fluid heat-meter system

Heat-meter

Secondary circuit

Primary circuit

(Room)
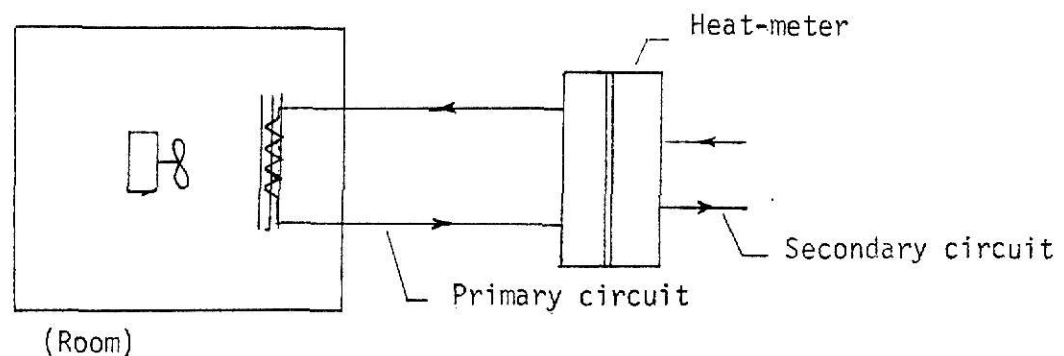
Figure 1.2 - Heat-meter Application

mined by recording the ouput of the thermopile measuring the temperature difference established across the thickness of the semi-conductive plate. In this application, the conventional method of determining the cooling load for the room would be to do an energy balance on the fluid entering and leaving the air space [1]. This requires measuring the fluid flow rate and its temperature change. Accurate results obtained using this method not only require accurate measurement of the fluid temperature change and flow rate but also require detailed knowledge of the properties of the fluid. Hence, this method is difficult to use for accurate measurement of the heat-transfer rate, particularly when the fluid temperature change is very small.

The heat-meter may also have applications in certain process control areas such as chemical processing.

1.2 Advantages

The major advantage of this particular type of heat-meter is in providing a direct calibrated electrical output proportional to the heat trans-

fer rate from the primary to secondary fluid. Also, because of its simple geometry, its range and sensitivity could be easily changed by replacing the semi-conductive plate. It was expected that the effect of fluid flow rates on the heat-meter performance would be small, and therefore the heat-meter would provide an accurate measurement of heat transfer rate for a wide range of fluid flow rates. As another advantage, fluid contamination would not affect the heat-meter sensitivity. Accurate measurements of the heat transfer rate would not require precise information about material properties, geometry or fluid properties. Furthermore, the heat-meter would have bi-directional heat flow capability.

1.3 Engineering Relevance

The fluid-to-fluid heat-meter idea appears to be a new concept. The closest types of heat flow measuring devices in terms of the concept of operation were found to be a heat flow meter [2], used for determining the thermal transmission properties of loose insulating materials, a guarded hot box [3], used for determining the thermal performance of building assemblies and a special purpose thermoelectric heat flux transducer [4], used for measuring the heat flux from various surfaces. All of the above mentioned conventional heat-meters operate on the concept of measuring the heat flow by measuring the temperature difference established across a thermally conductive material. One of the unique features of the fluid-to-fluid heat-meter is that the fluid-to-fluid heat-meter, by being basically a heat-exchanger, can transfer heat to or from an air space in addition to providing an accurate measurement of the heat flow rate.

1.4 Overview of the Chapters

Chapter II is concerned with designing and constructing the components

of the heat-meter prototype. In Chapter III, the feasibilty of the heat-meter concept is examined by testing the heat-meter. Chapter IV is concerned with construction of an additional test facility for calibrating the heat-meter. In Chapter V, heat-meter calibration tests and results are discussed. Chapter VI is the summary of the work with recommendations for future study.

CHAPTER II

PRELIMINARY DESIGN AND CONSTRUCTION OF THE HEAT-METER PROTOTYPE

The heat-meter basically consists of a thermally semi-conductive plate sandwiched between two aluminum slabs. Flow channels are machined in the slabs for fluid circulation. The purpose of this chapter will be to specify geometrical dimensions of the flow channels, thickness and material of the semi-conductive plate, and the thickness of the slabs for a scaled down heat-meter prototype of 0-1 KW range. This will also include designing of a thermopile section for providing an indirect measure of heat transfer by measuring the temperature difference across the semi-conductive plate.

2.1 Derivation of the Heat Transfer Equations

In this section, a set of equations will be developed to describe the relationship between the heat-meter heat transfer rate, heat-meter dimensions, fluid flow rates, inlet and outlet temperatures of the fluids and the thermal properties of the separating plate. In the analysis that follows it will be assumed that the inlet temperatures of the hot and cold fluids, flow rates of each fluid, dimensions of the heat-meter and the thickness and properties of the semi-conductive plate are known.

A possible configuration for machining the flow channels in the aluminum slabs is shown in Figure 2.2. The fluid stream entering the inlet port is divided into two streams until the exit port. This arrangement of the flow channels along with the high thermal conductivity of the aluminum slabs

6

would create a relatively uniform temperature in the slabs. Therefore, in deriving the energy equations, the aluminum slabs are assumed to have uniform temperatures. Figure 2.1 is a typical section of the flow channels of the aluminum slab shown in Figure 2.2.
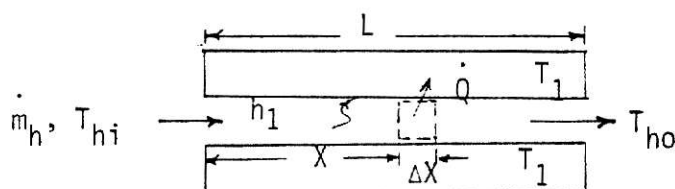
Figure 2.1 - Heat convection to a constant wall temperature
flow channel.

$\dot{Q}$, the heat transfer rate due to convection from the fluid to the constant temperature flow channel wall, is calculated as follows

$$\dot{Q} = \int_0^L h_1 \, P \, (T_{bh}(x) - T_1)dx \qquad (2\text{-}1)$$

where h_1 is the convective heat transfer coefficient, L is the length of the flow channel, $T_{bh}(x)$ is the bulk temperature of the hot fluid, T_1 is the temperature of the flow channel wall and P is the perimeter of the flow channel cross section.

Assuming fully developed conditions for which h_1 is constant, equation (2-1) yields

$$\dot{Q} = h_1 \, P \int_0^L (T_{bh}(x) - T_1) \, dx \qquad (2\text{-}2)$$

An energy balance on the fluid element shown in Figure 2.1 yields

$$\dot{m}_h h'_x - \dot{m}_h h'_{x+\Delta x} - \int_x^{x+\Delta x} h_1 \, P(T_{bh}(x) - T_1) \, dx = 0 \qquad (2\text{-}3)$$

where $\dot{m}_h$ is the hot fluid flow rate and h' is the enthalpy per unit mass of the hot fluid. Dividing equation (2-3) by Δx and taking the limit as Δx approaches zero, yields
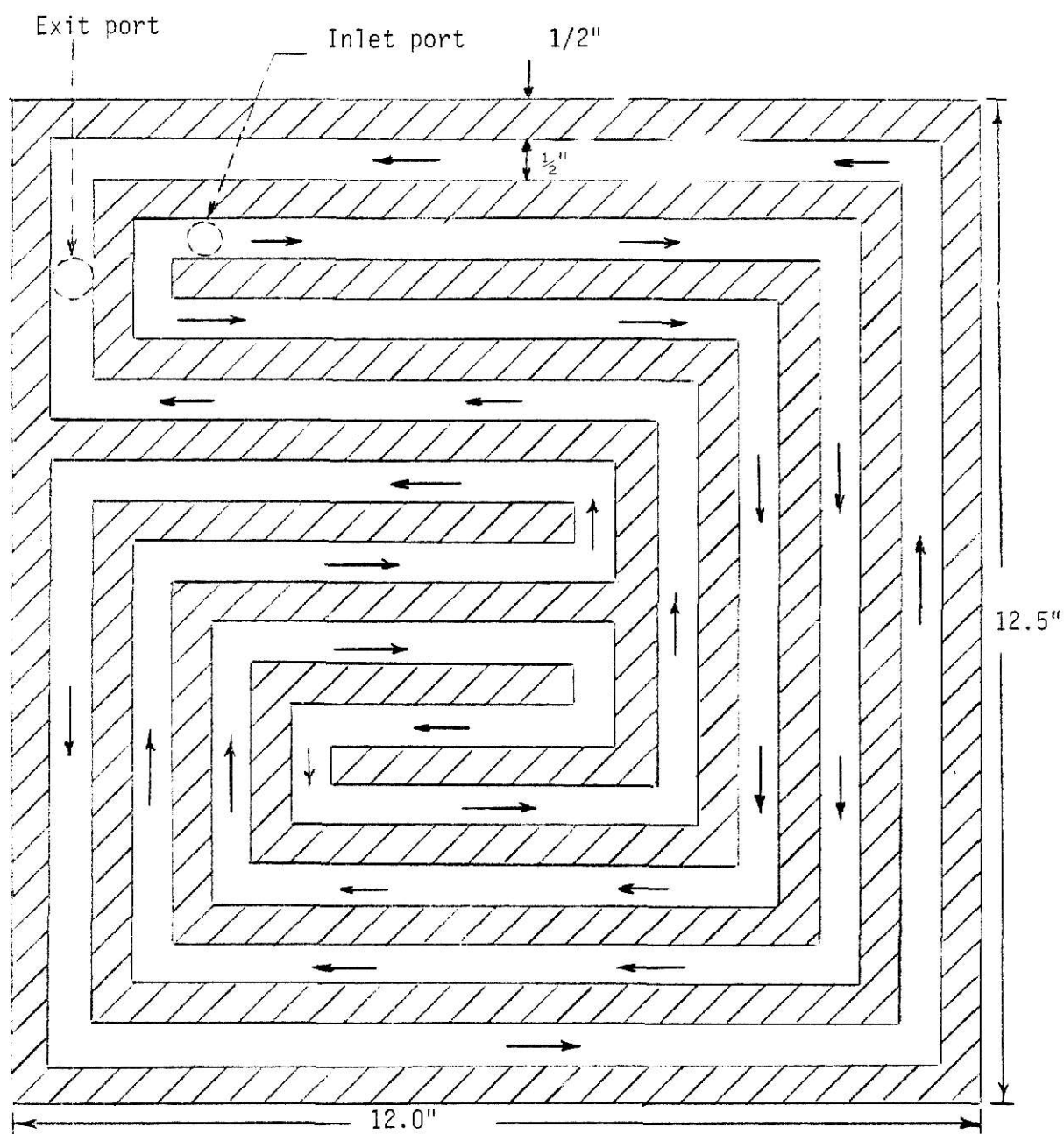
Figure 2.2 - A possible configuration for machining the flow channels in the heat-meter slabs

$$-\dot{m}_h \left(\frac{dh'}{dx}\right) - h_1 P(T_{bh}(x) - T_1) = 0 \tag{2-4}$$

Assuming constant properties and constant T_1, the first term in equation (2-4) may be written

$$\frac{dh'}{dx} = C_{ph} \left(\frac{dT_{bh}}{dx}\right) = C_{ph} \frac{d(T_{bh} - T_1)}{dx} \tag{2-5}$$

where C_{ph} is the specific heat per unit mass of the hot fluid at constant pressure. Therefore, substituting eq. (2-5) in eq. (2-4) yields

$$\dot{m}_h C_{ph}\left(\frac{d(T_{bh} - T_1)}{dx}\right) + h_1 P(T_{bh} - T_1) = 0 \tag{2-6}$$

The boundary condition for the eq. (2-6) is

$$T_{bh} = T_{hi} \text{ at } x=0 \tag{2-7}$$

where T_{hi} is the hot fluid inlet temperature.

Equation (2-6) is solved subject to eq. (2-7) yielding

$$T_{bh} - T_1 = (T_{hi} - T_1)e^{(-h_1 Px/\dot{m}_h C_{ph})} \tag{2-8}$$

Substituting eq. (2-8) in eq. (2-2) yields

$$\dot{Q} = h_1 P \int_b^L (T_{hi} - T_1)e^{(-h_1 Px/\dot{m}_h C_{ph})}dx \tag{2-9}$$

Performing the integration in eq. (2-9) yields

$$\dot{Q} = \dot{m}_h C_{ph}(T_{hi} - T_1)(1 - e^{(-h_1 PL/\dot{m}_h C_{ph})}) \tag{2-10}$$
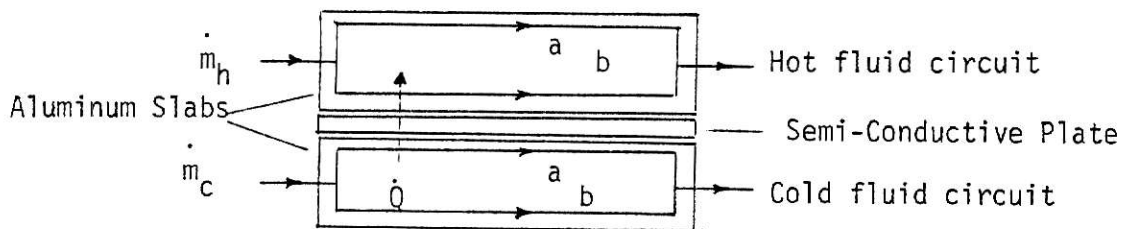
Figure 2.3 - Simplified sketch of the heat-meter assembly.

Referring to Figure (2.2) and (2.3), the lengths of the two parallel flow channels "a" and "b" machined in each slab may be slightly different.

Therefore eq. (2-10) can be written to express the heat transfer rate from the fluid in channel "a" and the fluid in channel "b", to the constant temperature slab in which they are flowing.

Equation (2-10), for channel "a" can be written as

$$\dot{Q}_{a1} = \dot{m}_h C_{ph}(T_{hi} - T_1)(1 - e^{(-h_1 P L_a / \dot{m}_h C_{ph})}) \qquad (2-11)$$

where L_a is the length of the flow channel "a" and $\dot{Q}_{a1}$ is the heat convection rate from the fluid in channel "a" to the aluminum slab at temperature T_1.

For the fluid entering and leaving channel "a", overall energy balance can also be written as

$$\dot{Q}_{a1} = \dot{m}_h C_{ph}(T_{hi} - T_{hoa}) \qquad (2-12)$$

where T_{hoa} is the temperature of the hot fluid leaving the flow channel "a".

Assuming the same flow rate and convective heat transfer coefficient for the fluids in channels "a" and "b", eqs. (2-10) and (2-12) for the fluid in channel "b" can be written as

$$\dot{Q}_{b1} = \dot{m}_h C_{ph}(T_{hi} - T_1)(1 - e^{(-h_1 P L_b / \dot{m}_h C_{ph})}) \qquad (2-13)$$

and

$$\dot{Q}_{b1} = \dot{m}_h C_{ph}(T_{hi} - T_{hob}) \qquad (2-14)$$

where T_{hob} is the hot fluid temperature leaving the channel "b" of length L_b and $\dot{Q}_{b1}$ is the heat convection rate from the fluid in channel "b".

A similar set of equations can be written to describe the heat convection rate between the cold fluid and the aluminum slab in which it is flowing. Therefore for channel "a" of the cold fluid, eqs. (2-10) and (2-12) are written as

$$\dot{Q}_{a2} = \dot{m}_c C_{pc}(T_2 - T_{ci})(1 - e^{(-h_2 P L_a / \dot{m}_c C_{pc})}) \qquad (2-15)$$

and

$$\dot{Q}_{a2} = \dot{m} \, C_{pc}(T_{coa} - T_{ci})$$ (2-16)

where the constants are as previously defined and subscript c refers to the cold fluid.

Equations (2-10) and (2-12), for the cold fluid in channel "b", are as follows

$$\dot{Q}_{b2} = \dot{m}_c P_{pc}(T_2 - T_{ci})(1 - e^{(-h_2 P L_b / \dot{m}_c C_{pc})})$$ (2-17)

$$\dot{Q}_{b2} = \dot{m}_c \, C_{pc}(T_{cob} - T_{ci})$$ (2-18)

where T_{cob} is the temperature of the cold fluid leaving channel "b" and $\dot{Q}_{b2}$ is the heat convection rate between the fluid in channel "b" and the slab in which it is flowing.

Assuming no heat losses from the heat-meter to the surroundings and constant thermal conductivity for the separating plate, the heat conducted through the plate separating the two slabs can be expressed as follows:

$$\dot{Q}_{a1} + \dot{Q}_{b1} = \dot{Q}_{a2} + \dot{Q}_{b2} = K_S A(\frac{T_1 - T_2}{t})$$ (2-19)

where K_S, A and t are thermal conductivity, area and thickness of the separating plate, respectively.

The convective heat transfer coefficient, h, is estimated using the "Dittus-Boelter" correlation [5]. Therefore

$$Nu_d = .023 \, Re^{.8}(Pr)^n \text{ where } \begin{array}{l} n = .3 \text{ cooling} \\ n = .4 \text{ heating} \end{array}$$ (2-20)

Nu_d is the local Nusselt number based on the hydraulic diameter, Re is the Reynolds number and Pr is the Prandtl number.

The Nusselt number is defined as:

$$Nu_d = \frac{hD}{K}$$ (2-21)

where K is the thermal conductivity of the fluid and D is the hydraulic
diameter defined as:

$$D = \frac{4(\text{cross sectional area of the flow channel})}{\text{wetted perimeter}} \qquad (2\text{-}22)$$

2.2 Estimating the Heat Transfer Rate

Using the equations developed, for flow channels of dimensions and configuration shown in Figure 2.2, the heat transfer rate and the temperature difference across the separating plate were estimated. Values of T_{hi}, T_{ci}, $\dot{m}_c$, $\dot{m}_h$ and K_g that were used to make the estimation are listed in Table 2.1. The results of such calculations along with the estimates of the pressure drop in the flow channels are shown in Table 2.1. The results indicate that using the easily available glass plate as the separating plate, pumping of the cold and hot water at the rate of .126 $\frac{1}{S}$ (2 GPM) through the flow channels of dimensions and configuration indicated, would require a moderately small pump and also establish a measurable temperature difference across the thickness of the separating plate. Therefore, a decision was made to construct the aluminum slabs of the heat-meter prototype using the dimensions and the flow channels configuration shown in Figure 2.2.

2.3 Estimation of the Pressure Drop

The following is an estimation of the pressure drop of water in the flow channels of dimensions indicated in Table 2.1 and the configuration shown in Figure 2.2. Such a configuration, as opposed to a single flow channel configuration, would minimize the pressure drop by dividing the fluid stream into two smaller streams. In estimating the pressure drop, it is assumed that the flow is fully-developed and that the fluid has constant properties. Relative roughness of the flow channels is assumed to be equivalent

Fluid Flow Channel		Hot		Cold
	Shape	1.27 cm x 1.27 cm (0.5 in. x 0.5 in.) square channel		
	Length	l_a = 1.37 m,		l_b = 2.13 m
Fluid Properties	T_{in}, °C	40		20
	ρ, $\frac{Kg}{m^3}$	994.59		1000.52
	C_p, $\frac{J}{Kg-°K}$	4810		4181.8
	ν, $\frac{m^2}{sec}$	0.658×10^{-6}		1.006×10^{-6}
	K, $\frac{w}{m-°K}$	0.628		0.597
	Pr	4.34		7.02
Heat-Meter Plate	Area, m²		0.0968	
	Thickness, m		0.005	
	K_s, $\frac{w}{m-°K}$		0.761	
$\dot{V}$, Total Flow Rate		.126 ℓ/s (2 GPM)		.126 ℓ/s (2 GPM)
T_1, °C			39.03	
T_2, °C			21.00	
T_{out}, °C		39.49		20.50
$\dot{Q}$, W			265.76	
ΔP, psi		0.21 (1.44 $\frac{KN}{m^2}$)		0.21 (1.44 $\frac{KN}{m^2}$)

Table 2.1 - Estimation of the heat transfer rate for the heat-meter

to the relative roughness of a drawn tube. Pressure drop in the bends is expressed in terms of an equivalent length of straight flow channel. The hydraulic diameter, defined by eq. (2-22), is used as the equivalent diameter of the flow channels. Referring to Table 2.1 for properties of the hot fluid, for a volumetric flow rate of $\dot{V}$ = .0631 $\frac{1}{S}$ (1 GPM) in each channel of the parallel flow channels, the Reynolds number is calculated to be:

$$Re_d = \frac{\dot{V}}{D\nu} = \frac{(0.631 \times 10^{-3} \frac{m^3}{S})}{(0.127m)(.658 \times 10^{-6} \frac{m^2}{S})} = 7551 \tag{2-23}$$

From reference [6], the absolute roughness of the drawn tube is taken to be $e = 1.52 \times 10^{-6}$ m, which gives the following relative roughness.

$$\frac{e}{D} = 12 \times 10^{-5} \tag{2-24}$$

Using the moody diagram in reference [6], at Re_d = 7551 and $\frac{e}{D}$ = 12 x 10^{-5}, f, the average friction factor is determined to be f = .034.

From reference [6], the equivalent length for a 90^0 standard elbow is

$$\frac{L_e}{D} = 30 \tag{2-25}$$

Referring to Figure 2.2 and Table 2.1 for dimensions of the flow channels, n, the number of the bends in fluid path "a" is 15 and m, the number of bends in fluid path "b", is 13. Therefore, using eq. (2-25), L_{ea} and L_{eb}, the equivalent lengths for bends in fluid paths "a" and "b", respectively, are calculated as follows

$$L_{ea} = (D)(n)(30) = (.0127m)(15)(30) = 5.72 \ m$$

$$L_{eb} = (D)(m)(30) = (.0127m)(13)(30) = 4.95 \ m$$

Therefore, the total equivalent length for each fluid path is

$$L_{ta} = L_{ea} + L_a = 5.72 + 1.37 = 7.09 \text{ m} \qquad (2\text{-}26)$$

and

$$L_{tb} = L_{eb} + L_b = 4.95 + 2.13 = 7.08 \text{ m} \qquad (2\text{-}27)$$

Then ΔP, the pressure drop in each fluid path, can be calculated from the following equation

$$\Delta P = (f)(\frac{L_e}{D})(\frac{\rho \overline{V}^2}{2}) \qquad (2\text{-}28)$$

where $\overline{V}$ is the average fluid velocity and L_e is the total equivalent length.

Substituting values in eq. (2-30) yields

$$\Delta P_a = \Delta P_b = (.034)(\frac{7.09 \text{ m}}{.0127 \text{ m}})(\frac{(994.6 \frac{Kg}{m^3})(.391 \frac{m}{S})^2}{2}) = 1.44 \frac{kN}{m^2} (0.21 \text{ psi})$$

Since in the range of the operation of the heat-meter, the fluids flow rate was not expected to exceed $.126 \frac{1}{S}$ (2 GPM), therefore, a moderately small pump could be used to overcome the pressure drop of $1.44 \frac{kN}{m^2}$ in the flow channels of dimensions and configuration shown in Figure 2.2. After the construction of the heat-meter prototype, its pressure drop character- istics were determined experimentally. The predicted and the experimentally determined characteristic curves are shown in Figure A.3 of Appendix A. Comparison between the two curves indicates that, at a flow rate of $.126 \frac{1}{S}$ (1 GPM), the predicted pressure drop is 72% less than the actual pressure drop. Assumptions made in estimating the pressure drop, the losses due to exit and inlet ports, various fittings used in the fluid circuit, and the difference between the viscosity of water at $40^{\circ}C$ and $15^{\circ}C$, are thought to be the major sources of error in the estimate.

2.4 <u>Aluminum Slabs Thickness Design</u>

In designing the heat-meter slabs, the thickness of the aluminum slabs
was chosen such that it would provide an approximately uniform temperature
distribution over the surface in contact with the separating conductive
plate. A relatively uniform temperature distribution would cause the
heat transfer process between the two slabs to be approximately one-dimen-
sional heat conduction. The temperature distribution in the aluminum slabs
was simulated using an electrical analog model of the problem. Then, the
aluminum slab thickness was selected based on the temperature profiles
that were determined.

2.4.1 <u>Conductive Sheet Analog</u>. A side view of a typical section of the
aluminum slab that was simulated to determine its temperature profiles, is
shown in Figure 2.4. The complete side view of the aluminum slabs is shown
in Figure 2.10. The simulated section of the aluminum slab was part of the
slab between the two neighboring flow channels. The simulation was possible
because of the analogy that exists between the steady state temperature
distribution in heat conduction and the steady state voltage distribution
in electrical conduction. By proper scaling and appropriately changing the
variables, experimental voltage data obtained for the model can be used to
obtain the temperature distribution for the heat conduction problem.

The conductive sheet analog model used in the simulation was constructed
from a carbon impregnated ("Teledeltos") resistance paper, using a scale of
six to one. Figure 2.5 is a schematic diagram of the model. The boundary
conditions of the analogous problem of heat conduction were simulated by
establishing appropriate voltages across points A, B and points A, C, shown
in Figure 2.5. A voltmeter was used to locate the points of constant voltage
on the conductive sheet. Such points corresponded to the points of constant
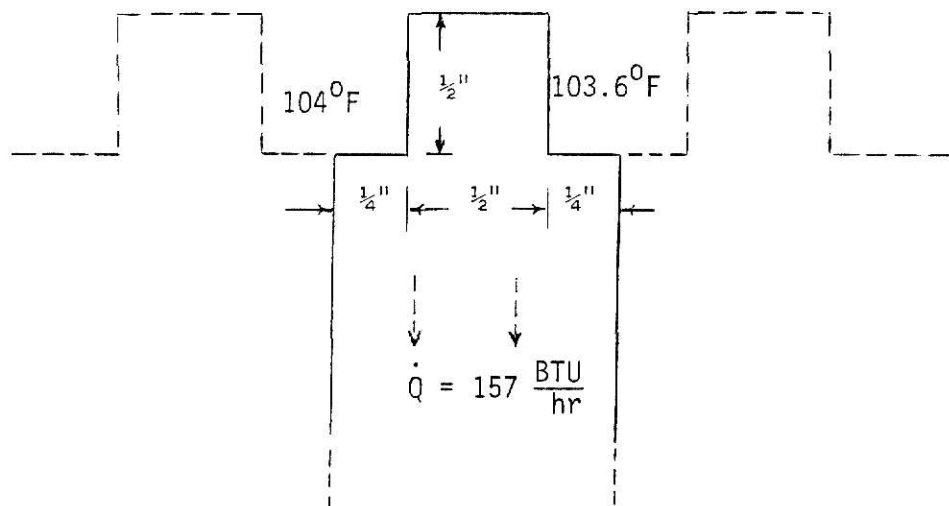
Figure 2.4 - Heat conduction in the aluminum slab
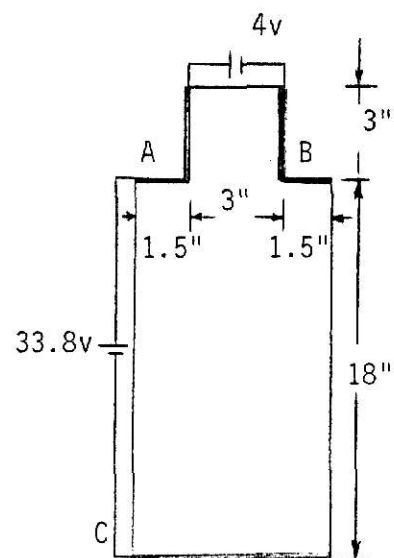
Figure 2.5 - Conductive sheet analog

temperature in the analogous problem of heat conduction.

2.4.2 <u>Scaling and the Boundary Conditions</u>. In simulating the boundary conditions of the heat conduction problem shown in Figure 2.4, it was assumed that there would be no heat flux in the asymetrical direction. Using the heat transfer equations developed earlier, for typical conditions, the heat transfer through the simulated section of the aluminum slab was calculated to be 46 W (157 $\frac{BTU}{hr}$). Also, it was determined that for that condition the fluids in the two neighboring flow channels of the slab would be at $104^{O}F$ $(40^{O}C)$ and $103.6^{O}F(39.8^{O}C)$. Therefore, the transformation equation for the temperature and the voltage could be written as follows

$$T = 104 - C_T V \qquad (2\text{-}29)$$

where C_T is a transformation constant for convenience taken to be $0.1 \frac{^{O}F}{V}$.

From reference [7], the relationship between the heat transfer and the electrical current could be written as follows

$$I = (\frac{K_e t_e}{Kt}) \frac{\dot{Q}}{C_T} \qquad (2\text{-}30)$$

where I is the current, $\dot{Q}$ is the heat transfer rate, K is the thermal conductivity of the aluminum slab, t is the width of the simulated section of the slab, K_e is the electrical conductivity of the resistance paper and t_e is the thickness of the paper.

Equation (2-30) could also be written as follows

$$V_{ac} = IR = (R) (\frac{K_e t_e}{Kt}) \frac{\dot{Q}}{C_T} \qquad (2\text{-}31)$$

where V_{ac} is the voltage and R is the electrical resistance of the conductive sheet.

To determine the voltage difference between points A and C, shown in Figure 2.5, to simulate the heat transfer rate of 157 $\frac{BTU}{hr}$ (46 W), substituting

values for the thermal conductivity of the aluminum and the electrical resistance of the paper in eq. (2-31) yields

$$V_{ac} = (4670 \text{ ohms})(\frac{\text{volts}}{0.1^\circ F})(\frac{5.44 \times 10^{-4} \text{ ohms}^{-1}}{118 \frac{BTU}{hr - ^\circ F - Ft}(1 \text{ Ft})}) \ (157 \frac{BTU}{hr})$$

$$V_{ac} = 33.8 \text{ volts}$$

Referring to Figure 2.4, a temperature difference exists between the two neighboring flow channels of the slab to be simulated. To simulate this condition, the corresponding voltage difference, ΔV, was calculated using eq. (2-31), yielding

$$\Delta V = \frac{104 - T}{C_T} = \frac{(104 - 103.6)^\circ}{.1 \frac{^\circ F}{\text{volts}}} = 4 \text{ volts}$$

This voltage difference was established across points A and B, shown in Figure 2.5.

2.4.3 <u>Test Procedure</u>. Referring to Figure 2.5, a d.c. power supply was used to establish 33.8 volts across points A and C, and 4 volts across points A and B on the conductive sheet analog model. Using a digital volt-meter, points of constant voltage with respect to point A, were located. By putting a transparency over the conductive sheet, points of constant voltage were connected to each other to form the corresponding isotherms in the analogous problem of heat conduction. Figure 2.6 is a graphical representation of these isotherms. Two other similar tests were conducted to determine the effect of closely spaced flow channels and fluids of the same temperature in the neighboring flow channels. The graphical representation of the isotherms for these two tests are shown in Figures 2.7 and 2.8.

2.4.4 <u>Conclusions</u>. Temperature profiles in Figures 2.6 through 2.8
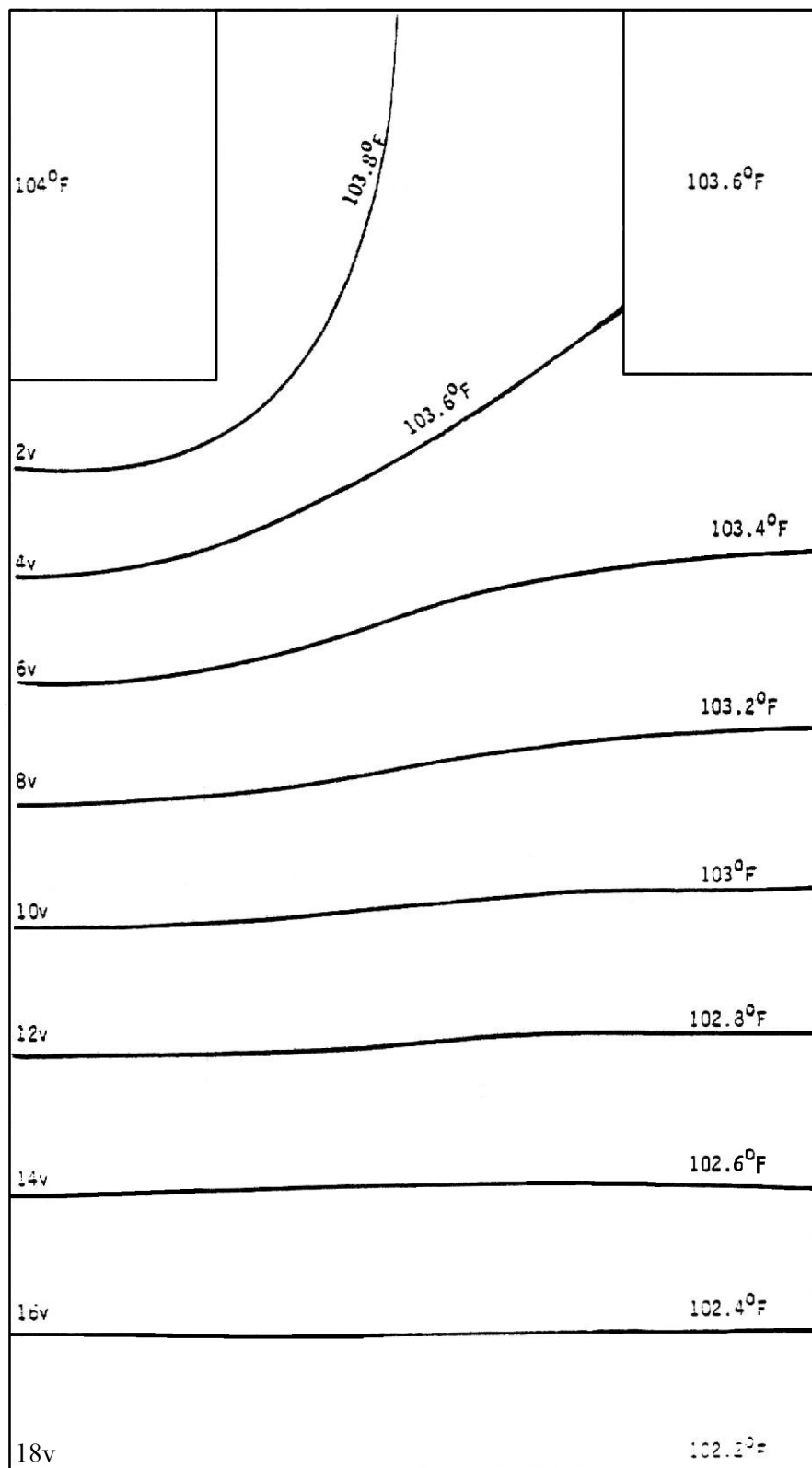
Figure 2.6 - Temperature distribution in the aluminum slab of Figure 2.4
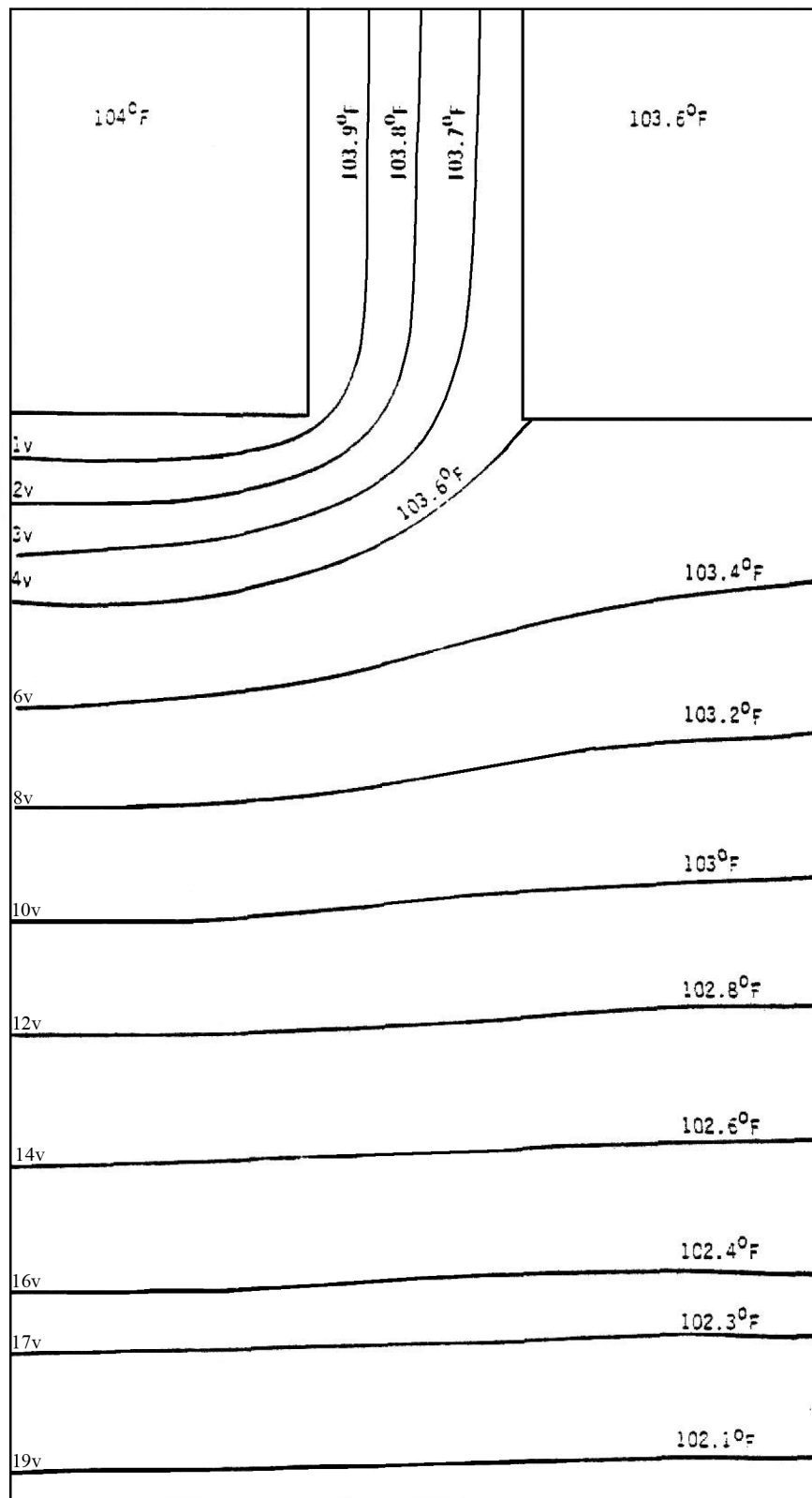
Figure 2.7 - Temmperature distribution in the aluminum slab of Figure 2.4,
with closely spaced flow channels.
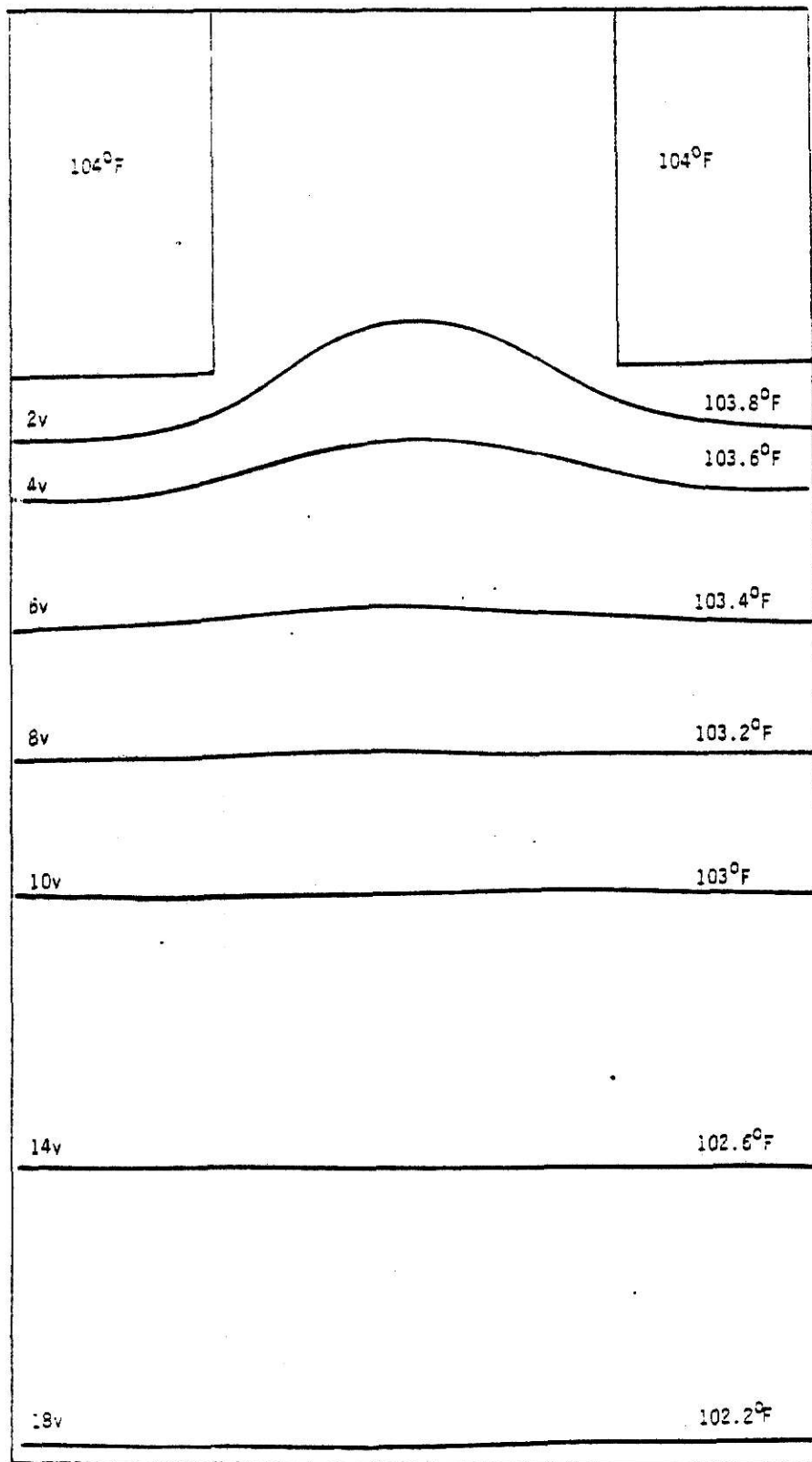
Figure 2.8 - Temperature distribution in the aluminum slab of Figure 2.4, with flow channels of same temperature.

indicate that the temperature distribution in the aluminum slab becomes relatively uniform at the thickness of about 1.5 inches. Since using the one inch thick aluminum slabs that were readily available would still give a fairly uniform temperature distribution in the bottom of the slab and the performance of the heat-meter would not be greatly affected, therefore the decision was made to use them as the heat-meter slabs.

2.5 Aluminum Slab Construction

Two identical one inch thick slabs of aluminum were machined into the dimensions 12 in. x 12.5 in (30.5 cm x 31.8 cm). As shown in Figure 2.9, two parallel flow channels, of dimensions .5 in. x .5 in. (1.27 cm x 1.27 cm), were machined into one side of each of the two aluminum slabs. Aluminum plates of dimensions 5/8 in. x 12 in. x 12.5 in (1.6 cm x 30.5 cm x 31.8 cm) with 3/16 in. screw holes drilled in them, were bolted onto the aluminum slabs to cover and seal the flow channels as shown in Figure 2.10. On each plate, two entry ports were tapped for 1/4 in. F.P.T. In Figure 2.9, the locations of the 26 screw holes tapped in each aluminum slab are shown. Rubber sheet, 12 in. x 12.5 in x 1/16 in. (30.5 cm x 31.8 cm x .16 cm) was cut to form a gasket between the cover plate and the top of the channel wall for each slab.

For measurement of the temperature difference between the two aluminum slabs, a thermopile was connected between two aluminum plates of dimensions 1/4 in. x 12 in. x 12.5 in (.64 cm x 30.5 cm x 31.8 cm). The plates acted as support for the thermocouple junctions which were epoxied in grooves of 1/8 in. (.32 cm) deep by 3/16 in. wide on each plate. The thermopile consisted of 24 pairs of copper-constantan thermocouple junctions electrically insulated from the aluminum plate using shrink tubing. Referring to Figure 2.11,

Exit port   Inlet port   Drilled and Tapped to fit screw #10-32

1.250"

2.00"

1.00"

1.00"

1.00"

1.00"

1.00"

1.00"

2.00"

1.250"

1.250" 1.00" 1.00"   2.00"   0.75" .750"   2.00"   1.00" 1.00" 1.250"
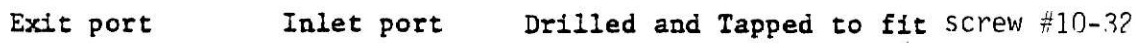
Figure 2.9 - Top view of the heat-meter slab
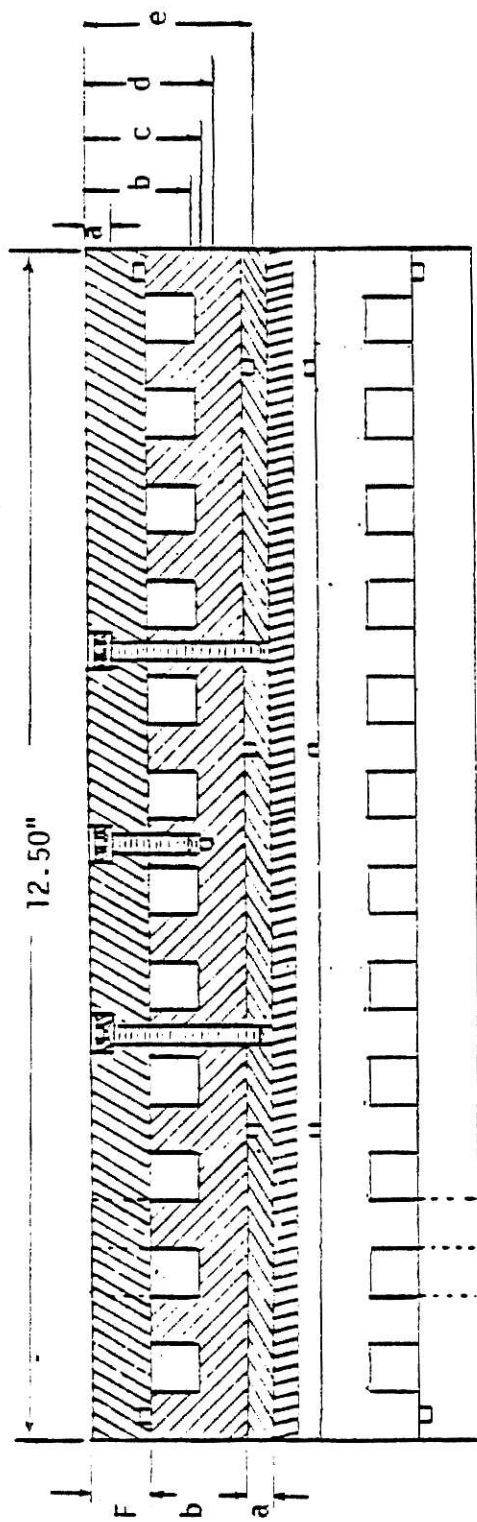
Figure 2.10 - Side view of the heat-meter plates

Dimensions:

a = .250"
b = 1.00"
c = 1.050"
d = 1.10"
e = 1.50"
f = 0.625"
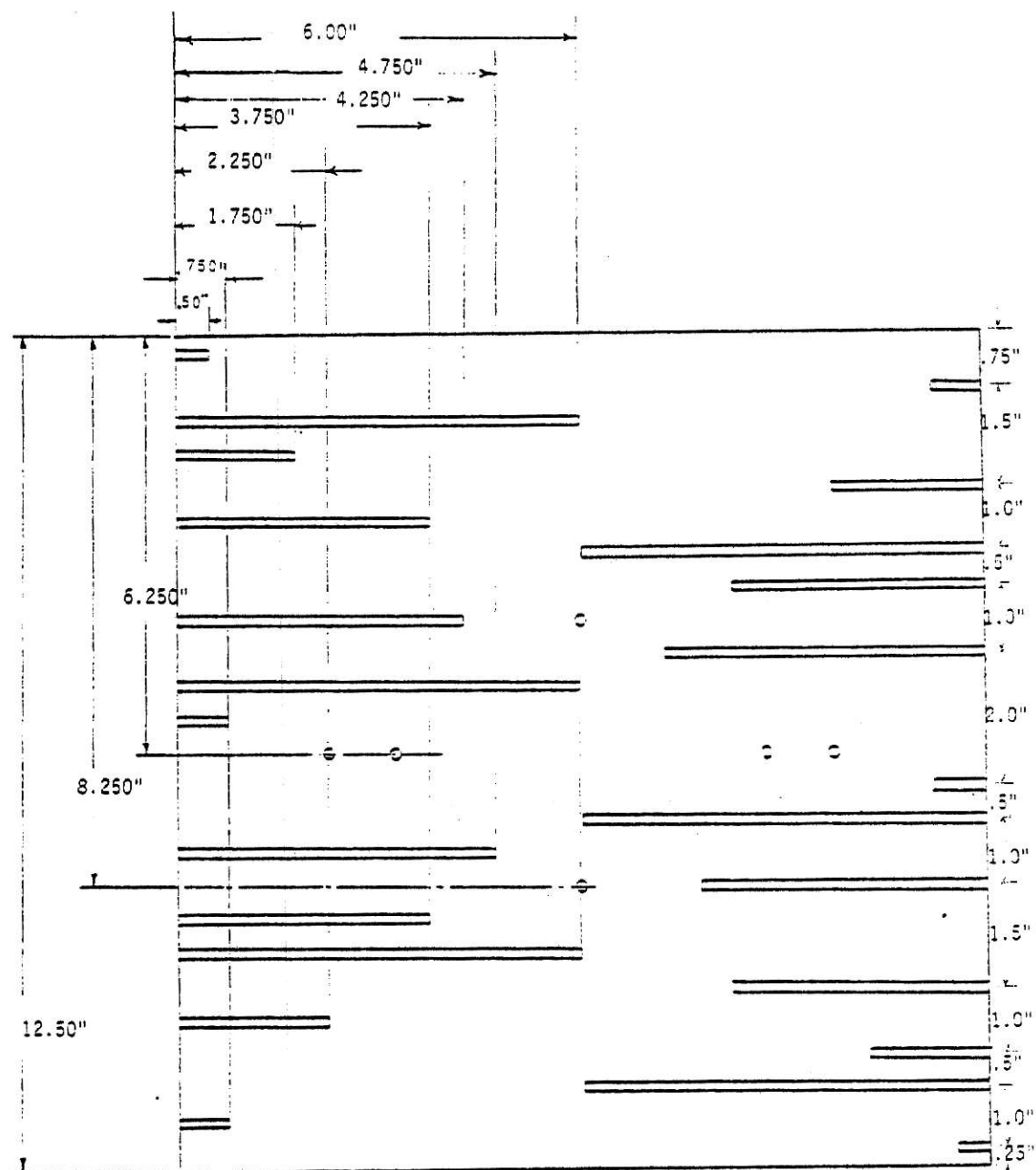
Figure 2.11 - Relative position of the thermocouples in the grooves of the
thermopile plate.

the grooves machined in the aluminum plates were spaced such that once the thermocouples were embedded in them, the reading of the thermopile would represent an estimate of the average temperature difference between the two aluminum slabs. Two terminal strips with 24 copper-constantan pins on each were screwed to the side of each aluminum slab to connect the ends of the thermocouples of the thermopile.

A glass plate of dimensions 1/8 in. x 12 in. x 12.5 in. (.32 cm x 30.5 cm x 31.8 cm) was cut to be used as the semi-conductive plate, separating the two aluminum slabs. By using the glass plate as the separating plate, as a result of its thermal conductivity, heat could be transferred between the slabs in the expected heat-meter range and establish a measurable temperature difference across the thickness of the plate.

Two plywood sheets of dimensions $16 \frac{3}{8}$ in. x 16 in. x $\frac{3}{4}$ in. (41.6 cm x 40.6 cm x 1.9 cm) along with two plexiglass plates of dimensions 1/4 in. x 12 in. x 12.5 in. (.64 cm x 30.5 cm x 31.8 cm) were used to support the heat-meter sections together. The entire assembly was clamped together using twelve 5/16 in. x 7 in. long bolts.

2.6 Construction of Thermopiles for Measurement of Fluid Temperature Difference

Two identical thermopiles were constructed for measurement of the temperature difference of the fluids entering and leaving the heat-meter. The readings of the thermopiles were used to estimate the amount of heat gained or lost by the fluids circulating in the heat-meter.

Each thermopile consisted of two identical brass cylinders as shown in Figure 2.12. On the circumference of each three inch long brass cylinder, a total of ten holes were drilled radially through the cylinder wall. Ten, 24-gauge copper-constantan thermocouple junctions were electrically insulated
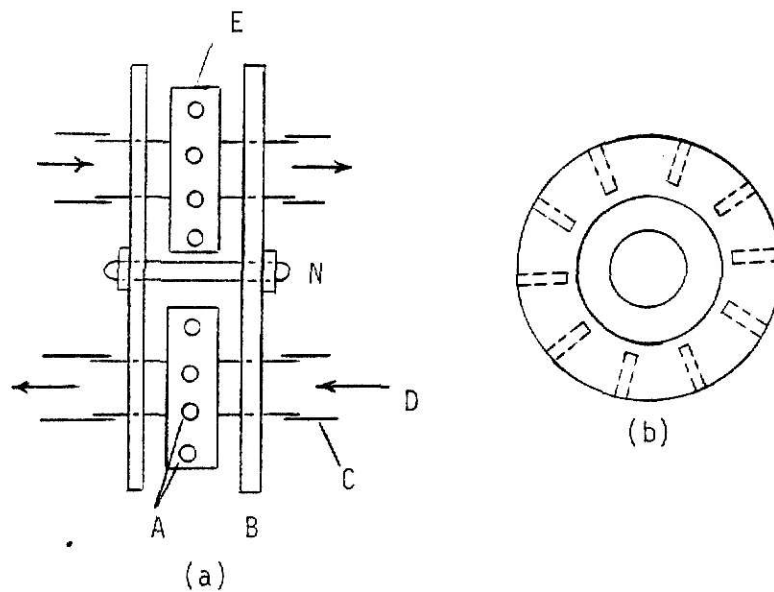
Figure 2.12 - Schematic diagram of the thermopile for measurement of fluid temperature difference. (a) end view of brass cylinder.

Legend:

A   Location of thermcouple junctions

B   Plastic plates for mechanically connecting the two brass cylinders

C   Hose connection for fluid flow

D   Direction of fluid flow

E   Brass cylinder

N   Threaded nylon rod and nuts

from the brass support using shrink tubing and expoxied into the holes of each brass cylinder. The separate thermocouples from each cylinder were connected in series to form a thermopile. When using the thermopiles, they were insulated from the ambient using blanket type insulation.

CHAPTER III

PRELIMINARY TESTING OF THE HEAT-METER PROTOTYPE

The main purpose of the preliminary testing of the heat-meter prototype was to establish the feasibility of the heat-meter concept. In the preliminary testing of the heat-meter, measurements of the hot fluid heat loss, the cold fluid heat gain and the heat-meter output were made to determine whether a relationship exists between the heat transfer rate and the heat-meter output.

3.1 Test Setup

A schematic of the test setup used in the preliminary testing of the heat-meter is shown in Figure 3.1. Four, 1/4" x 5 in. long, brass nipples were connected to the inlet and outlet ports of the heat-meter. To each nipple, a 90° brass elbow was connected. Four other 1/4" x 3 in. long, brass nipples were connected to the elbows. The thermopiles, for measuring the temperature difference of the fluids entering and leaving the heat-meter, were connected to these heat-meter nipples using short pieces of 1/2 in. rubber hoses to thermally isolate them from the heat-meter assembly. The thermopiles were then insulated from the surrounding air by wrapping them with blanket type insulation. Using 1/2 in. rubber hoses, hot and cold water were directly connected from the tap to each side of the heat-meter. Number 24 gauge copper-constantan thermocouples were inserted into the outlet of the hot and cold fluid hoses to measure the outlet temperature of both fluids. A digital thermometer with reference junction at 0° C, was used to make direct
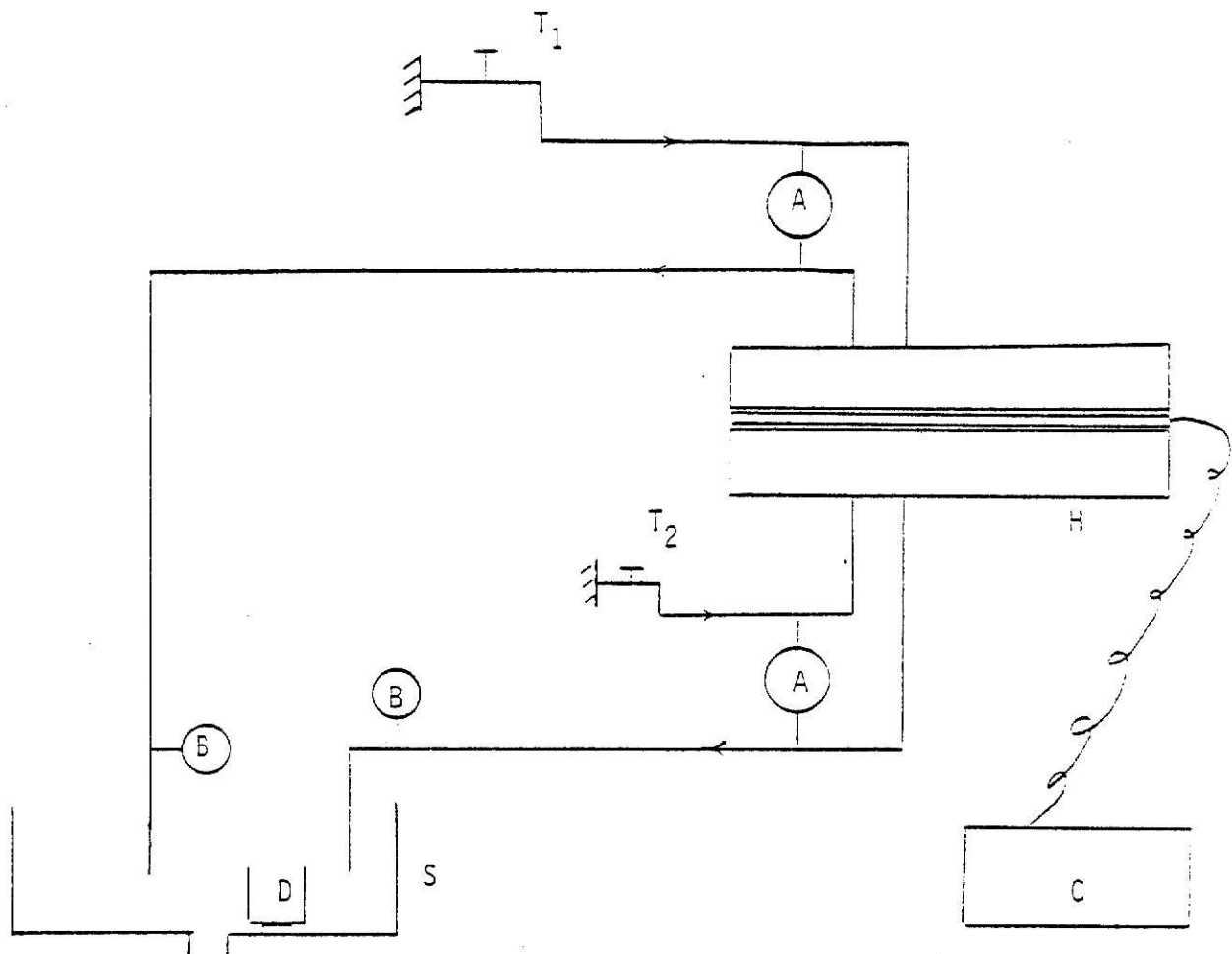
Figure 3.1 - Schematic diagram of the set up for preliminary testing of the heat-meter

Legend:

A   Thermopile measuring the fluid temperature change

B   Thermocouple measuring the exit fluid temperature

C   Storage scope

D   1000 ml beaker

H   Heat-meter

S   Sink

T_1 Hot water tap

T_2 Cold water tap

measurements of the temperature of the outlet fluids. By a volume collection method, fluid flow rates were measured, using a 1000 ml beaker and a digital stop watch.

3.2 Test Procedure

During the initial testing of the heat-meter prototype, no specific attempt was made to insulate it. Hot tap water was circulated in one side of the heat-meter while cold tap water was circulated in the other side. Both fluids were emptied into a sink after leaving the heat-meter. In measuring the temperature of the hot fluid, it was noticed that the fluid temperature was not stable because of the way that the hot tap water temperature controls functioned. A storage scope was then used to monitor the hot and cold fluids temperature along with the output of the thermopiles. The hot fluid temperature was changing in a periodic way, causing the thermopile outputs and the cold fluid temperature to change in a similar way with a time lag. Since controlling the hot fluid temperature in the source was not possible, using the storage scope approximate average values were determined for the fluid temperatures, for the outputs of the thermopiles measuring the fluid temperatures changes and for the heat-meter output. An energy balance on the fluids indicated a large difference between the heat lost by the hot fluid and the heat gained by the cold fluid. The difference was attributed to a net heat transfer taking place between the heat-meter and the surrounding air. Therefore, using 2 inch thick polystyrene foam, the heat-meter was insulated and tested again using the same procedure. Table 3.1 is a summary of the data taken for both insulated and unsulated tests.

3.2.1 <u>Sample Calculation</u>. A sample calculation of the heat lost by the hot fluid and the cold fluid heat gain will now be shown for testing of

$\bar{T}_{ho}$ °C	$\bar{T}_{co}$ °C	$\Delta\bar{V}_4$ mv	$\Delta\bar{V}_5$ mv	$\Delta\bar{V}_6$ mv	Vol_h ml	Δt_h sec	Vol_c ml	Δt_c sec	ΔT_h °C	ΔT_c °C	ΔT_{LM} °C	$\dot{Q}_h$ W	$\dot{Q}_c$ W	$\dot{V}_h$ $\frac{\ell}{min}$	$\dot{V}_c$ $\frac{\ell}{min}$	ρ_h $\frac{Kg}{\ell}$	ρ_c $\frac{Kg}{\ell}$
56.8	18	.65	.31	33.4	558	6.15	648	5.95	1.66	.793	35.6	619	360	5.44	6.53	.9847	.9985
36.4	17.5	.375	.15	15.98	270	3.06	227	1.95	.959	.384	17	351	186	5.29	6.98	.9936	.9985
45.5	16.5	.38	.215	25.6	670	4.5	500	4.83	.97	.549	27.2	597	237.2	8.93	6.21	.9898	.9988
57.9	17.6	.90	.510	34.6	1018	18.94	977	13.04	2.08	1.275	34.7	455	401	3.22	4.50	.9843	.9985
57.8	18.6	.770	.850	33.0	958	19.15	1014	22.6	1.76	2.14	33.12	362	400	3.00	2.69	.9843	.9985
38.9	17.6	.355	.545	17.8	992	15.92	933	23.47	.846	1.37	18.09	220	228	3.76	2.39	.9926	.9985
20.85	16.8	.064	.120	4.17	987	17.43	975	28.07	.16	.302	4.32	37.8	43.7	3.40	2.08	.9979	.9988
49.6	19.1	.955	.900	25.70	1001	30.29	920	29.62	2.23	2.26	25.78	307	292	1.98	1.86	.9980	.9984

Uninsulated H.M. (first three rows); Insulated H.M. (last five rows).

Table 3.1 - Summary of the data for preliminary testing of the heat-meter.

the uninsulated heat-meter. The heat gain by the cold fluid is given by

$$Q_c = (\dot{V}_c)(\rho_c)(C_p)(\frac{\Delta V_5}{n})(m) \tag{3-1}$$

where $\dot{V}$ is the volumetric flow rate, ΔV_5 is the output of the cold fluid thermopile, n is the number of the thermocouple pairs in the thermopile, ρ is the water density and m is the slope of the temperature-voltage curve for a copper-constantan thermocouple in the operating temperature range.

$$\dot{V} = \frac{\text{volume collected}}{\text{collection time}} = \frac{Vol_c}{\Delta t_c} \tag{3-2}$$

Substituting values from Table 3.1 in eq. (3-2) yields

$$\dot{V} = \frac{.658(\ell)}{5.95(S)} = .109 \frac{\ell}{S}$$

Substituting appropriate values from Table 3.1 in eq. (3-1) yields

$$\dot{Q}_c = (.109 \frac{\ell}{S})(.9985 \frac{Kg}{\ell})(4180 \frac{J}{Kg\text{-}^oC})(\frac{.31}{10} mv)(25.58 \frac{^oC}{mv}) = 360 \text{ W}$$

Similarly, the heat lost by the hot fluid is given by

$$\dot{Q}_h = (\dot{V}_h)(C_p)(\rho_h)(\frac{\Delta V_4}{n})(m) \tag{3-3}$$

where ΔV_4 is the output of the thermopile measuring the hot fluid temperature change and n is the number of thermocouple pairs in the corresponding thermopile.

$$\dot{V}_h = \frac{Vol_h}{\Delta t_h} = \frac{\text{volume collected}}{\text{collection time}} = \frac{.558(\ell)}{6.15(S)} = .0907 \frac{\ell}{S} \tag{3-4}$$

Substituting the appropriate values from Table 3.1 in eq. (3-3) yields

$$\dot{Q}_h = (.0907\frac{\ell}{S})(.9847\frac{Kg}{\ell})(4180\frac{J}{Kg\text{-}^oC})(\frac{.65}{10} mv)(25.58\frac{^oC}{mv}) = 621 \text{ W}$$

3.3 Discussion of Preliminary Test Results

The results of the preliminary testing of the heat-meter are shown graphically in Figures 3.2 and 3.3. In these figures, the heat lost by the hot fluid and the heat gained by the cold fluid are plotted versus the
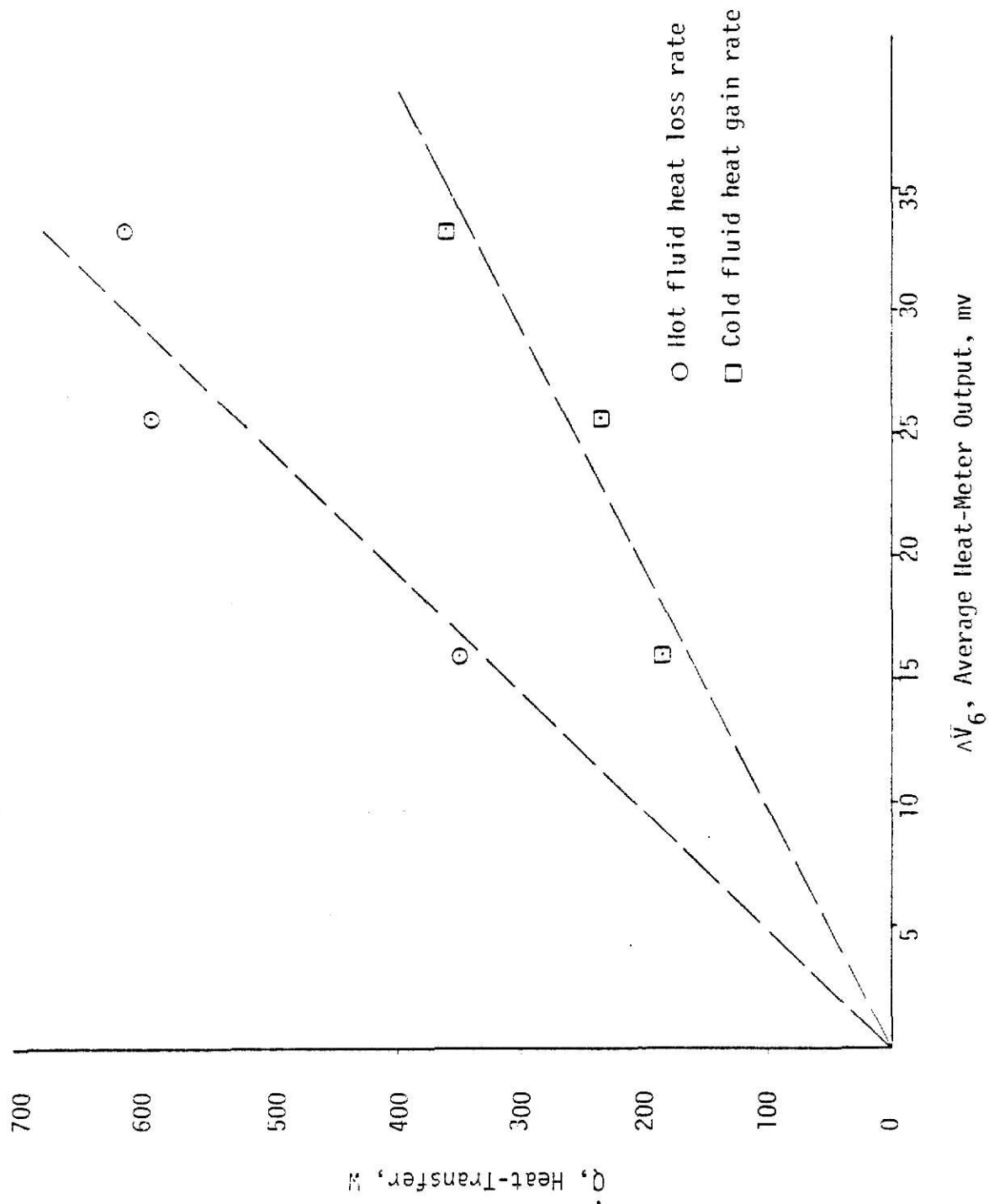
Figure 3.2 - Heat-transfer vs. uninsulated heat-meter output
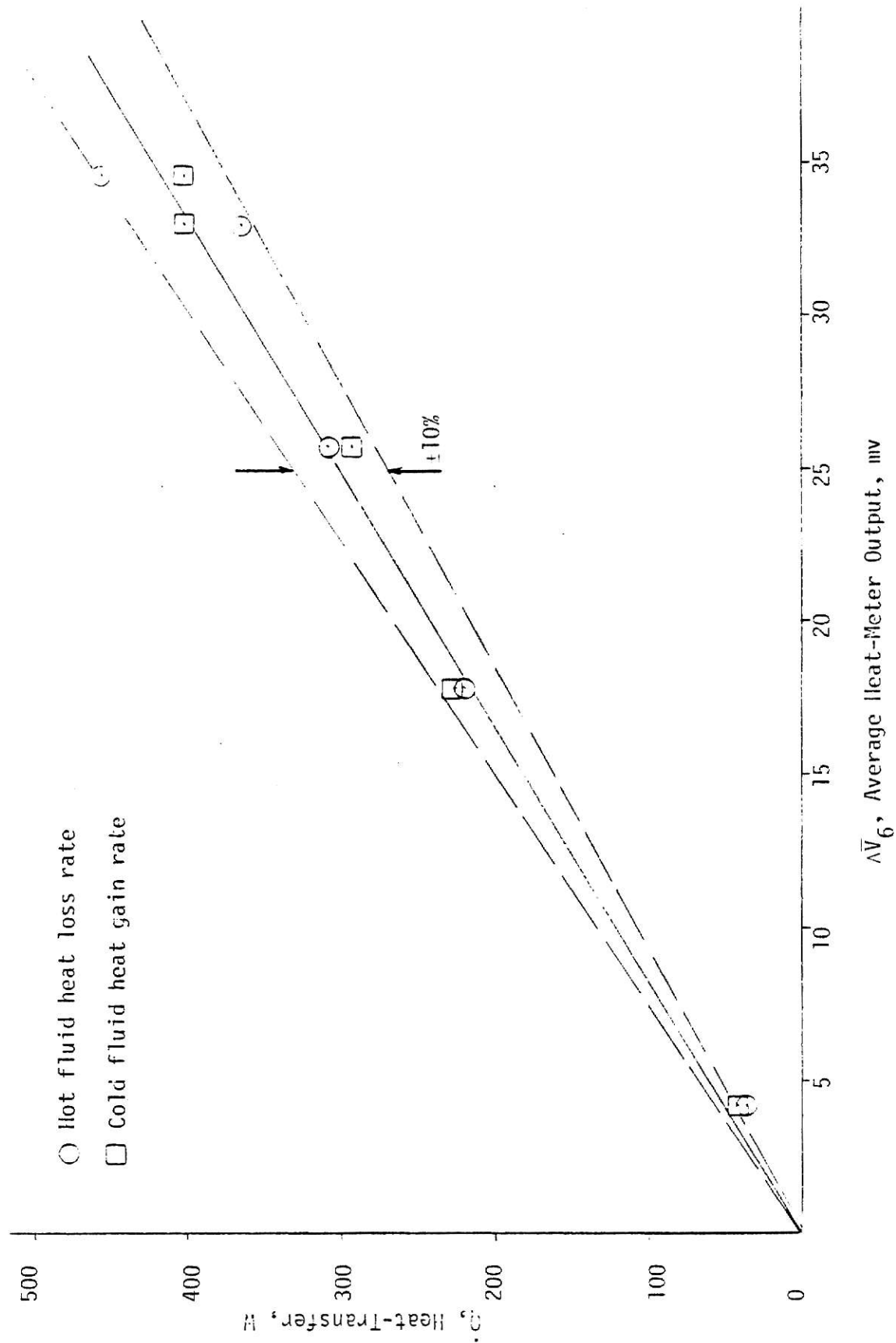
Figure 3.3 - Heat-transfer vs. insulated heat-meter output

millivolt output of the heat-meter. Both the insulated and the uninsulated
heat-meter test results are shown for comparison. As is evident from the
graphs in Figures 3.2 and 3.3, insulating the heat-meter appears to have
greatly reduced the heat transfer from the heat-meter to the ambient.
Within our ability to measure, the heat gained by the cold fluid and the
heat transferred from the hot fluid agree to within about ±10 percent of
the heat transferred when the heat meter was insulated.

Calibrating the heat-meter to an intended accuracy of ±1 percent
or better would require careful measurement of the heat transfer to the
hot fluid. Measurement of the fluid temperature change to estimate the
heat transfer would not give accurage results particularly when the fluid
temperature was fluctuating. In the preliminary testing of the heat-meter,
lack of control over the hot fluid temperature made it impossible to study
the effect of a change in the mean temperature of the separating plate on
the heat-meter performance. By directly connecting the heat-meter to the
water taps for fluid circulation, studying the effect of flow rate change
was not possible because of the constant drift in the tap water flow rate
due to line pressure fluctuations.

The conclusion drawn from the preliminary testing of the heat-meter is
that indeed a relationship exists between the heat transfer rate and the out-
put of the heat-meter. Therefore, the next step was to study the performance
of the heat-meter and determine its accuracy and repeatibility with a more
refined testing of it.

CHAPTER IV

MODIFIED TEST FACILITY FOR HEAT-METER CALIBRATION

Accurately calibrating the heat-meter prototype, and studying the performance of it under controlled conditions, required an additional test facility. For this purpose, a calorimeter box was constructed to accurately measure and control the heat input to the hot fluid circuit. The setup was used to study the heat-meter accuracy, repeatibility, the effect of fluid flow rates and the effect of the mean temperature of the semi-conductive plate on the heat-meter performance.

4.1 Construction of the Calorimeter Box

To house and insulate the components of the hot fluid circuit, a cubical insulating box with a removable lid was constructed. The box had inside dimensions of 18"x18"x18" (45.7cm x 45.7cm x 45.7cm) and six inch thick walls constructed by using three, 2 inch thick layers of "thermax" insulation fastened together with aluminum tape.

4.1.1 Construction of the Calorimeter Box Thermopile. To account for the heat losses from the calorimeter box during the heat-meter calibration, twenty four pairs of 24 gauge copper-constantan thermocouples were connected to the inside and outside surfaces of the calorimeter box. The junctions of the thermocouples were electrically insulated from the calorimeter box using shrink tubing. A thermopile was formed to measure the average temperature difference across the walls of the box, by connecting the ends of the thermocouple wires in series to a terminal strip which was epoxied to the outside

surface of the calorimeter box. Details of the heat loss calibration tests are discussed in Appendix C.

4.1.2 _Construction of the Heating Element._ A heat exchanger that would be used in the hot fluid circuit for heat input, was constructed by housing a 1500 watt electrical water heating element in a 2.5 in. O.D. x 15 in. long copper tube. Two, $\frac{1}{2}$ in. F.P.T. brass fittings were silver brazed to the ends of the copper tubing as the inlet and outlet ports of the heat exchanger. Using a small wood support, the heat exchanger was mounted on a 17 in. x 17 in. x 1/4 in. (43.2cm x 43.2cm x .64cm) plywood sheet and housed inside the calorimeter box. Power input to the heating element was supplied from a terminal strip epoxied to the outside surface of the calorimeter box.

4.1.3 _The Hot Fluid Pump._ For hot fluid circulation, initially a Teel Magnetic Drive Pump Model 1P876 was mounted inside the calorimeter box. During the heat-meter calibration tests, however, the high temperature of the air inside the calorimeter box indicated that the pump was transferring an excessive amount of heat to the air inside of the box. This would increase the heat loss from the calorimeter box to the ambient air and also cause a temperature difference between the air inside the calorimeter box and the connecting tunnel, which is explained in Section 4.2. Referring to Appendix C, since the heat loss calibration tests were based on equal temperatures inside the calorimeter box and the connecting tunnel, therefore using the heat loss calibration curve for estimating the heat loss from the system would not give correct results. To solve the problem, it was decided to use a submersible Little Giant Pump model 2E-N for the hot fluid circulation loop. In this arrangement the pump would be cooled by the fluid being circulated through it, and hence there would be virtually no additional heating of the

internal air. From standard 8.5 in dia. x 1/4 in. thick P.V.C. pipe, an 11 inch long cylindrical canister was constructed to house the submersible pump. On the top surface and on the side near the bottom of the canister, two separate holes were drilled and tapped to receive 1/4 in. x 3 in. long brass nipples as the exit and inlet ports of the pump. Another hole, on the top surface of the canister was drilled and tapped for a 3/8 in. x 2 in. long brass nipple. During the heat-meter calibration tests, a partially inflated balloon was fitted over the nipple to maintain approximately atmospheric pressure over the water in the canister and prevent evaporation from the canister to the air inside the calorimeter box. During operation of the system, such an arrangement would protect the fluid circuit against the stresses caused by thermal expansion of the water, and would also allow for volume expansion due to operation of flow control valves. Power was supplied to the pump through a compression fitting seal on top of the canister. The external power cord passed through the calorimeter box and was connected to a terminal strip expoxied to the outside surface of the box.

4.1.4 <u>Calorimeter Box Support</u>. The calorimeter box was suspended off a table using a support in the shape of a cross made from standard 2 in x 4 in. pine.

4.2 <u>Construction of the Connecting Tunnel</u>

To insulate the part of the hot fluid circuit between the calorimeter box and the heat-meter hot side, an insulating box, referred to as the connecting tunnel, was constructed with a removable top and outside dimensions of 15.5 in. x 20.5 in x 20.0 in (39.4cm x 52.1cm x 50.8cm). The four-inch thick walls of the connecting tunnel consisted of two layers of 2 inch thick "thermax" foam insulating material bonded together with aluminum

tape. For determination of the heat loss from the connecting tunnel, by measuring the average temperature difference from its walls, 8 pairs of 24 gauge copper-constantan thermocouples were connected between the inside and outside surfaces of the connecting tunnel. The junctions of the thermocouples were electrically insulated from the connecting tunnel by using shrink tubing. The connecting tunnel was connected to the calorimeter box using aluminum tape and was suspended on a small wooden table along with the heat-meter assembly. The relative position of the connecting tunnel with respect to the calorimeter box is shown in Appendix Figure C.1.

4.3 Air Circulation within Connecting Tunnel and Calorimeter Box

A small electrical fan was mounted both inside the calorimeter box and inside the connecting tunnel to circulate the internal air and maintain the internal air temperature approximately uniform. Details of the electrical circuits for the fans are shown in Figure C.3 of Appendix C.

4.4 Heat-Meter Assembly

The glass plate used in the preliminary testing of the heat-meter was replaced by a phenolic plate of 1.5mm (0.6 in.) thickness and a nominal thermal conductivity of .29 $\frac{W}{m-^{o}C}$ (.17 $\frac{BTU}{hr-Ft-^{o}F}$). Prior to assembling the heat-meter, to minimize the contact resistance to heat flow between the slabs, a thin layer of "thermalmastic", a commercially available highly conductive paste, was applied to both surfaces of each of the heat-meter thermopile plates. In preliminary testing of the heat-meter, "thermalmastic" was only applied to the surface of the thermopile plates in contact with the bottom surface of the heat-meter slabs. After assembling the heat-meter, blanket type insulation was wrapped around the heat-meter slab sides and then using 2-inch thick layers of "thermax" insulating material, the heat-meter assembly

was insulated on all sides. To indicate the temperature difference across the insulation, twelve pairs of 24 gauge copper-constantan thermocouples with electrically insulated junctions were connected to the inside and outside surfaces of the heat-meter insulation to form a thermopile. The ends of the thermocouples were connected in series to a terminal strip epoxied to the outside surface of the heat-meter insulation. The heat-meter assembly was then oriented vertically and attached to the connecting tunnel as shown in Figure 4.1. This arrangement would thermally guard the hot side of the heat-meter because the connecting tunnel and the heat-meter hot side slab would be at approximately the same temperature as the hot fluid. Figure 4.2 is a photographic view of the modified test setup for heat-meter calibration.

4.5 Hot and Cold Fluid Circuits

4.5.1 Hot Water Circuit. The hot water circuit shown in Figure 4.1 was setup using 1/2 inch rubber hose connecting lines. The basic components of the circuit were a submersible pump for hot water circulation, turbine flow meter for measurement of the fluid flow rate, heating element for power input to the hot fluid, flow control values for controlling the fluid flow rate and thermopile section for measuring the hot fluid temperature change. To make it possible to control the hot fluid flow rate after sealing the system for testing, an opening of 5 in. x 5 in. (12.7cm x 12.7cm) dimensions with a replacable plug of insulation was made on the wall of the calorimeter box to give access to the globe control valve V1 shown in Figure 4.1. For charging the hot fluid circuit, using 1/2 inch rubber hose, a connection was made between the water tap and the inlet of globe valve A shown in Figure 4.1. Another connection was made between globe valve B and the sink. Valve V was closed and globe valve V1 was fully opened. By slowly
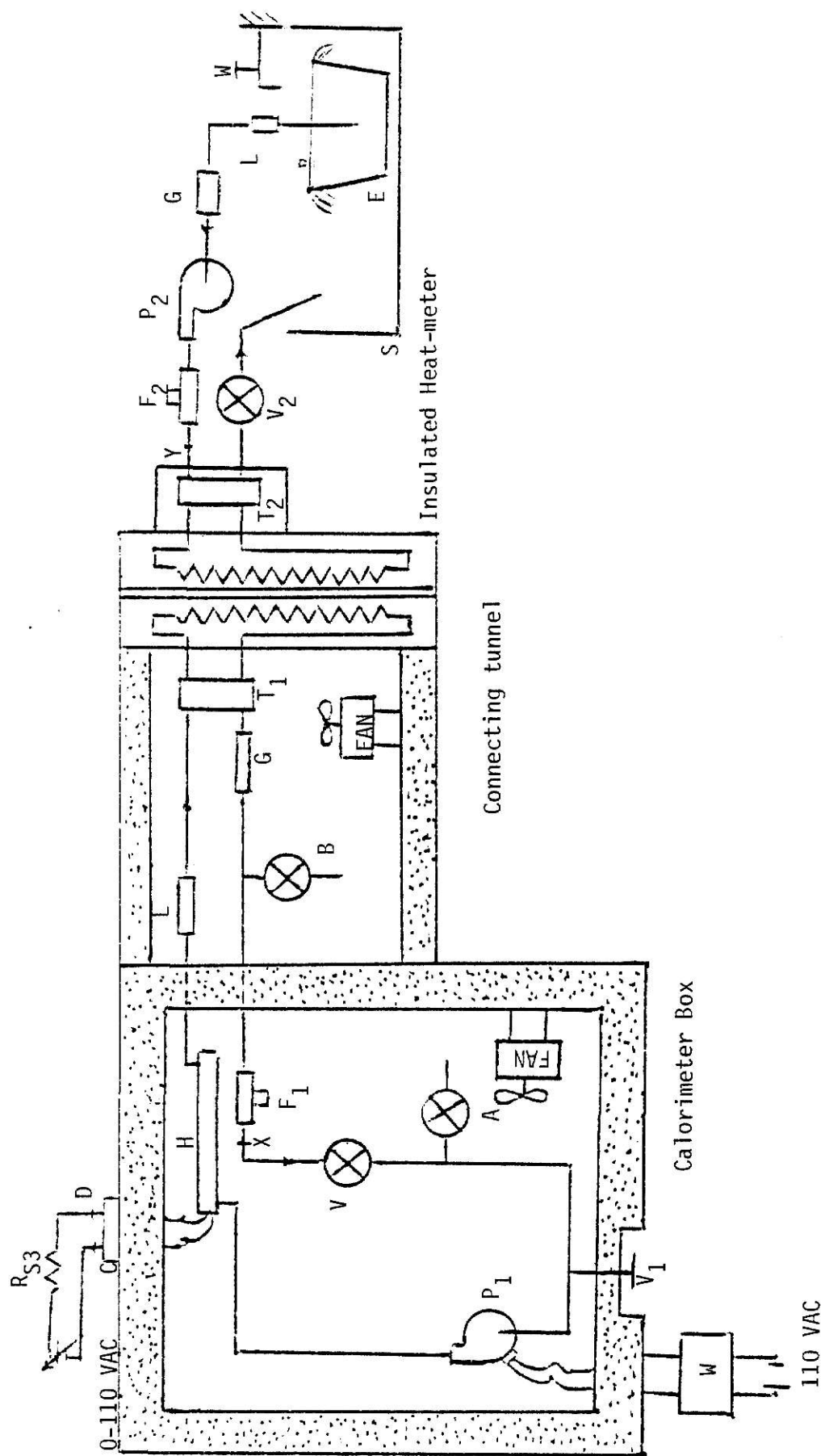
Figure 4.1 - Schematic diagram of test set up for heat-meter calibration

Legend:

A   Globe valve for charging the hot fluid circuit

B   Globe valve for charging the hot fluid circuit

E   Bucket overfilled with water

F_1 Turbine flow-meter in the hot fluid circuit (ME-3907)

F_2 Turbine flow-meter in the cold fluid circuit (ME-3909)

G   Sight glass

H   Heating element

L   Filter

P_1 Submersible

P_2 Cold fluid pump

R_{S3} Standard resistor in the heating element electrical circuit

S   Sink

T_1 Thermopile measuring hot fluid temperature change

T_2 Thermopile measuring cold fluid temperature change

V   Check valve

V_1 Globe flow control valve in the hot fluid circuit

V_2 Globe flow control valve in the cold fluid circuit

W   Water tap

X   Thermocouple measuring of the hot fluid temperature

Y   Thermocouple measuring of the cold fluid temperature
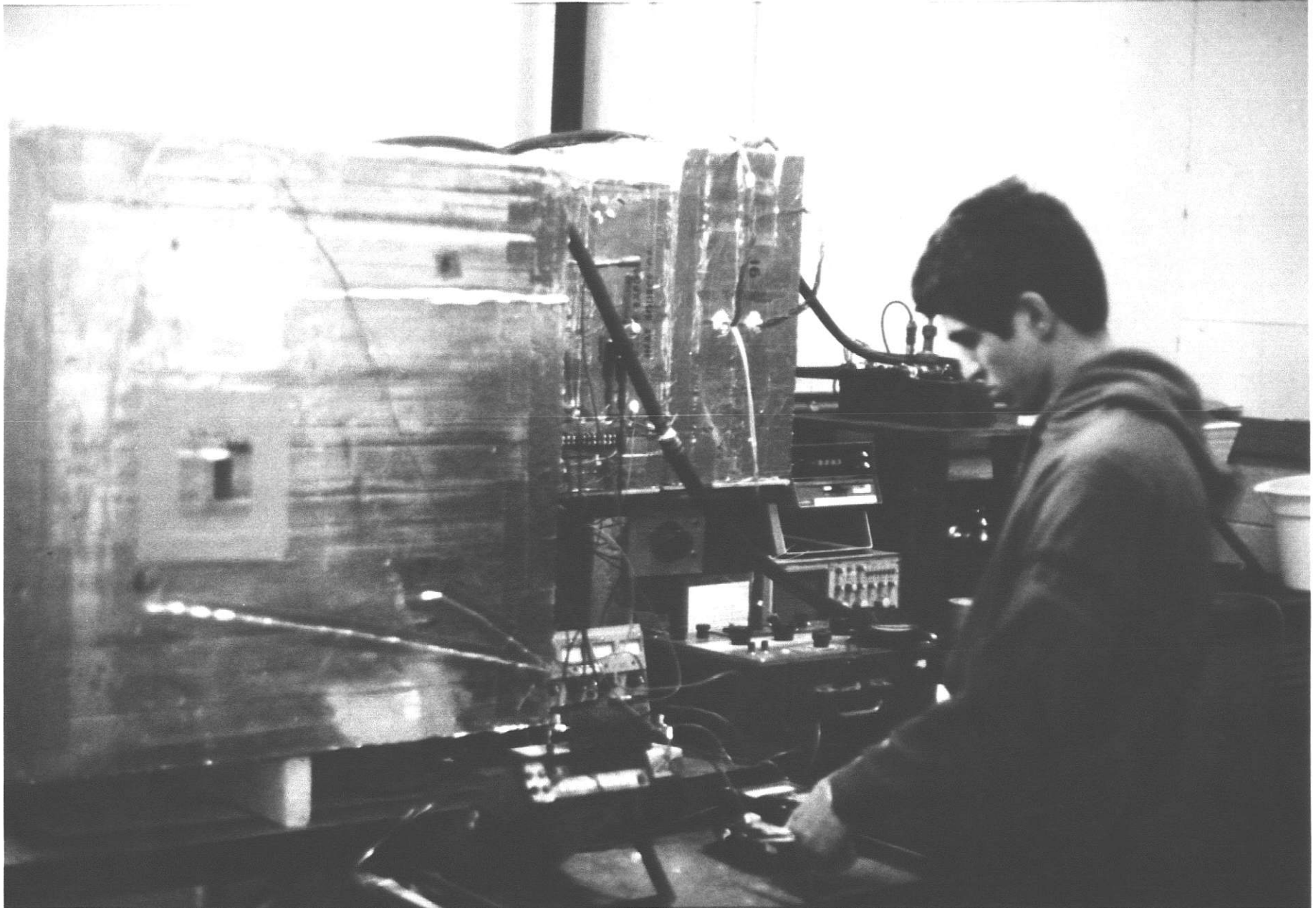
Figure 4.2 A photographic view of the modified test set up.

opening the valve A, water from the tap was forced into the heat-meter hot side and out to the sink through the valve B. Valve B was slowly closed until the submersible pump cannister had only about one inch of air column above the water level in it. Both valves A and B were closed and the hose connections to them were removed. By turning the pump on and opening valve V, water was circulated in the system and charging of the hot fluid circuit was complete.

4.5.2 <u>Cold Water Circuit</u>. A schematic diagram of the cold water circuit is shown in Figure 4.1. The circuit basically consists of a Potter turbine flow meter for measurement of the fluid flow rate, a globe valve for flow control, a Teel Magnetic Drive Pump for cold water circulation and another thermopile section for measuring the cold water temperature change. Initially, the cold fluid thermopile was insulated from the surroundings by encasing it in a box of "thermax" insulating material.

4.5.3 <u>Measurement of Coolant Flow Rates</u>. Two Potter turbine flow meters model 5/8 - 215 B, were calibrated and used in the hot and cold fluid circuits for flow rate measurements. The frequency outputs of the turbine flow meters were connected to a Hewlett Packard Electronic Counter model 5212A. The detailed discussion of the turbine flow meters calibration is presented in Appendix B.

4.6 <u>Measurement of the Power Inputs to the Calorimeter Box</u>

4.6.1 <u>Measurement of the Power Input to the Heating Element</u>. Power was supplied to the heating element in the hot water circuit from a 0-150 volt variac. The variac and the pump were connected to a 0-500 W constant voltage transformer to maintain a constant supply voltage. The electrical

circuit for power input to the heating element is shown in Figure 4.1. The resistance of the standard resistor used in the circuit was determined to be .330 Ω ± .27%, following the same procedure used for measuring the resistance of the standard resistors in the fan circuits as discussed in Section C.3 of Appendix C. The power input to the heating element was determined by measuring the voltage drop across the standard resistor and between points C and D of the circuit shown in Figure 4.1. The instrument used for measuring the voltage was a Fluke Digital Multimeter model 8600A.

4.6.2 <u>Power Input to the Hot Water Pump</u>. Power input to the hot water pump was directly measured by using a 0-250 W Weston A.C. wattmeter. The pump circuit is shown in Figure 4.1.

4.6.3 <u>Measurement of the Power Inputs to the Fans</u>. Using the Fluke Digital Multimeter model 8600A, power inputs to the fans in the calorimeter box and the connecting tunnel, were measured by recording the voltage drop across the standard resistor and between points A and B of each circuit. as shown in Figure C.1.

4.7 <u>Temperature Measurements</u>

Accurate determination of mass flow rates, for use in the energy balances on the hot and cold water circuits, required measurement of the fluid temperatures at the turbine flow meters. Therefore, 24 gauge copper-constantan thermocouples were inserted into the hot and the cold fluid circuits close to the exit of each turbine flow meter. Thermocouples, used for measurement of temperature difference and absolute temperature, were connected to a millivolt potentiometer and a thermocouple thermometer through a multiple position selector switch. A Digitec digital thermocouple thermometer model

590 TC Type T was used to make temperature measurements of the air inside the calorimeter box and the connecting tunnel, the ambient air, the outside surface of the calorimeter box and the hot and cold water at the turbine flow meters. A Leeds and Northrup millivolt potentiometer model 8686 was used to measure the output of the thermopiles for the heat-meter output, the temperature difference across the calorimeter box, the temperature difference across the connecting tunnel, the hot fluid temperature change, the cold fluid temperature change and the temperature difference across the heat-meter insulation.

Table 1b. (Continued)

No.	Compound Structure & Name	T_c (°K) experiment	T_c (°K) prediction	T_c (°K) deviation	P_c (atm) experiment	P_c (atm) prediction	P_c (atm) deviation	V_c ($\frac{cm^3}{g\ mole}$) experiment	V_c ($\frac{cm^3}{g\ mole}$) prediction	V_c ($\frac{cm^3}{g\ mole}$) deviation
85.	$CH_3COC_2H_5$ methyl ethyl ketone	535.6	537.0	1.4	41.0	42.0	1.0	267.0	265.0	-2.0
86.	CH_3OH methanal	512.6	512.6	0.3	79.9	81.5	1.6	118.0	113.0	-5.0
87.	C_2H_5OH ethanal	516.2	521.4	5.2	63.0	63.2	-0.2	167.0	168.0	1.0
88.	C_4H_9OH n-butanal	562.9	556.2	-6.7	43.3	43.3	0.0	274.0	278.0	4.0
89.	C_4H_9OH 2-butanol	536.0	534.5	-1.5	41.4	44.5	3.1	268.0	274.0	6.0
90.	C_4H_9OH tert-butarol	506.2	516.2	10.0	39.2	44.5	5.3	275.0	264.0	-11.0
91.	$C_6H_{13}OH$ n-hexanol	610.0	590.7	-19.3	40.0	32.9	-7.1	381.0	388.0	7.0
92.	C_6H_5OH phenol	694.2	693.4	-0.8	60.5	60.6	0.1	229.0	229.0	0.0
93.	$C_6H_{11}OH$ cyclo-hexanol	625.0	620.0	-5.0	37.0	44.63	7.63	327.0	327.0	0.0
94.	C_7H_7HO benzyl alcohol	677.0	675.9	-1.1	46.0	44.9	-1.1	334.0	329.0	-5.0
95.	$C_6H_4CH_3OH$ o-aesol	697.6	701.5	3.1	49.4	50.1	0.7	282.0	290.0	8.0
96.	$C_6H_4CH_3OH$ m-aesol	705.8	732.3	26.5	45.0	46.6	1.6	310.0	289.0	21.0

Table 1b. (Continued)

No.	Compound Structure & Name	T_c (°K)			P_c (atm)			V_c ($\frac{cm^3}{g\ mole}$)		
		experiment	prediction	deviation	experiment	prediction	deviation	experiment	prediction	deviation
97.	$C_6H_4CH_3OH$ p-cresol	704.6	711.9	7.3	50.8	47.2	-3.6	—	302.0	—
98.	CH_3OCH_3 dimethyl ether	400.0	399.2	-0.8	53.0	55.1	2.1	178.0	175.0	-3.0
99.	$C_2H_3OCH_3$ vinyl methyl ether	436.0	437.2	1.2	47.0	49.2	2.2	205.0	209.5	4.5
100.	$C_3H_5OC_2H_5$ vinyl ethyl ether	475.0	473.3	-1.7	40.2	41.8	1.6	260.0	264.0	4.0
101.	$C_3H_7OC_3H_7$ diiso-propyl ether	500.0	506.4	6.4	28.4	32.0	3.6	386.0	387.0	1.0
102.	$C_2H_5OC_4H_9$ ethyl butyl ether	531.0	532.5	1.5	30.0	30.8	0.8	390.0	395.0	5.0
103.	CH_3COOH acetic acid	594.4	593.9	-0.5	57.1	56.9	-0.2	171.0	172.0	1.0
104.	C_2H_5COOH propionic acid	612.0	614.2	2.2	53.0	47.1	5.9	230.0	227.0	-3.0
105.	C_3H_7COOH n-butyric acid	628.0	633.6	5.6	52.0	40.2	-11.8	292.0	282.0	-10.0
106.	C_6H_5COOH benzoic acid	752.0	753.1	1.1	45.0	44.0	-1.0	341.0	341.0	0.0
107.	CH_3COOCH_3 methyl acetate	506.8	510.6	3.8	46.8	46.4	-0.4	228.0	230.0	2.0

Table 1b. (Continued)

No.	Compound Structure & Name	T_c (°K)			P_c (atm)			$V_c (\frac{cm^3}{g\ mole})$		
		experiment	prediction	deviation	experiment	prediction	deviation	experiment	prediction	deviation
108.	$HCOOC_2H_5$ ethyl formate	508.4	506.5	-1.9	46.8	49.9	3.1	229.0	230.0	1.0
109.	$HCOOC_3H_3$ vinyl formate	475.0	476.3	1.3	57.0	53.1	-3.9	210.0	209.5	-0.5
110.	$CH_3COOC_2H_3$ vinyl acetate	525.0	524.7	-0.3	43.0	41.7	-1.3	265.0	264.5	-0.5
111.	$CH_3COOC_2H_5$ ethyl acetate	523.2	528.7	5.5	37.8	39.6	1.8	286.0	285.0	-1.0
112.	$C_2H_5COOCH_3$ methyl propionate	530.6	532.8	-2.2	39.5	39.6	0.1	282.0	285.0	-3.0
113.	CH_3CN acetonitrile	548.0	553.8	5.8	47.7	47.8	0.1	173.0	175.0	2.0
114.	C_2H_5CN propionitrile	564.4	563.9	-0.5	41.3	41.4	0.1	230.0	230.0	0.0
115.	C_3H_5CN allyl cyanide	585.0	586.1	1.1	39	38.0	-0.9	265.0	264.0	-1.0
116.	C_3H_7CN butyro-nitrile	582.2	581.3	-0.9	37.4	36.2	-1.2	285.0	285.0	0.0
117.	CH_3NO_2 nitro-methane	588.0	588.3	0.3	62.3	62.6	0.3	173.0	173.0	0.0
118.	CH_3NH_2 methyl anime	430.0	429.6	-0.4	73.6	73.1	-0.5	140.0	132.0	-8.0

Table 1b.   (Continued)

No.	Compound Structure & Name	T_c (°K)			P_c (atm)			$V_c \left(\frac{cm^3}{g\ mole}\right)$		
		experiment	prediction	deviation	experiment	prediction	deviation	experiment	prediction	deviation
119.	$C_2H_5NH_2$ ethyl amine	456.0	453.8	-2.2	55.5	58.4	2.9	178.0	178.0	0.0
120.	C_2H_6NH di-methyl amine	437.6	446.6	9.0	52.4	55.2	2.8	187.0	187.0	0.0
121.	$C_3H_7NH_2$ n-propyl amine	497.0	491.4	-5.6	46.8	48.3	1.5	233.0	233.0	0.0
122.	$C_3H_7NH_2$ iso-propyl amine	476.0	471.3	-4.7	50.0	49.8	-0.2	229.0	229.0	0.0
123.	C_3H_9N trimethyl amine	433.2	436.2	3.0	40.2	42.7	2.5	254.0	243.0	-11
124.	$C_6H_{15}N$ tri-ethyl amine	535.0	532.7	-2.3	30.0	29.3	-0.7	390.0	408	18
125.	$C_6H_5NH_2$ aniline	699.0	689.7	9.3	52.4	52.4	0.0	270.0	276.0	6.0
126.	$C_6H_{14}NH$ dipropyl amine	550.0	551.0	4.0	31.0	30.8	-0.2	407.0	407.0	0.0
127.	$C_7H_7NH_2$ o-toluidine	634.0	707.7	13.7	37.0	46.26	7.26	343.0	337.0	-6.0
128.	$C_7H_7NH_2$ m-toluidine	709.0	725.9	16.9	41.0	41.3	0.3	343.0	336.0	-7.0
129.	$C_7H_7NH_2$ p-toluidine	667.0	706.7	39.6	—	41.8	—	—	343.0	—
130.	CH_3SH methyl mercapton	470.0	469.7	-0.3	71.4	71.2	-0.2	145.0	145.0	0.0

Table 1b. (Continued)

No.	Compound Structure & Name	T_c (°K)			P_c (atm)			$V_c (\frac{cm^3}{g \cdot mole})$		
		experiment	prediction	deviation	experiment	prediction	deviation	experiment	prediction	deviation
131.	C_2H_5SH ethyl mercaptan	499.0	503.0	4.0	54.2	56.5	2.3	207.0	200.0	-7.0
132.	$CH_3SC_2H_5$ dimethyl sulfide	503.1	501.6	-1.5	54.6	51.9	-2.7	201	205.0	4.0
133.	$CH_3SC_2H_5$ methyl ethyl sulfide	533.0	534.0	1.0	42.0	43.6	1.6	—	260.0	—
134.	$C_2H_5SC_2H_5$ diethyl sulfide	557.0	559.4	2.4	39.1	37.6	-1.5	318.0	315.0	-3.0

Table 1c. Comparison between Predicted and Experimental Values of the Critical Compressibility, Z_c

No.	Structure and name	Experiment	Prediction	Deviation
1	C_2H_6 ethane	0.285	0.284	-0.0035
2	C_3H_8 propane	0.281	0.279	-0.0071
3	C_4H_{10} n-butane	0.274	0.275	0.0036
4	C_4H_{10} iso-butane	0.283	0.275	-0.0283
5	C_5H_{12} n-pentane	0.262	0.270	0.0305
6	C_5H_{12} 2-methylbutane	0.271	0.270	-0.0037
7	C_5H_{12} neo-pentane	0.269	0.269	0.0000
8	C_6H_{14} n-hexane	0.260	0.265	0.0192
9	C_6H_{14} 2-methylpentane	0.267	0.266	-0.0037
10	C_6H_{14} 3-methylpentane	0.273	0.266	-0.0256
11	C_6H_{14} 2,2-dimethylbutane	0.272	0.264	-0.0294
12	C_7H_{16} n-pentane	0.263	0.261	-0.0076
13	C_7H_{16} 2,2,3-trimethylbutane	0.267	0.260	-0.0262
14	C_2H_4 ethylene	0.276	0.276	0.000

Table 1c. (Continued)

No.	Structure and name	Experiment	Prediction	Deviation
15	C_3H_6 propylene	0.275	0.277	0.0073
16	C_4H_8 1-butene	0.277	0.272	-0.0180
17	C_4H_8 cis-2-butene	0.272	0.270	-0.0074
18	C_4H_8 trans-2-butene	0.274	0.273	-0.0036
19	C_6H_{12} 1-hexene	0.260	0.263	0.0115
20	C_3H_4 propadiene	0.271	0.271	0.0000
21	C_4H_6 1,3 butadiene	0.270	0.270	0.0000
22	C_2H_2 acetylene	0.271	0.271	0.0000
23	C_3H_4 propyne	0.270	0.270	0.0000
24	C_5H_{10} cyclopentane	0.276	0.275	-0.0036
25	C_6H_{12} methylcyclopentane	0.273	0.270	-0.0110
26	C_6H_{12} cyclohexane	0.273	0.272	-0.0037
27	C_5H_8 cyclopentene	0.272	0.272	0.0000
28	C_6H_6 benzene	0.271	0.271	0.0000

Table 1c. (Continued)

No.	Structure and name	Experiment	Prediction	Deviation
29	C_7H_8 toluene	0.264	0.268	0.0152
30	C_8H_{10} o-xylene	0.263	0.267	0.0303
31	C_8H_{10} m-xylene	0.260	0.268	0.0308
32	C_8H_{10} p-xylene	0.260	0.277	0.0654
33	C_7H_{16} 3-ethylpentane	0.267	0.261	-0.0225
34	C_8H_{18} n-octane	0.259	0.256	-0.0116
35	$C_{12}H_{26}$ n-dodecane	0.240	0.238	-0.0083
36	C_8H_{18} 2,3 dimethylhexane	0.262	0.256	-0.0229
37	C_8H_{18} 2,5 dimethylhexane	0.262	0.256	-0.0229
38	$C_{17}H_{36}$ n-heptadecane	0.220	0.215	-0.0227
39	C_5H_{10} cis-2-pentene	0.280	0.263	-0.0607
40	C_5H_{10} trans-2-pentene	0.280	0.265	-0.0536
41	C_5H_{10} 3-methyl-1-butene	0.282	0.268	-0.0496
42	C_6H_{10} 1,5 hexadiene	0.260	0.261	0.0038

Table 1c. (Continued)

No.	Structure and name	Experiment	Prediction	Deviation
43	C_7H_{14} ethylcyclopentane	0.269	0.260	0.0335
44	C_9H_{12} 1,2,3 trimethylbenzene	0.276	0.277	0.0036
45	C_9H_{12} 1,2,4 trimethylbenzene	0.258	0.254	-0.0155
46	C_9H_{12} 1,2,5 trimethylbenzene	0.260	0.260	0.0
47	C_9H_{12} n-propylbenzene	0.265	0.259	-0.0226
48	CH_3OH methanol	0.224	0.223	-0.0045
49	C_3H_8O 1-propanol	0.253	0.251	-0.0079
50	$C_4H_{10}O$ isobutanol	0.257	0.252	-0.0186
51	C_6H_6O phenol	0.240	0.240	0.0.
52	C_7H_8O o-cresol	0.240	0.239	0.0042
53	C_7H_8O m-cresol	0.241	0.240	-0.0041
54	C_7H_8O p-cresol	0.246	0.249	0.0122
55	C_2H_6O dimethyl ether	0.287	0.277	-0.0348
56	C_3H_8O ethylmethyl ether	0.267	0.272	0.0187

Table 1c. (Continued)

No.	Structure and name	Experiment	Prediction	Deviation
57	$C_5H_{12}O$ ethylpropyl ether	0.265	0.263	-0.00755
58	$C_{12}H_{10}O$ diphenyl ether	0.260	0.236	-0.0923
59	C_4H_8O vinylethyl ether	0.270	0.272	0.0074
60	C_3H_6O acetone	0.232	0.231	-0.0043
61	$C_5H_{10}O$ diethylketone	0.269	0.222	-0.1747
62	$C_5H_{10}O$ methyl-n-proylketone	0.250	0.222	-0.1120
63	$C_2H_4O_2$ acetic acid	0.200	0.245	-0.2250
64	$C_4H_8O_2$ n-butyric acid	0.295	0.291	-0.0136
65	$C_2H_4O_2$ methyl formate	0.255	0.26	0.0196
66	$C_4H_8O_2$ n-propyl formate	0.259	0.251	-0.0309
67	$C_4H_8O_2$ ethyl acetate	0.252	0.243	-0.0159
68	$C_4H_8O_2$ methyl propionate	0.256	0.248	-0.0313
69	C_3H_9N n-propyl amine	0.267	0.270	0.0112

Table 2a. Group Contributions for Ideal Gas Heat Capacity

No.	Group	a	$b \times 10^2$	$c \times 10^4$	$d \times 10^6$
1	-C-	-5.8307	4.4541	-0.4208	0.012630
2	-CH	-3.5232	3.4158	-0.2816	0.008015
3	-CH2	-2.301	3.061	-0.2132	0.005596
4	-CH3	0.646	2.127	-0.08285	0.001041
5	CH4	0.6087	2.1433	-0.0852	0.001135
6	=C-	-0.9439	2.0500	-0.1829	0.005414
7	=CH	-0.2866	1.6393	-0.09885	0.002275
8	=CH2	0.5266	1.8357	-0.0954	0.001950
9	=C=	1.9627	0.8316	-0.0648	0.001778
10	≡C-	2.32	0.235	0.02125	-0.001875
11	≡CH	2.8443	1.0172	-0.0690	0.001866
12	-C- (ring)	-5.8307	4.4541	-0.4208	0.012630
13	-CH (ring)	-3.5232	3.4158	-0.2816	0.008015
14	-CH2 (ring)	0.3945	2.1363	-0.1197	0.002596
15	=C- (ring)	-0.9439	2.0500	-0.1829	0.005414
16	=CH (ring)	-0.2493	1.6223	-0.0964	0.00218
17	=C= (ring)	1.9627	0.8316	-0.0648	0.001778

Table 2a. (Continued)

No.	Group	a	$b \times 10^2$	$c \times 10^4$	$d \times 10^6$
18	≡C- (ring)	-	-	-	-
19	↔C⟨	0.1219	1.2170	-0.0855	0.002122
20	-C⟨	-1.3883	1.5159	-0.1069	0.002659
21	HC⟨	-1.4572	1.9147	-0.1233	0.002985
22	⊃C↔	-	-	-	-
23	H⊃C↔	-	-	-	-
24	H2C↔	-	-	-	-
25	-0-	2.8461	-0.0100	0.0454	-0.00218
26	=0	-	-	-	-
27	-0- (ring)	-7.4888	5.4531	-0.4395	0.01694
28	0⟨	-3.7344	1.3727	-0.1265	0.003789
29	-OH (to -C-)	6.5128	-0.1347	0.0414	-0.00162
30	-OH (to -CH)	6.5128	-0.1347	0.0414	-0.00162
31	-OH (to -CH2)	6.5128	-0.1347	0.0414	-0.00162
32	-OH (to -CH3)	4.2128	-0.0237	0.0414	-0.00162
33	-OH (to -CH ring)	-4.832	2.3509	-0.0614	-0.001916
34	-OH (aromatic)	0.1133	-3.2	-0.4296	0.018886

Table 2a. (Continued)

No.	Group	a	$b \times 10^2$	$c \times 10^4$	$d \times 10^6$
35	$-\overset{\mid}{C}=0$	1.0016	2.0763	-0.1636	0.004494
36	$\overset{H}{\underset{\mid}{-C}}=0$	3.5184	0.9437	0.0614	-0.00698
37	$\overset{H}{\underset{\mid}{H-C}}=0$	5.607	0.754	0.0713	-0.005494
38	$\overset{C}{\underset{\parallel}{-C}}-0-$	2.7350	1.0751	0.0667	-0.00923
39	$\overset{O}{\underset{\parallel}{-C}}-OH$	1.4055	3.4632	-0.2557	0.006886
40	$\overset{O}{\underset{\parallel}{H-C}}-OH$	2.798	3.243	-0.2009	0.004817
41	$\overset{O}{\underset{\parallel}{-0-C}}-H$	4.8898	1.2524	-0.02613	-0.009069
42	$\overset{O}{\underset{\parallel}{-C}}-$ (ring)	-4.1212	1.7667	0.1665	-0.01918
43	$\overset{O}{\underset{\parallel}{-C}}-0$ (ring)	-	-	-	-
44	$\overset{O}{\underset{\parallel}{-C}}-OH$ (ring)	-	-	-	-
45	$\overset{H}{\underset{\mid}{-C}}=0$ (aromatic)	5.7743	0.7606	0.044	-0.005244
46	$-\overset{\mid}{N}-$	-3.4677	2.9433	-0.2673	0.007828
47	$-\overset{\mid}{N}H$	-1.2530	2.1932	-0.1604	0.004237
48	$-NH2$	4.1783	0.7378	0.0679	-0.00731
49	$=\overset{\mid}{N}$	-	-	-	-
50	$=NH$	-	-	-	-
51	$\equiv N$	-	-	-	-

Table 2a. (Continued)

No.	Group	a	bx10^2	cx10^4	dx10^6
52	-N- (ring)	-3.4677	2.9433	-0.2673	0.007828
53	-NH (ring)	-1.2530	2.1932	-0.1604	0.004237
54	-NH2 (ring)	4.1783	0.7378	0.0679	-0.00731
55	-NH2 (aromatic)	-1.0027	4.1606	-0.5026	0.02143
56	=NH (aromatic)	-	-	-	-
57	≡N (aromatic)	-	-	-	-
58	N⟨S	2.4458	0.3436	0.0171	-0.00272
59	-N=O	7.009	-0.0224	0.2328	-0.001
60	-NO2	1.0898	2.6401	-0.1871	0.004750
61	-N≡C	5.186	0.3492	0.0259	-0.00244
62	N≡C-	4.5104	0.5461	0.0269	-0.00379
63	-S-	4.2256	0.1127	-0.0026	-0.00007
64	-SH	2.5597	1.3347	-0.1189	0.003820
65	=S	-	-	-	-
66	-SO	-	-	-	-
67	-SO2	-	-	-	-
68	-SO3H	6.9218	2.4735	0.1776	-0.02245

Table 2a. (Continued)

No.	Group	a	$b \times 10^2$	$c \times 10^4$	$d \times 10^6$
69	-S- (ring)	4.2256	0.1127	-0.0026	-0.00007
70	-SO (ring)	-	-	-	-
71	-SO2 (ring)	-	-	-	-
72	S	4.0824	-0.0301	0.0731	-0.00708
73	-F	1.9382	0.3452	-0.0106	-0.001128
74	-Cℓ	3.5035	0.2122	-0.02355	0.000276
75	-Br	2.9605	0.4731	-0.0455	0.001420
76	-I	3.2651	0.4901	-0.0539	0.001782
77	-Si-	4.6977	0.5272	0.001945	0.0013
78	-B-	2.2716	0.000	0.000	0.000
79	CiS	1.4705	0.5614	-0.0431	0.001144
80	trans	1.4776	-0.2542	0.0179	-0.00044
81	ortho (1,2)	4.602	-0.7372	-0.3058	-0.001548
82	meta (1,3)	0.422	0.0628	-0.3784	0.000722
83	para (1,4)	0.000	0.000	0.000	0.000
84	1,2,3 position	-	-	-	-
85	1,2,4 position	-	-	-	-

Table 2a. (Continued)

No.	Group	a	$b \times 10^2$	$c \times 10^4$	$d \times 10^6$
86	1,2,5 position	-	-	-	-
87	1,3,5 position	-	-	-	-
*88	side-chain with 2 or more C atoms	-	-	-	-
*89	3 adjacent -CH2 groups	-	-	-	-
*90	-C- adjacent to -CH	-	-	-	-
91	2 adjacent -C- groups	-	-	-	-
**92	single branching	-	-	-	-
**93	double branching (1,1)	-	-	-	-
**94	cis (1,2)	-	-	-	-
**95	trans (1,2)	-	-	-	-
**96	cis (1,3)	-	-	-	-
**97	trans (1,3)	-	-	-	-
**98	cis (1,4)	-	-	-	-
**99	trans (1,4)	-	-	-	-
***100	single branching	-	-	-	-
***101	double branching (1,1)	-	-	-	-
***102	cis (1,2)	-	-	-	-

Table 2a. (Continued)

No.	Group	a	$b \times 10^2$	$c \times 10^4$	$d \times 10^6$
[***]103	trans (1,2)	-	-	-	-
[***]104	cis (1,3)	-	-	-	-
[***]105	trans (1,3)	-	-	-	-
[****]106	double branching (1,2)	-	-	-	-
[****]107	double branching (1,3)	-	-	-	-
[****]108	double branching (1,4)	-	-	-	-
[****]109	triple branching (1,2,3)	-	-	-	-
[****]110	triple branching (1,2,4)	-	-	-	-
[****]111	triple branching (1,3,5)	-	-	-	-
[*****]112	C3 cycloparaffin ring	- 3.532	-0.03	0.0747	-0.00551
[*****]113	C4 cycloparaffin ring	- 4.505	1.078	0.0425	-0.0255
[*****]114	C5 cycloparaffin ring	-12.285	1.8609	-0.1037	0.002145
[*****]115	C6 cycloparaffin ring	-13.88	1.7818	-0.0345	0.000591
[*****]116	pentene ring	-10.9923	1.4892	-0.0429	-0.00187
[*****]117	hexene ring	- 8.0233	2.2239	-0.1915	0.005473
* ** *** **** *****	branching in paraffin chains branching in six-membered rings (cycloparaffins) branching in five-membered rings (cycloparaffins) branching in aromatic ring correction				

Table 2b. Comparison between Experimental and Predicted Values of Gas Heat Capacity

No.	Structure and Name	Temperature, °K	Experiment, cal/gmole, °K	Prediction, cal/gmole, °K	Deviation, %
1	CH_4 methane	300 800	8.54 13.88	8.55 13.88	0.12 0.0
2	C_2H_6 ethane	298 800	12.65 25.8	12.55 25.8	-1.0 0
3	C_3H_8 propane	298.15 1000	17.57 41.83	17.64 41.93	0.38 0.24
4	C_7H_{16} n-heptane	298.15 1000	39.67 91.2	37.95 92.27	-4.34 1.17
5	C_7H_{16} 2,2,3-trimethyl butane	298.15 1000	39.33 92.32	39.75 93.03	1.06 0.76
6	C_2H_4 ethylene	298.15 700	10.41 18.76	10.40 18.74	-0.1 -0.11
7	C_4H_8 1-butene	298.15 700	20.47 38.71	20.34 38.93	-0.62 0.57
8	C_4H_8 trans-2-butene	298 800	20.99 41.50	20.99 41.50	0 0
9	C_6H_{12} 3,3-dimethyl-1-butene	298 800	30.23 63.60	31.85 65.79	5.36 3.44
10	C_4H_6 1,2-butadiene	298.15 1000	19.01 40.52	18.07 39.61	-4.94 -2.25
11	C_5H_8 2-methyl-1,3-butadiene	298 800	25.0 48.0	24.14 47.29	-3.44 -1.48
12	C_2H_2 acetylene	273.15 700	10.53 14.37	10.29 14.45	-2.28 0.56
13	C_3H_4 methylacetylene	298.15 1000	14.50 27.71	14.75 27.57	-1.74 -0.49
14	C_5H_8 2-pentyne	298 800	23.59 45.90	23.95 46.39	1.53 1.07

Table 2b. (Continued)

No.	Structure and Name	Temperature, °K	Experiment, $\frac{cal}{gmole, °K}$	Prediction, $\frac{cal}{gmole, °K}$	Deviation, %
15	C_5H_{10} cyclopentane	700 1000	47.81 59.80	48.26 60.02	0.95 0.37
16	C_6H_{12} cyclohexane	300 800	25.6 66.8	25.95 6t.39	1.37 -2.11
17	C_6H_{12} methylcyclopentane	750 1100	60.87 75.80	61.87 76.00	1.64 0.27
18	C_5H_8 cyclopentene	300 800	18.0 45.8	18.05 46.03	0.28 0.50
19	C_7H_{14} cis-1,3-dimethylcyclopentane	298 800	32.14 75.84	33.26 73.47	3.48 -3.13
20	C_6H_6 benzene	400 800	27.18 44.92	26.52 44.99	-2.43 0.16
21	C_8H_{10} $C_6H_5C_2H_5$	300 700	30.87 61.77	30.45 61.74	-1.36 -0.05
22	C_8H_{10} o-xylene	300 800	31.89 74.35	30.95 73.91	-2.94 -0.60
23	C_8H_{10} m-xylene	300 800	30.44 61.44	29.97 61.16	-1.57 0.46
24	C_8H_{10} p-xylene	300 800	30.48 66.22	30.19 66.29	-0.95 0.11
25	C_9H_{12} p-ethyltoluene	298 800	36.22 77.60	35.06 77.70	-3.2 0.13
26	$C_{11}H_{10}$ 2-methylnaphthalene	298 800	38.19 82.03	37.24 81.58	-2.49 -0.55
27	CH_3CH methanol	300 800	10.5 19.0	10.78 18.74	2.67 1.37
28	C_3H_7OH iso-propyl alcohol	500	24.9	24.39	-2.07

Table 2b. (Continued)

No.	Structure and Name	Temperature, °K	Experiment, $\frac{cal}{gmole, °K}$	Prediction, $\frac{cal}{gmole, °K}$	Deviation, %
29	C_3H_7OH iso-propyl alcohol	— 350	— 26.6	— 26.05	— -2.08
30	C_7H_8 toluene	400 800	33.76 55.55	33.13 55.64	-1.87 0.16
31	C_4H_9OH 2-butanol	298 800	27.08 52.68	28.43 54.33	4.55 3.13
32	$C_6H_4(CH_3)(OH)$ p-cresol	298 800	29.75 61.11	30.74 61.29	1.65 0.29
33	CH_3OCH_3 dimethyl ether	300 —	15.8 —	15.78 —	0.13 —
34	$C_3H_7OC_3H_7$ isopropyl ether	298 800	37.83 74.39	37.0 75.89	-2.19 2.01
35	CH_3COCH_3 acetone	300 800	18.0 34.9	18.50 35.23	2.76 0.94
36	$CH_3COC_2H_5$ methyl ethyl ketone	298 800	24.59 46.08	23.48 46.64	-4.51 1.22
37	CH_3CHO acetaldehyde	300 800	13.20 24.20	13.02 24.32	-1.38 0.5
38	$CH_3COOC_2H_5$ ethyl acetate	400 500	29.70 35.30	30.19 35.68	1.66 1.07
39	CH_3CN acetonitrile	300 800	12.5 21.3	12.59 21.55	0.72 1.17
40	C_2N_2 cyanogen	400 700	13.6 16.9	13.77 16.70	1.22 -1.20
41	$(CH_3)_3N$ trimethylamine	298 800	21.93 45.62	21.97 45.66	0.18 0.09
42	C_2H_5CN propionitrile	298 800	17.46 32.14	17.63 32.96	1.0 2.55

Table 2b. (Continued)

No.	Structure and Name	Temperature, °K	Experiment, cal / gmole, °K	Prediction, cal / gmole, °K	Deviation, %
43	$C_4H_9NO_2$ 2-nitrobutane	298 300	29.51 59.44	29.42 59.75	-0.3 0.52
44	CH_3Cl methyl chloride	300 800	9.7 17.0	10.25 16.73	5.62 -1.58
45	CH_2Cl_2 methylene chloride	300 800	13.3 19.1	13.0 19.08	5.80 0.1
46	$CHCl_3$ Chloroform	300 700	15.6 21.2	16.21 21.39	3.91 0.89
47	CCl_4 carbon tetrachloride	300 800	19.9 24.6	19.83 24.68	0.35 0.33
48	CCl_2F_2 dichlorodifluoromethane	300 800	17.3 24.4	17.65 23.90	2.02 -2.07
49	CH_3I methyl iodide	300 800	10.6 17.5	10.61 17.54	0.07 0.24
50	$C_2H_4F_2$ 1,1-difluoroethane	298 800	16.24 29.69	16.33 29.66	0.55 -0.1
51	C_4F_8 octafluorocyclobutane	298 800	37.32 58.65	37.31 58.69	0.027 0.07
52	C_6H_5Br bromobenzene	298 800	23.35 47.78	22.42 47.31	-3.98 -0.98
53	C_2HCl_3 trichloroethylene	298 800	19.17 26.94	18.24 26.45	-4.85 -1.82
54	C_2H_5SH ethyl mercaptan	300 1000	17.6 35.2	17.02 35.09	-3.29 -0.3
55	C_4H_3SH thiophene	298 1000	17.3 27.2	17.07 26.01	-1.33 -4.4
56	$C_4H_9SCH_3$ butyl methyl sulfide	298 800	33.64 66.53	32.32 64.93	-3.92 -2.40

Table 2b. (Continued)

No.	Structure and Name	Temperature, °K	Experiment, $\frac{cal}{gmole, °K}$	Prediction, $\frac{cal}{gmole, °K}$	Deviation, %
57	CH_3Br methyl bromide	300	10.2	10.32	1.18
		800	17.3	17.45	0.87
58	CH_3NC	300	12.8	12.71	-0.7
		800	21.3	21.3	0
59	CH_3COOH acetic acid	300	16.0	16.0	0
		800	29.1	29.16	0.22
60	$(CH_3)_3N$ trimethyl amine	300	22.1	22.1	0
		800	45.6	45.7	0.2
61	$SiCl_4$	300	21.7	22.07	1.70
		800	25.1	25.07	-0.21

CHAPTER VI

SUMMARY AND CONCLUSIONS WITH RECOMMENDATIONS FOR FUTURE WORK

6.1 Summary and Conclusions

This research project was specifically concerned with the design, con-
struction and performance testing of a special-purpose prototype heat exchange
device referred to as a fluid-to-fluid heat-meter. The heat-meter prototype
consists of a thermally semi-conductive plate, sandwiched between two aluminum
slabs in which flow channels were machined for fluid circulation. Its function
is to provide a calibrated measure of the heat flow between the fluids indi-
cated by the output of a thermopile measuring the temperature difference across
the semi-conductive plate.

In the preliminary design of the heat-meter prototype, heat-transfer
equations were developed to describe the relationship between the coolant
flow rates, coolant temperatures, slab temperatures, dimensions of the flow
channels, thermal conductivity and dimensions of the semi-conductive plate
and the heat-meter heat transfer rate. Using the heat transfer analysis,
along with estimates of the pressure drop in the flow channels, the dimensions
and the configuration of the flow channels were determined. A conductive
sheet analog simulation was used to design the thickness of the heat-meter
slabs such that the temperature distribution over the surface of the slabs
in contact with the semi-conductive plate would be approximately uniform.

Based on the results of the preliminary design, two identical slabs
for the heat-meter prototype were constructed. Each slab included a thermo-
pile section for measurement of the temperature difference across the heat-
meter semi-conductive plate.

71

After completing the construction of the heat-meter prototype it was first tested to determine the feasibility of the heat-meter concept by circulating hot and cold tap water in the heat-meter slabs. Results of the preliminary testing of the heat-meter without insulation were plotted as power versus heat-meter thermopile output. Although there was considerable scatter in the data, it indicated that the heat-meter was working satisfactorily. However, a large disagreement existed between the estimated values of the heat loss from the hot fluid and heat gain by the cold fluid. This suggested that heat loss from the heat-meter was significant. The simple addition of a layer of polystyrene foam insulation to the heat-meter seemed to reduce the effects of heat loss to a negligible level.

During the preliminary testing of the heat-meter, measurement problems were encountered due to instability in the supply tap water temperatures and flow rates. Therefore, an additional test facility consisting of a calorimeter box and a connecting tunnel was constructed to control and accurately measure the heat input to the hot fluid circuit. The heat loss from the calorimeter box and the connecting tunnel were taken into account. For accurate measurements of fluid flow rates which were used for an energy balance on each fluid, turbine flow meters were calibrated and used in the hot and cold fluid circuits.

A series of calibration tests were conducted to determine repeatibility, accuracy and the effect of flow rate and mean temperature on heat-meter performance. Plotting a calibration curve as power transferred versus heat-meter thermopile output for the basic calibration tests indicated very little scatter in data, in comparison with preliminary test results. The initial phase of tests showed that the heat-meter was repeatable to well within $\pm\frac{1}{2}\%$ of the power transferred, in the tested power range of 89W-450W.

The basic calibration test results also indicated that, for a given heat-meter output, there was disagreement between the calculated values of the net power input to the hot water, the heat transfer from the hot water and the cold water heat gain. The trend of the disagreement indicated the possibility of either heat loss from the heat-meter or a measurement error. Calculating the thermal conductivity of the heat-meter semi-conductive plate from the test results yielded a value within about 5% of the nominal thermal conductivity as specified by the manufacturers. This close agreement of the calculated value of the thermal conductivity with its nominal value suggested that the heat loss from the heat-meter was probably not entirely responsible for the disagreement mentioned above. This left instrument error associated with measurement of either the hot and cold fluid temperature change or the fluid flow rates as the most probable sources of the differences in calculation of the power transfer. Crudely insulating the thermopiles measuring the hot and cold fluid temperature changes improved the agreement somewhat, suggesting that the heat exchange between the thermopiles and the air surrounding them affected the temperature difference measurements.

Based on a heat transfer analysis of the heat-meter, a heat-meter sensitivity curve was plotted as net power input to the hot fluid divided by heat-meter thermopile output versus heat-meter mean temperature. Plotting of the sensitivity curve on this expanded scale, indicated that the heat-meter sensitivity was decreasing with increasing mean temperature.

A test was conducted to check the repeatibility of the heat-meter with respect to mean temperature. Analyzing the results of the test indicated that there was some heat loss from the heat-meter hot side and that it was apparently affecting the sensitivity of the heat-meter.

A heat-meter flow rate test was conducted to determine the effect of

decreasing the heat-meter coolants flow rate on its performance. The test results showed that, within the accuracy of the measurements, the data fell on the same sensitivity calibration curve; thus indicating that the performance of the heat-meter was not significantly affected by the fluid flow rates for the limited range of flow rates tested. It should be mentioned that accurate testing of the heat-meter over a wide range of flow rates was not possible due to instrumentation limitations and that the flow rate test of the heat-meter represented the effect of only a 30% decrease in the fluid flow rates.

6.2 Recommendation for Future Study

The heat-meter mean temperature testing indicated that the sensitivity of the heat-meter was being affected by the heat loss from the heat-meter. Therefore, for further studying the heat-meter repeatibility with respect to mean temperature, it is recommended that the prototype device be thermally guarded. The turbine flow meters measuring the fluid flow rates and the thermopiles measuring the fluids temperature change represent potential sources of the observed measurement errors. The thermopiles appear to be the most likely source of error and should be given further investigation. During the heat-meter calibration testing, the drift in the frequency output of the turbine flow meters was thought to be due to an actual change in the fluid flow rate. Therefore, checking the globe flow control valves as the potential sources of the problem is recommended. Finally, since the flow rate testing of the heat-meter was limited to only a small decrease in the fluid flow rates, therefore further investigation of the effect of the fluid flow rates on the heat-meter performance is recommended.

BIBLIOGRAPHY

1. "Method of Testing for Rating Room Air Conditioners", ASHRAE Standard 16-69.

2. "Standard Test Method for Steady-State Thermal Transmission Properties by Means of the Heat Flow Meter", ASTM C518-76.

3. "Standard Test Method for Steady-State Thermal Performance of Building Assemblies by Means of a Guarded Hot Box", ASTM C236-80.

4. THERMONETICS Corporation, Brochure on Heat Flux Transducers and Applications.

5. Karlekar, B. V. and R. M. Desmond, *Engineering Heat Transfer*, 2nd Edition, West Publishing Co., 1978, pp. 393-395.

6. Fox, R. W. and A. T. McDonald, *Introduction to Fluid Mechanics*, 2nd Edition, John Wiley & Sons, 1978, pp. 361-376.

7. Kelley, S. M., *Temperature Distribution in a Heat Sink*, Mechanical Engineering Lab I Report, Dept. of Mech. Engg., KANSAS STATE UNIVERSITY, 1981.

8. "Handbook of Chemistry and Physics", 62nd Edition, CRC Press, 1982.

9. Holman, J. P., *Heat Transfer*, 5th Edition, McGraw-Hill Book Company, New York, 1981, pp. 66-72.

APPENDIX A

PUMP SELECTION FOR HEAT-METER PROTOTYPE

Two separate pumps were needed to circulate the primary hot fluid and the secondary cold fluid in the heat-meter. In calibration of the heat-meter, for accurate measurements of the power input to the hot fluid circuit, the pump, intended for hot fluid circulation, had to operate on a power smaller than the externally controlled power input to the heating element in the hot fluid circuit. Both pumps were intended to circulate fluid in the heat-meter at the rate of about 1.5 GPM. In the absence of external piping, the minimum pumping requirements could only be specified after the flow characteristics of the heat-meter were determined.

A.1 Test Setup

A schematic diagram of the test setup, consisting of a pressure transducer, flow control valve, flow meter pump, and a typical heat-meter slab, whose pressure drop versus flow characteristics were to be determined, is shown in Figure A.1. A schematic diagram of a similar setup to determine the flow characteristics of a typical test pump is shown in Figure A.2.

A.2 Test Procedure

Tap water from the sink was pumped through the hot fluid slab of the heat-meter, through the flow meter and then back to the sink as shown in Figure A.1. A differential pressure transducer of 5 psi range manufactured by "Pace" was used to measure the pressure drop across the plate. The trans-

76
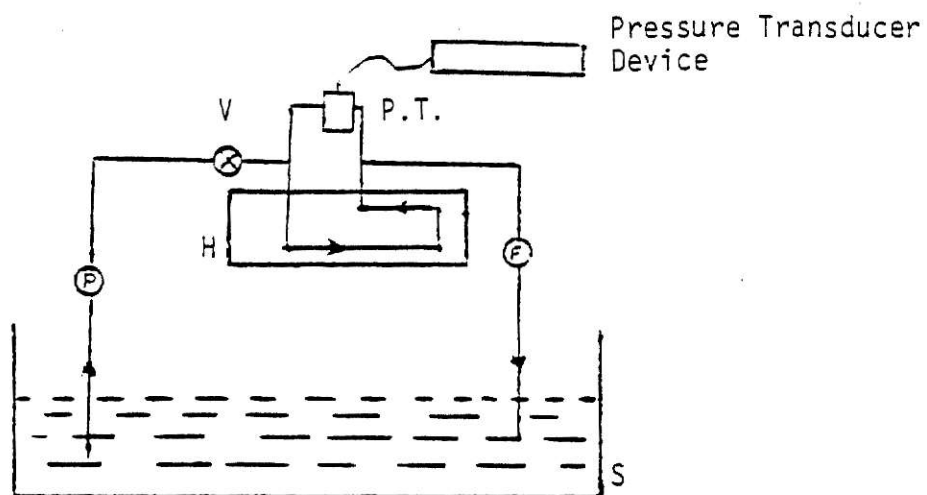
Figure A.1 - Test set up to determine the flow characteristics of the
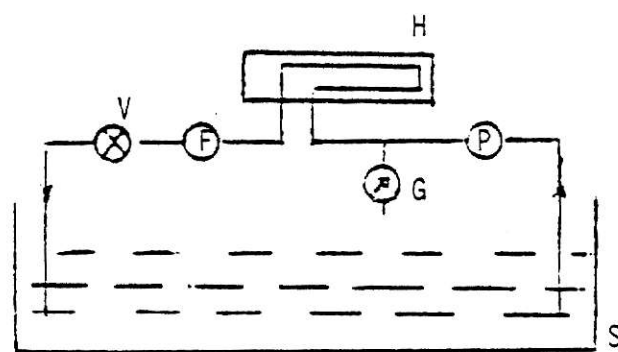
heat-meter

Figure A.2 - Test set up to determine the flow characteristics of the pumps

Legend:

F   Flow-meter

G   Pressure gauge

H   Heat-meter slab

P   Pump

P.T. Pressure transducer

S   Sink

V   Flow control valve

ducer was connected to the inlet and outlet ports of the heat-meter plate, through two identical 1/4 inch brass elbows and two 2 inch long 1/4 inch brass nipples. For different settings of the flow control valve, readings of the flow meter and the output of the pressure transducer were recorded. Following the same procedure, the heat-meter cold fluid slab was tested. Table A.1 lists the data taken for both slabs. Flow characteristic curves plotted as pressure drop versus volume flow rate for both slabs are shown in Figure A.3.

After determining the flow characteristics of the heat-meter slabs, two pumps of similar size and available from the mechanical engineering shop were tested using the setup shown in Figure A.2. The two pumps selected were a submersible Little Giant Pump model 2E-N and a Teel Magnetic Drive Pump model 1P876. Both pumps required power inputs of about 80 watts, and were able to pump water up to several gallons per minute through the heat-meter slabs. In the final design, the submersible pump, because of its lower power (75 watts) and the fact that it would be cooled by the fluid being circulated through it, was selected to be used in the hot fluid circulation.

Hot Fluid Slab		Cold Fluid Slab	
$\dot{V}$, GPM	ΔP, psi	$\dot{V}$, GPM	ΔP, psi
4.6	3.6	4.6	3.4
4.0	2.8	4.4	3.0
3.6	2.3	4.2	2.8
3.4	2.0	4.0	2.5
3.0	1.6	3.8	2.4
2.6	1.2	3.6	2.1
2.0	.80	3.2	1.7
1.6	.50	2.0	.80
1.0	.20	1.0	.30

Table A.1 - Summary of the data to determine
the flow characteristics of the
prototype heat-meter of dimensions
indicated in Table 2.1.
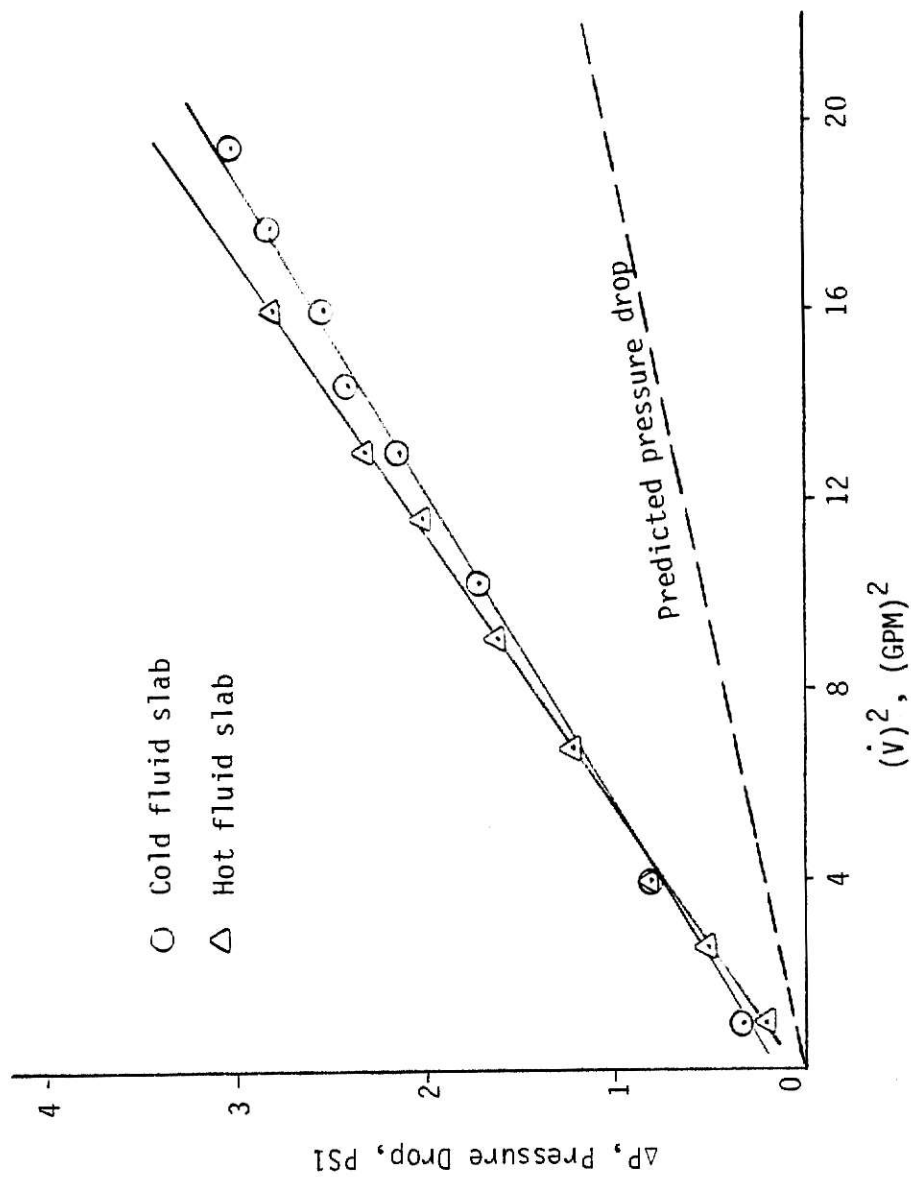
Figure A.3 – Flow characteristic curves of the heat-meter slabs

APPENDIX B

CALIBRATION OF THE TURBINE FLOW-METERS

Turbine flow-meters used in measuring the flow rate of the water cir-
culated in the heat-meter, were calibrated by a simple volume collection
method which consisted of collecting water for known periods of time and
measuring the frequency output, F, of the turbine flow-meter.

Since the flow-meters would be used to measure the flow rates of water
at different temperatures, it was therefore necessary to account for the
effect of viscosity change due to temperature change. The results of the
turbine flow-meter calibration were plotted as a universal curve. Such a
curve consists of a plot of K-factor, the frequency output of the flow meter
divided by the volume flow rate versus the frequency output divided by the
kinematic viscosity.

B.1 Test Setup

The fluid circuit, consisting of a submersible pump, a globe flow con-
trol valve and the turbine flow-meter, is shown in Figure B.1. Table B.1
indicates the name and the model number of the instruments used to make
measurements of time, mass, frequency and temperature.

B.2 Test Procedure

In order to have a constant head at the pump inlet, tap water was pumped
out of a bucket overflowing with water. The frequency counter was set to
indicate the output of the flow-meter every 10 seconds. A small capacitor
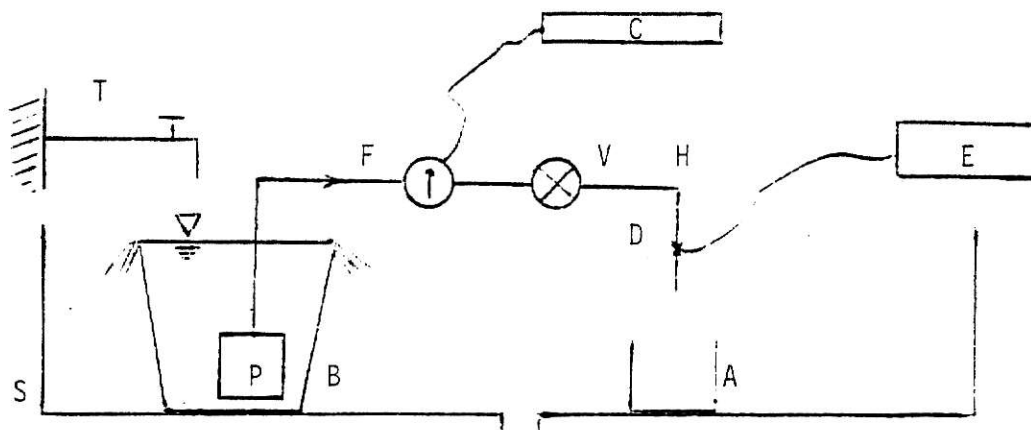
Figure B.1 - Schematic diagram of the apparatus set up for calibration
of the turbine flow-meter.

Legend:

A   1000 ml, beaker

B   Bucket constantly filled with water

C   Frequency counter

D   Location of the thermocouple junction

E   Digital thermocouple thermometer

F   Turbine flow-meter

H $\frac{1}{2}$ inch rubber hose

P   Submersible pump

S   Sink

T   Water tap

V   Flow control valve

was used to filter out background noise from the turbine flow-meter signal. A copper-constantan thermocouple inserted into the outlet flow stream was used to measure the water temperature. For every flow control valve setting, six consecutive readings of the frequency counter were recorded. Two readings were recorded prior to mass collection, two readings during mass collection and two after it. Water was collected in a 1000 ml beaker. Measurements of time were made by a digital stop watch. Data was taken for several different valve settings, covering the range of the operation of the flow-meters expected during the heat-meter calibration. Following this same procedure, additional data was taken over a period of several days to examine the repeatibility of the flow-meter calibration. Results of the calibration tests of the flow-meters are plotted as universal viscosity curves and presented in Figure B.2 and B.3.

B.3 Sample Calculation

A sample calculation is shown for test No. 1 to calculate the K-factor and $\overline{F}/\nu$ for turbine flow-meter No. ME-3909. A summary of the results of such calculations are listed in Table B.2 and Table B.3.

At $T=14.3^{O}C$, density and kinematic viscosity of water are as follows:

$$\rho = 999.2 \frac{g}{\ell} \quad \text{and} \quad \nu = 1.161 \text{ ctsk}$$

i) Volumetric Flow Rate

$$\dot{m} = \frac{\text{Mass collected}}{\text{time of collection}} = \frac{955.1g}{21.49S} = 44.44 \frac{g}{S}$$

$$\dot{V}, \text{ volumetric flow rate} = \frac{\dot{m}}{\rho} = \frac{44.44 \text{ g/S}}{999.2 \text{ g/}\ell} = 0.4448 \frac{\ell}{S}$$

ii) Average Frequency

$$\overline{F} = \frac{\sum_{i=1}^{6} fi}{6} = \frac{115.1+115.1+115.3+115.2+115.1+115.2}{6} = 115.2 \text{ Hz}$$
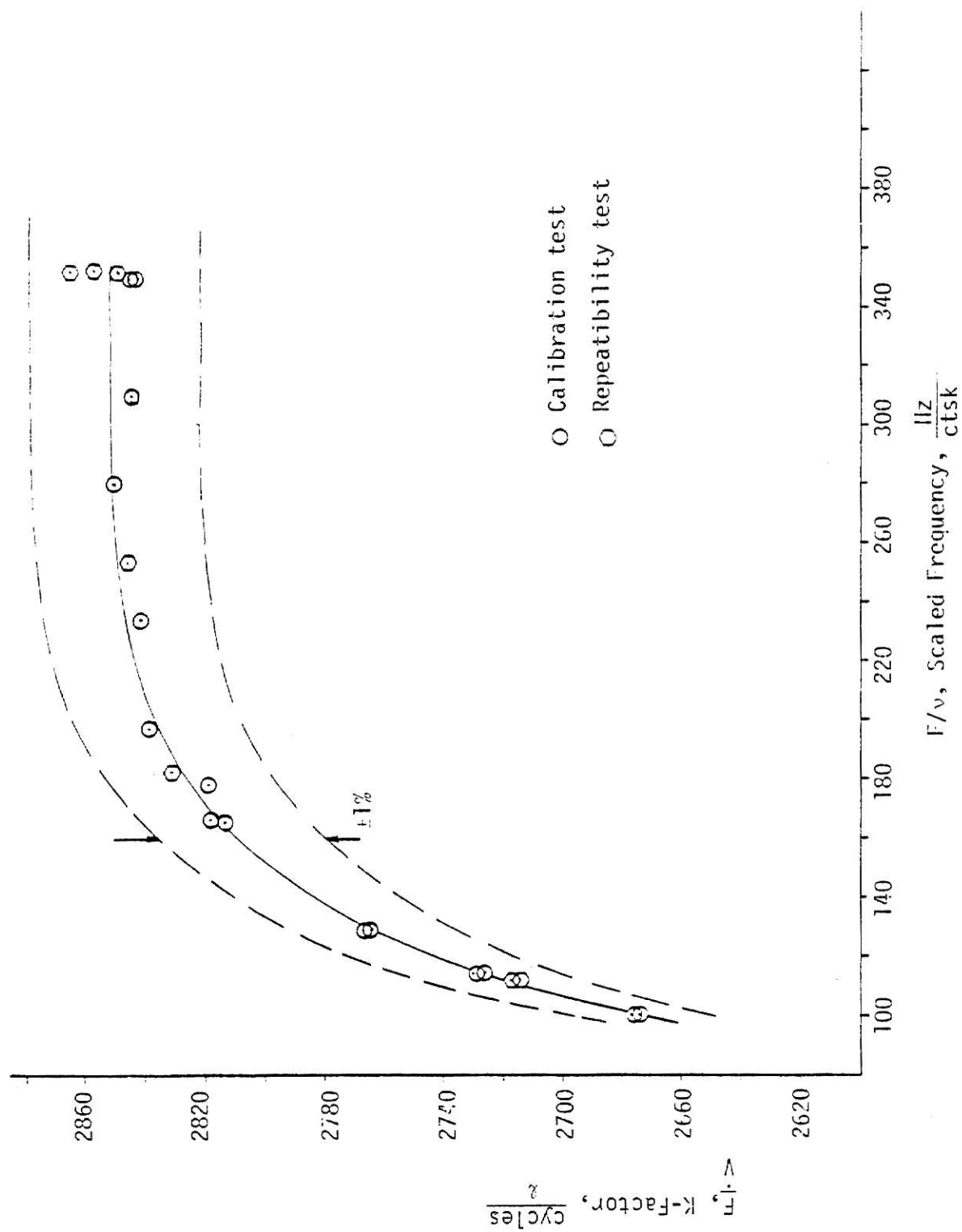
Figure B.2 - Universal viscosity curve for turbine flow meter no. ME-3907
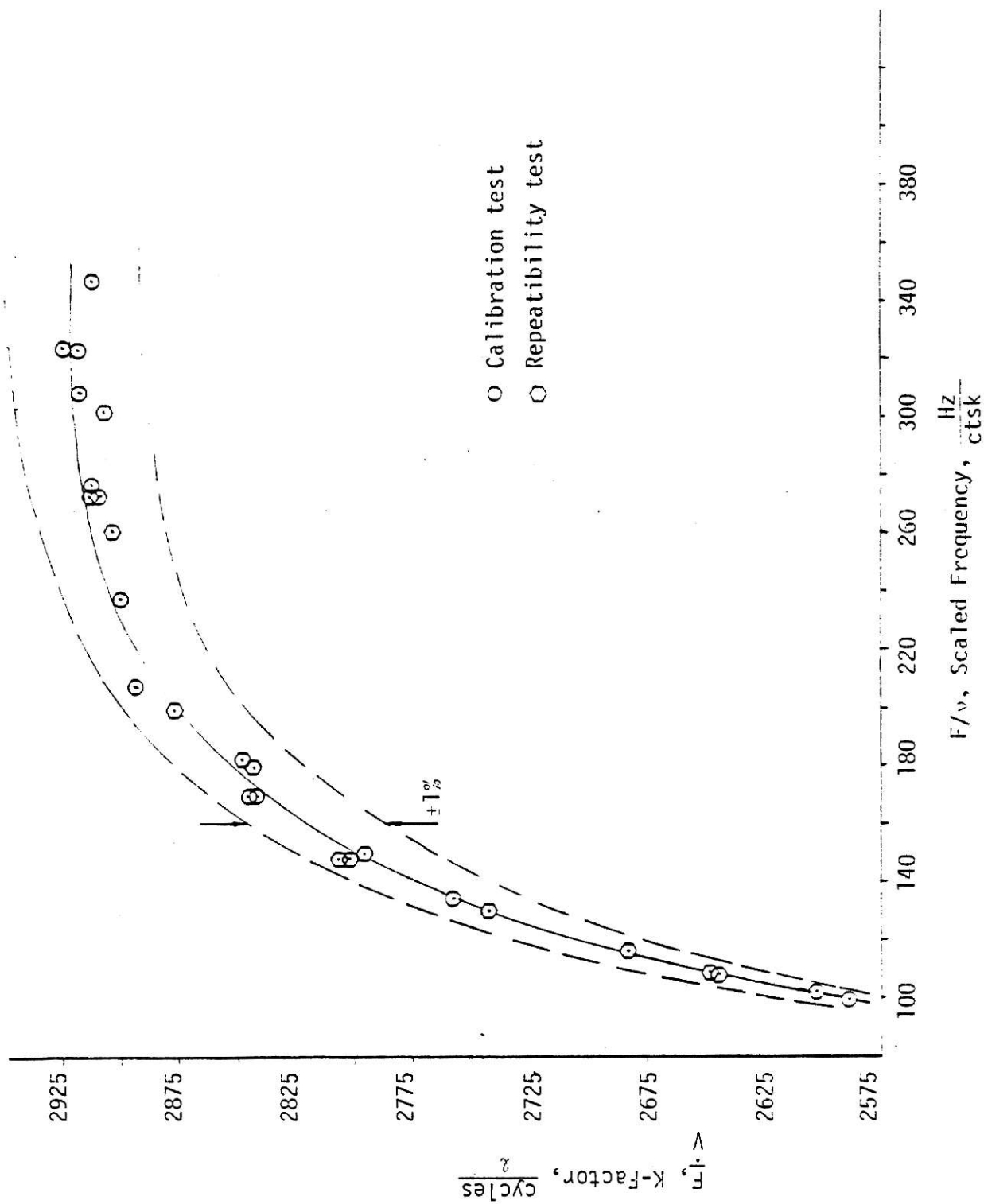
Figure B.3 - Universal viscosity curve for turbine flow meter no. ME-3909

iii) Scaled Frequency

$$\frac{\overline{F}}{\nu} = \frac{115.2 \text{ Hz}}{1.61 \text{ ctsk}} = 99.2 \frac{\text{Hz}}{\text{ctsk}}$$

iv) K-Factor

$$\frac{\overline{F}}{\overset{\cdot}{V}} = \frac{115.2 \text{ Hz}}{0.4448 \text{ } \ell/S} = 2590 \frac{\text{cycles}}{\ell}$$

B.4 Error Analysis

In the following section a sample calculation is shown for estimating the error in the value of the K-factor and the scaled frequency $\overline{F}/\nu$ associated with the universal calibration curve.

B.4.1 Error in Measurement of Mass. Error in measurement of the mass of the water has two components:

i)   Instrument uncertainty

σ = standard deviation = .05g

e_{m1} = limit of error (95% confidence) = 2σ = .1g

ii) Resolution error

e_{m2} = 2 (smallest scale division) = 2(.1g) = .2 g

Since e_{m1} and e_{m2} are two independent components of error, therefore, rms of them is taken to estimate the uncertainty in measuring the mass of the water.

$$e_m = \sqrt{e_{m1}^2 + e_{m2}^2} = \sqrt{(.1)^2 + (.2)^2} = .22g$$

B.4.2 Error in Time Interval Measurement. The uncertainty in measurement of time interval was thought to be due to the way that the fluid stream was directed into and out of the beaker at the beginning and the end of volume collection. To estimate the error, in a series of tests, three sets

of data were taken for two different flow rate settings. In Figure B.4, the relative position of the flow stream with respect to the side of the beaker is shown for the three different tests that were conducted. By assuming the small error in measurement of mass to be negligible, and the flow rate to be constant for each valve setting, the average flow rate for each setting was calculated. Then the maximum deviation of the flow rate from the average flow rate for each valve setting was calculated. The deviation expressed in percent of flow rate reading was multiplied by the corresponding value of the time measurement to get the error in measurement of time. The most likely error in time interval measurement, e_t = .047 sec, was calculated by taking the average of the error in time measurement for the two flow rate settings.

B.4.3 <u>Uncertainty in Frequency Measurement</u>. The standard deviation of the sample for the six measurements of the frequency is calculated as follows

$$S = \sqrt{\frac{\sum_{i=1}^{n} (F_i - \overline{F})^2}{n-1}} \tag{B-1}$$

where n is the number of measurements and $\overline{F}$ is the average frequency and is calculated from the following equation.

$$\overline{F} = \frac{\sum_{i=1}^{n} F_i}{n} \tag{B-2}$$

Therefore the standard deviation of the means would be

$$S_{\overline{F}} = \frac{S}{\sqrt{n}} \tag{B-3}$$

then

$$e_F = 2 S_{\overline{F}} \tag{B-4}$$
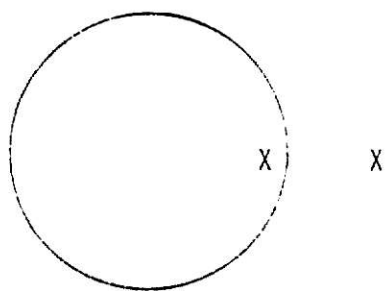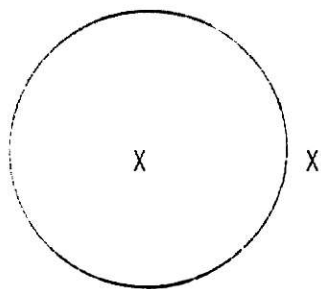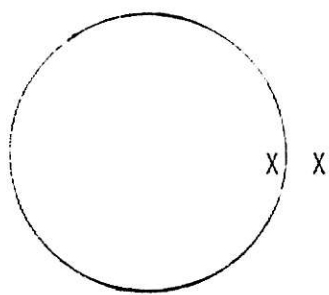
Figure B.4 - Relative position of the flow stream with respect to the
side of the beaker

where e_F is limit of error (95% confidence) in measurement of the frequency.

B.4.4 <u>Uncertainty in Temperature Measurement.</u> Error in measurement of the temperature of the water has two components:

i) Instrument uncertainty as specified by the manufacturer is

$$e_{T1} = \sqrt{(\text{ice point accuracy})^2 + (\text{conformity})^2 + (\text{analog to digital conversion})^2}$$

$$e_{T1} = \sqrt{(.3)^2 + (.5)^2 + (.02\% \text{ of Rdg} + 1 \text{ digit})^2} \quad {}^{\circ}C \qquad (B-5)$$

ii) Thermocouple wire error as specified by the manufacturer of the thermocouple wire used is

$$\lambda_2 = .75\% \text{ of Rdg}$$

Therefore the total error in temperature measurement is

$$\lambda_T = \sqrt{\lambda_1^2 + \lambda_2^2} \quad \% \text{ Rdg} \qquad (B-6)$$

where λ_1 is instrument uncertainty in percent of reading.

B.4.5 <u>Uncertainty in the Value of K-Factor and $\overline{F}/\nu$.</u>

$$\text{K-Factor} = \frac{\overline{F}}{\overline{V}} = \frac{\overline{F} t \rho}{m} \qquad (B-7)$$

where $\overline{F}$ is the average frequency, t is the time, ρ is the density and m is the mass.

Therefore, the uncertainty equation for K-factor could be expressed as

$$\lambda_K = \sqrt{\lambda_F^2 + \lambda_t^2 + \lambda_\rho^2 + \lambda_m^2} \qquad (B-8)$$

and for the scaled frequency

$$\lambda_{\overline{F}/\nu} = \sqrt{\lambda_F^2 + \lambda_\nu^2} \qquad (B-9)$$

where λ_F, λ_t, λ_ρ, λ_m and λ_ν are errors expressed as percents of reading in the values of frequency, time, density, mass and viscosity, respectively.

B.4.6 <u>Sample Calculation</u>. Sample calculation of the error in the value of the K-factor and the scaled frequency, $\overline{F}/\nu$, is performed for test number 1 of the calibration of turbine flow-meter No. ME-3909.

i) Error in measurements of mass

$$\lambda_m = \frac{e_m}{m} (100) = \frac{.22}{955.1} (100) = .023 \text{ % of Rdg} \tag{B-10}$$

ii) Error in measurement of time

$$\lambda_t = \frac{e_t}{t} (100) = \frac{.074}{21.49} (100) = .34 \text{ % of Rdg} \tag{B-11}$$

iii) Error in measurement of frequency

From eq. (B-1), S, the standard deviation of the sample is expressed as

$$S = \sqrt{\frac{\sum_{i=1}^{n} (F_i - \overline{F})^2}{n-1}}$$

Substituting the values for F_i and $\overline{F}$ from section (B-4) yields

$$S = .082 \text{ Hz}$$

Then from equation (B-3), $S_{\overline{F}}$, standard deviation of the means would be

$$S_{\overline{F}} = \frac{S}{\sqrt{n}} = \frac{.082}{\sqrt{6}} = .033 \text{ Hz}$$

Therefore

$$\lambda_F = \frac{2S_{\overline{F}}}{\overline{F}} (100) = \frac{(2)(.033)(100)}{115.2} = .057 \text{ % of Rdg} \tag{B-12}$$

where λ_F is the uncertainty in measurement of the frequency expressed as percent of reading.

iv) Error in measurement of the temperature

$$\lambda_1 = \frac{e_{T1}}{T} (100) \tag{B-13}$$

Substituting for e_{T1} from eq. (B-5) in eq. (B-13) yields

$$\lambda_1 = \frac{\sqrt{(.3)^2 + (.5)^2 + (.103)^2}}{14.3} (100) = 4.14 \text{ % Rdg}$$

But, from equation (B-6)

$$\lambda_2 = .75 \text{ % of Rdg.}$$

Therefore

$$\lambda_T = \sqrt{\lambda_1^2 + \lambda_2^2} = \sqrt{(4.14)^2 + (.75)^2} = 4.20 \text{ % Rdg}$$

where λ_T is limit of error as percent of reading in the value of the temperature.

$$\lambda_T = 4.20 \text{ % Rdg} = .60^o C \qquad (B-14)$$

The error in measurement of the density due to 4.2% error in temperature measurement is .0086% and is negligible compared to .34% error in time measurement.

Therefore, ignoring λ_ρ, the error in viscosity of water due to error in temperature measurement would be

$$e_\nu = (\tfrac{\partial \nu}{\partial T})_p \ e_T \qquad (B-15)$$

where $\frac{\partial \nu}{\partial T}$ is the rate of change of the viscosity with temperature in the temperature range of $10^o C$ to $20^o C$ and ΔT is the error in temperature measurement.

Substituting the values for $\frac{\partial \nu}{\partial T}$ and e_T, eq. (B-15) yields:

$$e_\nu = (.03 \ \frac{ctsk}{^o C}) \ (.6 \text{ deg C}) = .018 \text{ ctsks}$$

then

$$\lambda_\nu = \frac{e_\nu}{\nu} (100) = \frac{(.018)(100)}{1.161} = 1.57 \text{ % Rdg} \qquad (B-16)$$

where λ_ν is the error in the value of the viscosity of water expressed as a percent of reading and ν is the viscosity of water at $14.3^o C$.

From equation (B-8), the error in K-factor is expressed as

$$\lambda_K = \sqrt{\lambda_F^2 + \lambda_t^2 + \lambda_m^2 + \lambda_\rho^2}$$

Substituting into eq. (B-8) for λ_F, λ_t and λ_m from equations (B-12), (B-11) and (B-10) and neglecting λ_ρ yields

$$\lambda_K = \sqrt{(.057)^2 + (.34)^2 + (.023)^2} = .35 \text{ \% Rdg}$$

therefore

$$K = 2589 \frac{\text{cycles}}{\ell} \pm .35\% \left(\pm 9.1 \frac{\text{cycles}}{\ell}\right)$$

Also, from equation (B-9), the error in the scaled frequency is expressed as

$$\lambda_{\overline{F}/\nu} = \sqrt{\lambda_F^2 + \lambda_\nu^2}$$

Substituting into eq. (B-9) for λ_F and λ_ν from equations (B-12) and (B-16) yields

$$\lambda_{\overline{F}/\nu} = \sqrt{(0.57^2 + (1.57)^2} = 1.57 \text{ \% Rdg}$$

therefore

$$\frac{\overline{F}}{\nu} = 99.20 \frac{\text{cycles}}{\text{ctsk}} \pm 1.6\% \left(\pm 1.56 \frac{\text{cycles}}{\text{ctsk}}\right)$$

Following this same procedure, the values for λ_K and $\lambda_{\overline{F}/\nu}$, for calibration tests on the turbine flow-meters were calculated and are tabulated in Tables B.2 and B.3.

Frequency	Electronic Counter Model: 5212A Hewlett Packard
Mass	Sartorrus balance Model: 2250 Weighing range: 0-300 gr
Temperature	Digital Thermocouple Thermometer Model: 590 TC Type: T Range: -190 to 400^0C
Time	Digital Stop-Watch Model: Cronus

Table B.1 - Instruments used in calibration of turbine
          flow-meters

No.	$\dot{V}$	$\overline{F}$	$\overline{F}/\dot{V}$	λ_K	$\overline{F}/\nu$	$\lambda\,\overline{F}/\nu$
	1/min	Hz	C/1	% Rdg	Hz/ctsk	% Rdg
1	2.669	115.2	2589	.35	99.20	1.6
2	3.388	115.8	2758	.43	134.2	1.6
3	4.154	197.0	2845	.54	169.7	1.6
4	5.002	241.2	2894	.63	207.8	1.6
5	5.662	273.7	2900	.72	237.5	1.6
6	6.552	318.2	2913	.80	276.9	1.6
7	4.122	195.3	2842	.51	169.9	1.6
8	2.714	117.8	2603	.41	102.2	1.6
9	7.750	377.0	2919	.95	323.9	1.6
10	7.741	377.4	2925	.97	324.2	1.6
11	3.669	171.6	2806	.51	147.8	1.6
12	3.672	171.5	2802	.57	147.7	1.6
13	3.304	151.0	2743	.43	130.1	1.6
14	2.664	115.1	2592	.32	99.37	1.6
15	2.999	134.1	2683	.46	115.8	1.6
16	4.822	231.2	2877	.61	199.7	1.6
17	6.243	302.1	2904	.72	260.9	1.6
18	6.533	316.8	2910	.82	273.6	1.6
19	6.521	316.6	2913	.83	273.4	1.6
20	7.367	358.4	2919	.94	309.5	1.6
21	7.360	358.3	2920	.90	309.4	1.6
22	8.297	402.8	2913	.99	347.9	1.6
23	8.272	402.7	2921	1.0	347.8	1.6
24	2.824	124.7	2649	.31	109.1	1.6
25	2.824	124.5	2645	.41	108.7	1.6
26	4.415	209.5	2849	.58	182.9	1.6
27	7.141	346.0	2907	.84	301.9	1.6
28	7.122	346.0	2915	.95	301.1	1.6
29	4.377	207.5	2844	.55	180.6	1.6
30	3.703	172.5	2795	.48	150.5	1.6

Table B.2 - Summary of calibration for turbine flow-meter Model
5/8-215B, manufactured by Potter Aero Co. (ME-3909)

No.	$\dot{V}$	$\overline{F}$	$\overline{F}/\dot{V}$	λ_K	$\overline{F}/\nu$	$\lambda\overline{F}/\nu$
	l/min	Hz	C/l	% Rdg	Hz/ctsk	% Rdg
1	2.619	116.8	2676	.33	100.6	1.6
2	2.622	116.9	2674	.36	100.6	1.6
3	2.928	133.1	2728	.44	114.7	1.6
4	2.930	133.1	2727	.36	114.7	1.6
5	3.261	150.3	2766	.44	129.5	1.6
6	3.258	150.3	2768	.38	129.7	1.6
7	3.760	175.3	2798	.45	151.4	1.6
8	4.107	193.0	2819	.54	166.6	1.6
9	4.113	192.8	2813	.49	165.7	1.6
10	4.844	229.2	2839	.62	196.9	1.6
11	5.744	272.0	2842	.69	233.7	1.6
12	6.860	326.0	2851	.91	280.1	1.6
13	7.580	359.4	2845	.96	308.8	1.6
14	8.571	406.4	2845	1.1	349.1	1.6
15	8.567	406.4	2846	1.1	349.2	1.6
16	4.417	207.6	2820	.51	178.3	1.6
17	8.549	406.7	2854	1.1	351.2	1.6
18	8.513	406.7	2867	.98	351.2	1.6
19	8.538	406.8	2859	1.1	352.2	1.6
20	4.431	209.1	2831	.57	182.0	1.6
21	2.842	128.6	2715	.37	111.9	1.6
22	2.840	128.6	2717	.40	111.9	1.6
23	6.146	291.6	2847	.77	253.8	1.6

Table B.3 - Summary of calibration data for turbine flow-meter
Model 5/8-215B manufactured by Potter Aero Co.
(ME-3907)

APPENDIX C

HEAT LOSS CALIBRATION

In the calibration of the heat-meter, it was necessary to accurately account for the heat losses from the calorimeter box and the connecting tunnel. Therefore, heat loss calibration tests were conducted to measure the heat losses from the system at different temperature differences across the walls of it. A calibration curve was then plotted for the heat loss as a function of temperature difference across the walls of the system.

C.1 Estimation of the Heat Losses

Referring to Figures C.1 and C.2 for dimensions of the system, heat losses from the calorimeter box and the connecting tunnel were initially estimated as follows.

C.1.1 Heat Losses From the Calorimeter Box. Accounting for the heat losses from the edges and corners of the box, from reference [9], the total heat loss, $\dot{Q}$, from a cubical box is calculated as follows:

$$\dot{Q} = S_t \, k \, \Delta T \tag{C-1}$$

where ΔT is the temperature difference across the walls of the calorimeter box, k is the thermal conductivity of the box material and S_t is the total shape factor for the cubical box.

The total shape factor is calculated from the following equation:

$$S_T = S_e + S_c + S_w \tag{C-2}$$

where S_e is the shape factor for the edges of the calorimeter box, S_c is
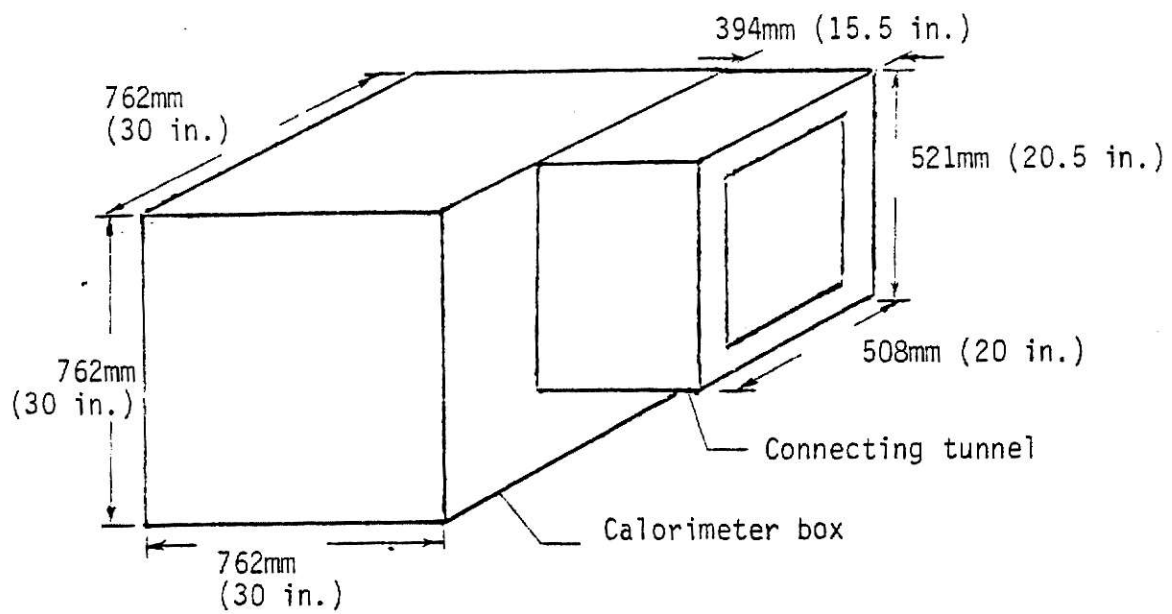
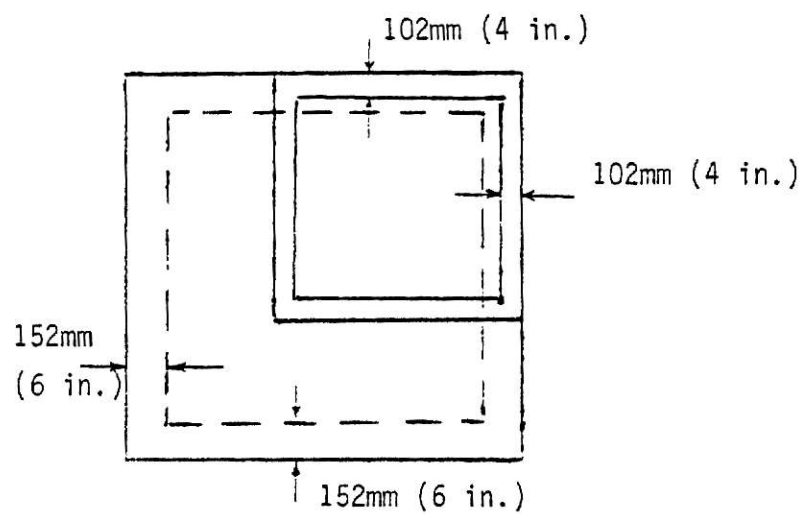Figure C.1 - Three-dimensional view of the calorimeter box and the connecting tunnel

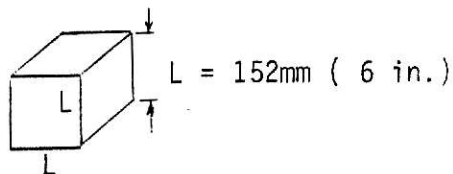Figure C.2 - Side view of the calorimeter box and the connecting tunnel

the shape factor for the corners of the box and S_w is the shape factor for the walls.

The shape factors S_e, S_C and S_w are calculated as follows:

i) Shape factor of the corners

$$S_C = (n)(.15)(L) \qquad (C-3)$$

where n = 8 is the number of corners.

ii) Shape factor of the edges

$$S_e = (m)(.54)(D) \qquad (C-4)$$

where m = 12 is the number of corners.
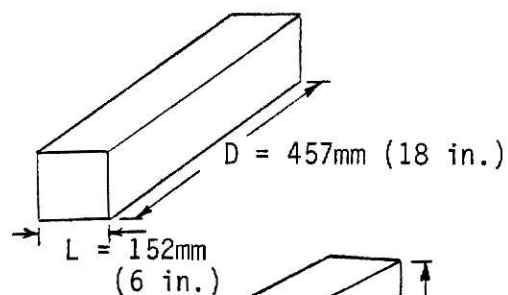
iii) Shape factor of the walls

$$S_w = (n_w)(\frac{A}{L}) \qquad (C-5)$$

where n_w = 6 is the number of the number of walls, A is the area and L is the thickness of the walls.
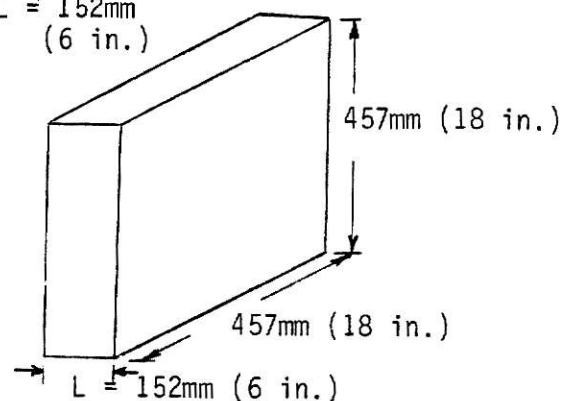
Referring to Figure C.1, for identical temperatures inside the calorimeter box and the connecting tunnel the surface of the calorimeter box in contact with the connecting tunnel would be an adiabatic surface. Therefore accounting for the percent of the surface area of the calorimeter box insulated by the connecting tunnel and using equations (C-1) through (C-5), the heat transfer equation for the calorimeter box can be expressed as follows.

$$\dot{Q}_C = (10.32) \; k \; \Delta T \qquad W \qquad (C-6)$$

where k, the thermal conductivity of the insulating material, is specified to be $0.020 \; \frac{W}{m-^{o}C}$ at a mean temperature of $24^{o}C$ and $0.018 \; \frac{W}{m-^{o}C}$ at a mean temperature of $5^{o}C$.

C.1.2 <u>Heat Loss From the Connecting Tunnel</u>. Accounting for the heat losses from the edges, the heat loss from the connecting tunnel is calculated as follows.

$$\dot{Q}_t = S'_t \ k \ \Delta T \tag{C-7}$$

where S'_t is the total shape factor for the connecting tunnel, k is the thermal conductivity of the connecting tunnel material, and ΔT is the temperature difference across the walls of the tunnel.

$$S'_t = S_e + S_w \tag{C-8}$$

where S_e is the shape factor for the edges and S_w is the shape factor for the walls of the connecting tunnel.

The shape factors S_e and S_w are calculated as follows, [9].

i) Shape factor for the edges

$$S_e = (m)(D)(.54) \tag{C-9}$$

where referring to Figure C.1 for dimensions, m, the number of the edges is 4 and D is equal to 394 mm.

ii) Shape factor for the walls

$$S_w = (n)(\frac{A}{L}) \tag{C-10}$$

where n=4 is the number of the walls, A=1929 (mm)^2 is the area of the connecting tunnel walls and L=102 mm is the wall thickness.

Using equations (C-7) through (C-10), the heat transfer equation for the connecting tunnel can be expressed as follows:

$$\dot{Q}_t = 5.67 \ k \ \Delta T \ \ W \tag{C-11}$$

where k is the same as the previously indicated thermal conductivity for the calorimeter box material.

C.2 Heat Loss Calibration Setup

A schematic diagram of the test setup, consisting of two electrical circuits for power input to the calorimeter box and the connecting tunnel, is shown in Figure C.3.

A dual regulated 0-20 VDC range power supply was used to control the power input to the calorimeter box and the connecting tunnel. Cold tap water mixed with hot water to give the same temperature as the air inside the connecting tunnel, was circulated in the heat-meter using a submersible pump. Water temperature was measured using a 24 gauge copper-constantan thermocouple inserted into the water flow. Two small electrical fans were used to circulate air inside the two chambers. Two thermopiles consisting of 23 and 8 copper-constantan thermocouples, were used to measure the temperature difference across the walls of the calorimeter box and the connecting tunnel, respectively. Thermocouples, used for measurement of temperature difference and absolute temperature, were connected to a millivolt potentivmeter and a thermocouple thermometer through a multiple position selector switch. The thermocouple thermometer was used to make temperature measurments of the air inside the two chambers, the ambient air, the circulating coolant water and the outside surface of the calorimeter box. The millivolt potentiometer was used to measure the voltage output of the thermopiles for determining the temperature difference across the walls of the calorimeter box, the connecting tunnel and the heat-meter insulation, as well as the heat-meter output and the temperature change of the water entering and leaving the heat-meter. The instruments used in the heat loss calibration tests are listed below in Table C.1.
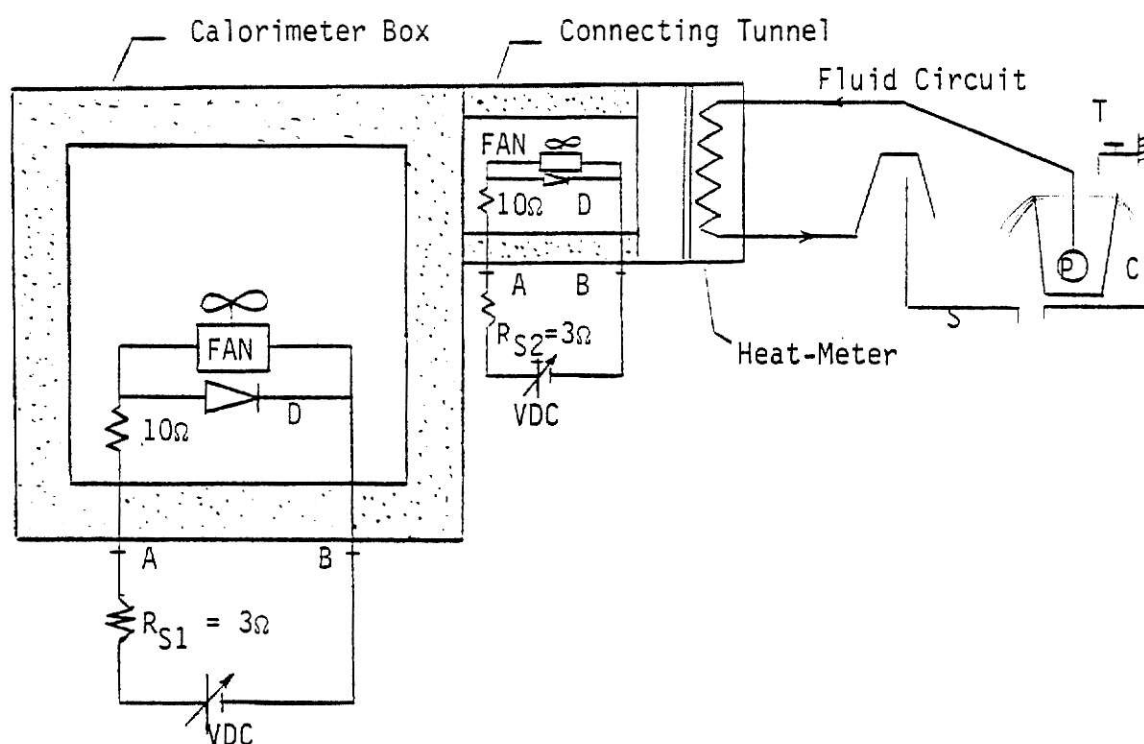
Figure C.3 - Schematic diagram of the apparatus set up for heat loss
calibration test

Legend:

C   Bucket

D   Silicon Diode (voltage regulator)

P   Submersible Pump

R_{S1} Standard Resistor of the calorimeter box $(3.00\Omega\pm.070\%)$

R_{S2} Standard Resistor of the connecting tunnel $(3.00\Omega\pm.019\%)$

VDC   0-20 VDC power supply

V_1 Voltage across points A and B on the calorimeter box circuit

V_2 Voltage across points A and B on the connecting tunnel circuit

V_{S1} Voltage across the standard resistor, R_{S1}

V_{S2} Voltage across the standard resistory, R_{S2}

S   Water sink

T   Water tap

Quantity Measured	
Absolute temperature	Thermocouple thermometer Model: 590 TC Type T Range: -190°C to 400°C
Millivolt output of the thermopiles	Millivolt Potentiometer 8686 Model: Leeds and Northrup Range: -10.1 mv to +100.1 mv
Voltage and Current	Digital Multimeter Model: Fluke 8600 A Range: Multiple range
Voltage supplied	Dual Regulated Power Supply Model: LAMBDA Range: 0-20 VDC

Table C.1 - Instruments used in heat loss calibration test.

C.3 Measurement of the Resistance of the Standard Resistors

Resistance of the standard resistors, used in the calorimeter box circuit and the connecting tunnel circuit for measuring current, were determined by setting up an electrical circuit as shown in Figure C.4.
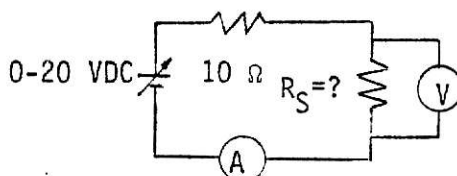
Figure C.4. - A, ammeter, V, voltmeter

For three different settings of the power supply, current through and voltage across the standard resistor were measured. This same procedure was repeated to measure the resistance of the second standard resistor. Tables C.2 and C.3 summarize the data taken, along with the estimated resistances of the two resistors. The estimated resistances were assumed to be constant during the heat loss calibration tests and the effect of temperature change on them was neglected.

Source Voltage	V_{S1}, Volts	I_1, A	$R_{S1} = \dfrac{V_S}{I}$, Ω	$\overline{R}_1$, Ω
5	.969 .967 .964	.323 .322 .321	3.000 3.003 3.003	3.00 ±.070%
10	2.034 2.031	.678	3.000 3.000	
15	3.115 3.124	1.039 1.043	2.998 2.995	

Table C.2 - Summary of the data for measurement of the resistance of the standard resistor number 1.

Source Voltage	V_{S2}, Volts	I_2, A	$R_{S2} = \dfrac{V_{S2}}{I2}$	$\overline{R}_2$, Ω
5	.977	.326	2.997	3.00 ±.019%
10	2.032	.678	2.997	
15	3.122 3.104	1.042 1.036	2.996 2.996	

Table C.3 - Summary of the data for measurement of the resistance of the standard resistor number 2.

C.4 Test Procedure

In calibrating the heat-meter, there was assumed to be essentially no heat transfer across the wall of the tunnel connected to the heat-meter. This assumption was based on the fact that during the testing, the air inside the connecting tunnel and the heat-meter hot side slab would be almost at the same temperature as the hot fluid being circulated in the heat-meter. The calorimeter box and the connecting tunnel were also assumed to be at the same temperature in steady state because of the hot fluid circulation in them. To simulate these conditions in the heat loss calibration test, warm tap water, at the same temperature as the air inside the connecting tunnel, was circulated in the heat-meter to prevent heat transfer from the tunnel to the heat-meter. Power inputs to the electrical heaters were adjusted to get the same steady-state temperatures in the calorimeter box and the connecting tunnel. A summary of the heat loss calibration data, for four different power inputs to the system, is given in Table C.4.

During the testing, it was noticed that for the same temperature inside the calorimeter box and the connecting tunnel, the ratio of the power inputs to them was different by a factor of two from the expected power ratio which was based on the estimates of the heat loss from the system. Uncertainty in the value of the thermal conductivity of the insulating material used in constructing the calorimeter box and the connecting tunnel, and the holes drilled in the walls of them to make various connections, are assumed to be responsible for the different power ratios.

C.4.1 Data Reduction. The total heat loss from the system is calculated as follows:

$$P_{total} = P_c + P_t = (V_1) \left(\frac{V_{s1}}{R_{s1}}\right) + (V_2) \left(\frac{V_{s2}}{R_{s2}}\right), \text{ W} \qquad \text{(C-12)}$$

Run	ΔV_1, mv	ΔV_2, mv	ΔV_3, mv	ΔV_5, mv	ΔV_6, mv	T_1, °C	T_2, °C	T_3, °C	T_4, °C	T_7, °C	V_1, v	V_2, v	V_{S1}, v	V_{S2}, v
1	15.705	4.855	4.855	0.0300	0.270	42.8	42.9	25.4	26.3	43.5	11.85	12.00	2.490	2.495
2	10.515	3.095	2.835	-0.0350	-0.290	36.5	36.2	24.8	25.4	36.6	9.630	9.756	2.006	2.010
3	5.8900	1.720	1.480	-0.0700	-0.590	30.6	30.3	24.5	24.6	30.6	7.189	7.326	1.470	1.479
4	7.4200	2.675	1.990	-0.0900	-0.690	32.3	33.4	24.0	24.4	32.5	8.414	8.518	1.740	1.740

Table C.4. Summary of the heat loss calibration data.

where P_c is the power input to the calorimeter box, P_t is the power input to the connecting tunnel, V_{s1} is the voltage across the calorimeter box standard resistor of resistance R_{s1}, V_{s2} is the voltage across the connecting tunnel standard resistor of resistance R_{s2} and referring to Figure C.3, V_1 and V_2 are voltages across points A,B in the calorimeter box power circuit and the connecting tunnel power circuit, respectively.

The average of the calorimeter box and the connecting tunnel thermopile outputs per thermocouple is calculated as follows:

$$\overline{V} = \frac{\Delta V_1}{2n_1} + \frac{\Delta V_2}{2n_2} = \frac{\Delta V_1}{(2)(23)} + \frac{\Delta V_2}{(2)(8)} , \quad mv \qquad (C-13)$$

where ΔV_1 is the output of the calorimeter box thermopile, ΔV_2 is the output of the connecting tunnel thermopile and n_1 and n_2 are number of the thermocouple junctions in the calorimeter box and the connecting tunnel thermopiles, respectively.

Using equations (C-12) and (C-13), the total heat loss and the average of the calorimeter box and the connecting tunnel thermopile outputs per thermo-couple, were calculated for the heat loss calibration tests and the results are summarized in Table C.5. The heat loss calibration curve plotted as P_{total} versus $\overline{V}$ is shown in Figure C.5.

C.5 Error Analysis

In the following section, to determine the uncertainty in the heat loss calibration curve, plotted as P_{total} versus $\overline{V}$, a sample calculation is shown for heat loss calibration test number one.

C.5.1 Error in the Value of $\overline{V}$. From equation (C-13) $\overline{V}$ is calculated as follows.

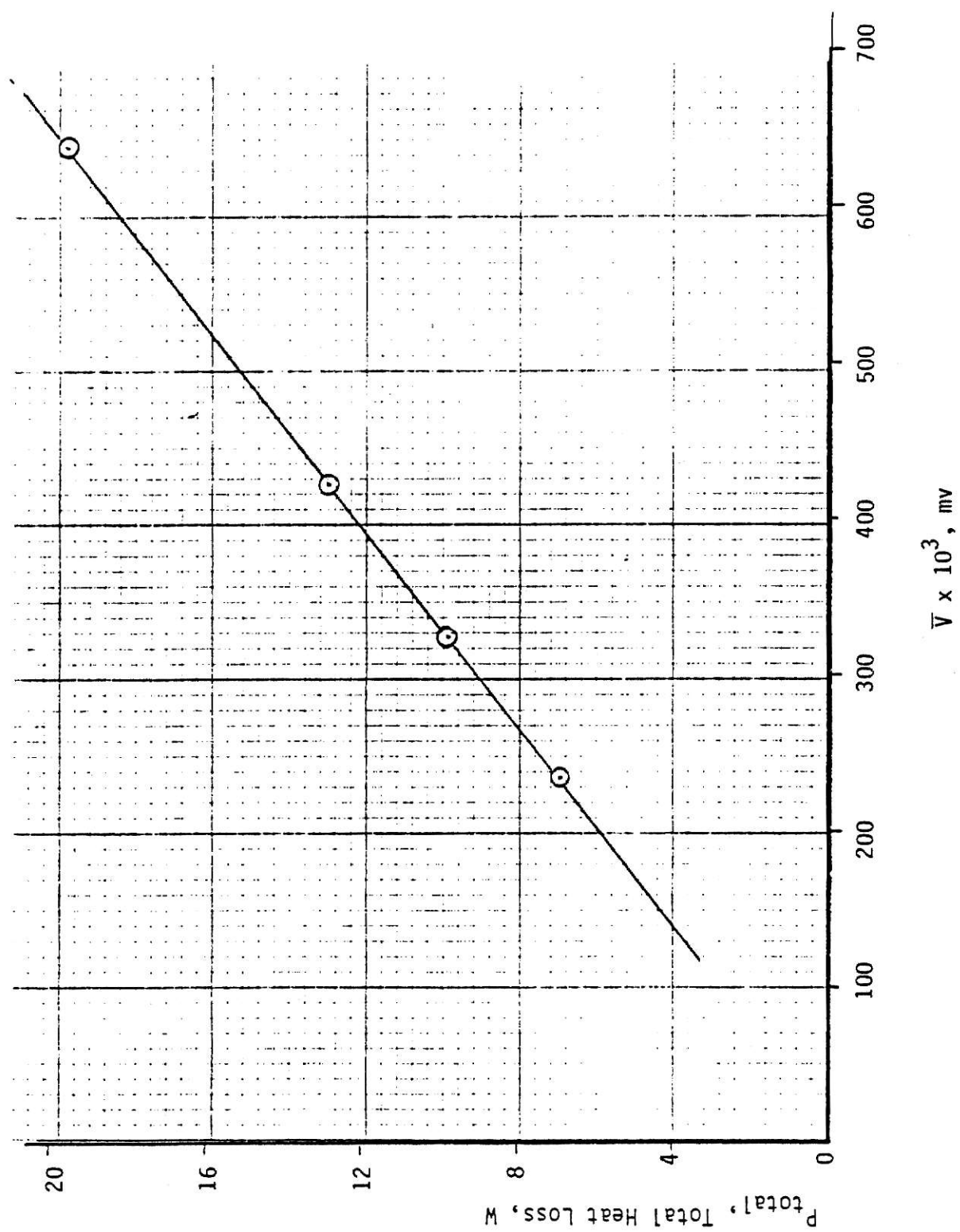$$\overline{V} = \frac{\Delta V_1}{2n_1} + \frac{\Delta V_2}{(2)n_2}$$

Figure C.5 – Heat loss calibration curve

From Table C.6, substituting values in eq. (C-13), yields

$$\overline{V} = \frac{15.71}{46} + \frac{4.855}{16} = .6449 \quad \text{mv}$$

$$e_V = \sqrt{(\frac{e_1}{46})^2 + (\frac{e_2}{16})^2} \tag{C-14}$$

where e_V is the error in $\overline{V}$, e_1 is the uncertainty in measurement of ΔV_1 and e_2 is the uncertainty in measurement of ΔV_2.

Uncertainties in the measurements of ΔV_1 and ΔV_2 have two components.

i) Instrument uncertainty = $\pm(.03\%$ of Rdg + $3\mu v)$

ii) Thermocouple wire error = $\pm.75\%$ of Rdg.

Therefore, e_1 and e_2 are calculated as follows:

$$e_1 = \sqrt{(.03\% \text{ of } \Delta V_1 + 3\mu V)^2 + (.75\% \text{ of } \Delta V_1)^2} \tag{C-15}$$

and

$$e_2 = \sqrt{(.03\% \text{ of } \Delta V_2 + 3\mu V)^2 + (.75\% \text{ of } \Delta V_2)^2} \tag{C-16}$$

Substituting values from Table C.6 in equations (C-15) and (C-16) yields

$$e_1 = \sqrt{(.0003 \times 15.71 + .003)^2 + (.0075 \times 15.71)^2} = .11 \text{ mv}$$

and

$$e_2 = \sqrt{(.0003 \times 4.855 + .003)^2 + (.0075 + 4.855)^2} = .036 \text{ mv}$$

Substituting for e_1 and e_2 in equation (C-14) yields

$$e_V = \sqrt{(\frac{.11}{46})^2 + (\frac{.036}{16})^2} = .0034 \text{ mv}$$

Therefore

$$\overline{V} = .6449 \pm .0034 \text{ mv } (.53\%)$$

C.5.2 <u>Uncertainty in the Resistance of the Standard Resistors.</u> $\overline{R}$, the average resistance is calculated as follows:

$$\overline{R} = \frac{\Sigma_{i=1}^{n} R_i}{n} \tag{C-17}$$

where $n = 6$ is the number of the measurements of the resistance.

S, the standard deviation of the sample is expressed as follows:

$$S = \left[\frac{\Sigma_{i=1}^{n}(R_i-\overline{R})^2}{n-1}\right]^{1/2} \tag{C-18}$$

Therefore the standard deviation of the means can be calculated from the following equation:

$$S_{\overline{R}} = \frac{S}{\sqrt{n}} \tag{C-19}$$

Then, λ_R, the limit of error is calculated using the following equation:

$$\lambda_R = \frac{2S_{\overline{R}}}{\overline{R}} \; (100) \qquad \% \; Rdg \tag{C-20}$$

Using the data in Tables C.2 and C.3 and equations (C-17) through (C-18), limits of error in measurement of the resistances of the standard resistors R_{s1} and R_{s2} were determined as follows:

$$\lambda_{R1} = .070\% \; of \; Rdg \; (\overline{R}_{S1} = 3.00 \; \Omega) \tag{C-21}$$

$$\Lambda_{R2} = .019\% \; of \; Rdg \; (\overline{R}_{S2} = 3.00 \; \Omega) \tag{C-22}$$

C.5.3 Uncertainty in P_{total}. The components of the error in reading the total heat loss value from the heat loss calibration curve shown in Figure C.5 are instrument uncertainty and resolution error. From eq. (C-12), P_{total} is expressed as follows:

$$P_{total} = P_c + P_t = (V_1)\left(\frac{V_{S1}}{R_{S1}}\right) + (V_2)\left(\frac{V_{S2}}{R_{S2}}\right)$$

Substituting values from Tables C.2, C.3 and C.4 in equation (C-12) yields

$$P_{total} = (11.854)\left(\frac{2.490}{3.00}\right) + (12.0)\left(\frac{2.495}{3.00}\right) = 19.83 \; W$$

The error equation for P_{total} is expressed as follows:

$$\lambda_p = \sqrt{\frac{e_{p1}^2 + e_{p2}^2 + e_{res}^2}{P_{total}^2}} \ (100) \quad \% \ Rdg \qquad (C-23)$$

where λ_p is the uncertainty in reading the value of the total heat loss from the heat loss calibration curve, e_{p1} is the uncertainty in the value of power input to the calorimeter box, e_{p2} is the uncertainty in the value of power input to the connecting tunnel and e_{res} is the resolution error in reading the heat loss value from the heat loss calibration curve.

i) Resolution error

Referring to Figure C.5., resolution error is estimated to be half of the smallest scale division.

$$e_{res} = \frac{1}{2} \ (.4W) = .2 \ W \qquad (C-24)$$

ii) Uncertainty in the power input to the calorimeter box

$$P_c = (V_1)(\frac{V_{S1}}{R_{S1}}) = (11.854)(\frac{2.49}{3.00}) = 9.84 \ W$$

$$\lambda_{p1} = \sqrt{(\lambda_{V1} + \lambda_{S1})^2 + \lambda_{R1}^2} \quad \% \ Rdg \qquad (C-25)$$

where λ_{p1} is the error in P_c, λ_{V1} is the uncertainty in measurement of V_1, λ_{S1} is the uncertainty in measurement of V_{S1} and λ_{R1} is the uncertainty of R_{S1}.

λ_{V1} and λ_{S1} are instrument uncertainties and are calculated as follows:

$$\lambda_{V1} = \frac{(.02\% \ of \ V_1 + .005\% \ of \ range)}{V_1} \ (100) \quad \% \ Rdg \qquad (C-26)$$

and

$$\lambda_{S1} = \frac{(.02\% \ of \ V_{S1} + .005\% \ of \ range)}{V_{S1}} \ (100) \quad \% \ Rdg \qquad (C-27)$$

Substituting values from Table C.4 in equations (C-26) and (C-27) yields

$$\lambda_{V1} = \frac{(.02)(11.854) + (.005)(20)}{11.854} = .028\%$$

$$\lambda_{S1} = \frac{(.02)(12) + (.005)(20)}{12} = .060\%$$

Substituting for λ_{V1}, λ_{S1} and λ_{R1} in equation (C-25) yields

$$\lambda_{p1} = \sqrt{(.028 + .060)^2 + (.070)^2} = .11\%$$

$$e_{p1} = (\lambda_{p1})(P_c) = (.11\%)(9.84) = .011 \text{ W} \qquad \text{(C-28)}$$

iii) Uncertainty in the power input to the connecting tunnel

$$P_t = (V_2)(\frac{V_{S2}}{R_{S2}}) = (12.0)(\frac{2.495}{3.00}) = 9.99 \text{ W}$$

$$\lambda_{p2} = \sqrt{(\lambda_{V2} + \lambda_{S2})^2 + \lambda_{R2}^2} \qquad \% \text{ Rdg} \qquad \text{(C-29)}$$

where λ_{p2} is the error in P_t, λ_{V2} is the error in V_2, λ_{S2} is the error in V_{S2} and λ_{R2} is the uncertainty in R_{S2}.

λ_{V2} and λ_{S2} are instrument uncertainties and are calculated as follows:

$$\lambda_{V2} = \frac{(.02\% \text{ of } V_2 + .005\% \text{ of range})}{V_2} (100) \qquad \% \text{ Rdg} \qquad \text{(C-30)}$$

$$\lambda_{S2} = \frac{(.02\% \text{ of } V_{S2} + .005\% \text{ of range})}{V_{S2}} (100) \qquad \% \text{ Rdg} \qquad \text{(C-31)}$$

Substituting for V_{S2} and V_2 from Table C.4 in equations (C-30) and (C-31) yields

$$\lambda_{V2} = \frac{(.02)(12) + (.005)(20)}{12} = .028\%$$

and

$$\lambda_{S2} = \frac{(.02)(2.495) + (.005)(20)}{2.495} = .060\%$$

Substituting for λ_{V2}, λ_{S2} and λ_{R2} in eq. (C-29) yields

$$\lambda_{p2} = \sqrt{(.060 + .028)^2 + (.019)^2} = .090\%$$

$$e_{p2} = (\lambda_{p2})(P_t) = (.090\%)(9.99) = .009 \text{ W} \qquad \text{(C-32)}$$

Substituting for e_{p1}, e_{p2} and e_{res} from equations (C-28), (C-32) and (C-24) in equation (C-23) yields

$$\lambda_p = \frac{(.011)^2 + (.009)^2 + (.2)^2}{19.83} \quad (100) = 1.0\%$$

Following this same procedure, P_{total}, $\overline{V}$, λ_p and λ_V where calculated for the heat loss calibration tests number two, three and four and the results are listed in Table C.5.

Test No.	$\bar{V}$, mv	λ_v, % Rdg	P_c, W	λ_{p1}, % Rdg	P_t, W	λ_{p2}, % Rdg	P_{total}, W	λ_{p1}, % Rdg
1	.6449	.53	9.839	.1129	9.917	.0890	19.83	1.0
2	.4220	.53	6.440	.1223	6.544	.1005	12.98	1.5
3	.2355	.53	3.522	.09266	3.6159	.0612	7.138	2.8
4	.3285	.53	4.880	.09067	4.946	.05835	9.826	2.0

Table C.5 - Uncertainties in heat loss calibration data.

Appendix D

ERROR ANALYSIS OF THE HEAT-METER CALIBRATION DATA

In the following section a sample calculation is given for P_n, the net power input to the hot water, $\dot{Q}_h$, the hot water heat loss, $\dot{Q}_c$, the cold fluid heat gain and $\bar{T}$, the heat-meter mean temperature. A sample calculation of error is given for the values of $\frac{P_n}{\Delta V_6}$, the heat-meter sensitivity, $\bar{T}$, $\dot{Q}_h$ and $\dot{Q}_c$. Experimental data from test no. 2 is used in each of the above mentioned calculations.

D.1 Sample Calculation of Performance

D.1.1 <u>Net Power Input</u>. Using the data listed in Table 5.2(b) for steady state conditions in test no. 2, the net power input to the hot fluid is calculated as follows

i) Power input to the fan circuit in the calorimeter box P_c, as defined in eq. (C-12), is

$$P_c = V_1 \left(\frac{V_{S1}}{R_{S1}} \right) \tag{D-1}$$

Substituting in eq. (D-1) for V_1, V_{S1} and R_{S1} from Tables 5.2(b) and C.4 yields

$$P_c = (5.910)\left(\frac{1.178}{3.00}\right) = 2.32 \text{ W}$$

ii) Power input to the fan circuit in the connecting tunnel P_t, as defined in the eq. (C-12), is

$$P_t = V_2 \left(\frac{V_{S2}}{R_{S2}} \right) \tag{D-2}$$

114

Substituting in eq. (D-2) for V_2, V_{S2} and R_{S2} from Tables 5.2(b) and C.5 yields

$$P_t = (4.521)(\frac{.8507}{3.00}) = 1.28 \text{ W}$$

iii) Power input to the heating element

$$P_h = V_3(\frac{V_{S3}}{R_{S3}}) \tag{D-3}$$

where V_3 is the voltage across points C and D in the heating element electrical circuit shown in Figure 5.1, V_{S3} is the voltage across the standard resistor of the circuit and $R_{S3} = .330 \ \Omega \pm .27\%$ is the resistance of the standard resistor.

Substituting in eq. (D-3) for V_3, V_{S3} and R_{S3} from Table 5.2(b) yields

$$P_h = (37.66)(\frac{.8572}{.330}) = 97.9 \text{ W}$$

iv) Power input to the pump

From Table 5.2(b), the power input to the hot water pump measured by the wattmeter is

$$P_p = 78 \text{ W} \tag{D-4}$$

v) Heat loss

Heat loss from the calorimeter box and the connecting tunnel is determined using the heat loss calibration curve in Figure C.3, which is plotted as the total heat loss versus $\overline{V}$. The voltage $\overline{V}$, as defined in eq. (C-13), is

$$\overline{V} = \frac{\Delta V_1}{46} + \frac{\Delta V_2}{16} \tag{D-5}$$

Substituting from Table 5.2(b) for ΔV_1 and ΔV_2, eq. (D-5) yields

$$\overline{V} = \frac{3.345}{46} + \frac{.5800}{16} = .1090 \text{ mv}$$

From the heat loss calibration curve in Figure C.5, at $\overline{V} = .1090$ mv the total

heat loss is determined to be

$$\dot{Q}_\ell = 3.2 \text{ W} \tag{D-6}$$

Therefore, P_n, the net power input to the hot fluid, is as follows:

$$P_n = P_c + P_t + P_h + P_p - Q_\ell \tag{D-7}$$

Substituting in eq. (D-7) for P_c, P_t, P_h, P_p and $\dot{Q}_\ell$, from eqs. (D-1), (D-2), (D-3), (D-4) and (D-6), yields

$$P_n = 2.32 + 1.28 + 97.9 + 78 - 3.2 = 176.3 \text{ W}$$

D.1.2 <u>Cold Fluid Heat Gain.</u> The cold fluid heat gain is calculated from the following equation.

$$\dot{Q}_c = \dot{V}_c \rho C_p (\Delta T_c) \tag{D-8}$$

where $\dot{V}_c$ is the volumetric flow rate, ρ is the density, C_p is the specific heat and ΔT_c is the cold fluid temperature change given by

$$\Delta T_c = (m_1)(\frac{\Delta V_5}{n}) \tag{D-9}$$

where m_1 is the slope of the copper-constantan thermocouple output versus temperature in the temperature range of $T_{ci} \pm 5^{\circ}C$, T_{ci} is the cold fluid temperature entering the heat-meter, ΔV_5 is the output of the thermopile measuring the cold fluid temperature change and n=10 is the number of the thermocouple junction pairs in the thermopile.

Substituting in eq. (D-9) from Table 5.2(b) yields

$$\Delta T_c = (25.13 \frac{^{\circ}C}{mv})(\frac{.2100}{10} \text{ mv}) = .5277 \text{ }^{\circ}C$$

The cold fluid temperature leaving the heat-meter is calculated as follows

$$T_{co} = T_{ci} + \Delta T_c \tag{D-10}$$

Substituting in eq. (D-10) for T_{ci} and ΔT_c from Table 5.2(b) and eq.

(D-9) yields

$$T_{co} = 16.0 + .5277 = 16.53 \,^{o}C$$

The average temperature of the cold fluid slab is calculated as follows

$$\bar{T}_c = \frac{T_{ci} + T_{co}}{2} \qquad (D-11)$$

Substituting in eq. (D-11) for T_{ci} and T_{co} from Table 5.2(b) and eq. (D-10) yields

$$\bar{T}_c = \frac{16.0 + 16.53}{2} = 16.27 \,^{o}C$$

Water density and specific heat at $\bar{T}_c = 16.27^{o}C$ and kinematic viscosity at $T_{ci} = 16.0^{o}C$ are as follows [8]:

$$\rho = .9989 \frac{Kg}{\ell} \quad , \quad C_p = 4185 \frac{J}{Kg - \,^{o}C} \quad , \quad \nu = 1.110 \text{ ctsk}$$

Using data in Table 5.2(b) and eq. (B-2), the average output frequency of the cold water turbine flow meter is calculated to be

$$\bar{F}_c = \frac{176.4 + 176.4 + 176.4 + 176.4 + 176.3 + 176.4}{6} = 176.4 \text{ Hz} \quad (D-12)$$

Therefore, the scaled frequency is

$$\frac{\bar{F}_c}{\nu} = \frac{176.4}{1.110} = 158.9 \frac{Hz}{ctsk} \qquad (D-13)$$

From the calibration curve shown in Figure B.3 for flowmeter no. ME-3909, at $\frac{\bar{F}_c}{\nu} = 158.9 \frac{Hz}{ctsk}$ the K-factor is

$$\text{K-factor} = \frac{\bar{F}_c}{\dot{V}_c} = 2810 \frac{cycles}{\ell} \qquad (D-14)$$

Substituting for $\dot{V}_c$, ℓ, C_p and ΔT_c into eq. (D-8) yields

$$\dot{Q}_c = (.06278 \,\ell/S)(.9989 \frac{Kg}{\ell})(4185 \frac{J}{Kg - \,^{o}C})(.5277^{o}C) = 138.5 \text{ W}$$

D.1.3 <u>Hot Fluid Heat Loss</u>. The hot fluid heat loss to the heat-meter cold fluid is calculated from the following equation:

$$\dot{Q}_h = \dot{V}_h \, \rho C_p (\Delta T_h) \qquad\qquad (D-15)$$

where $\dot{V}_h$ is the volumetric flow rate of the hot fluid, ρ is the density, C_p is the specific heat and ΔT_h is the hot fluid temperature change given by

$$\Delta T_h = (m_2)\left(\frac{\Delta V_4}{n}\right) \qquad\qquad (D-16)$$

where m_2 is the slope of the copper-constantan thermocouple output versus temperature in the temperature range of $T_{ho} \pm 5^\circ C$, T_{ho} is the hot water temperature leaving the heat-meter, ΔV_4 is the output of the thermopile measuring the hot fluid temperature change and $n=10$ is the number of the thermocouple junction pairs in the thermopile.

Substituting in eq. (D-16) from Table 5.2(b) yields

$$\Delta T_h = (24.33)\left(\frac{.2650}{10}\right) = .6448 \,^\circ C$$

The hot fluid temperature entering the heat-meter is calculated as follows:

$$T_{hi} = T_{ho} + \Delta T_h \qquad\qquad (D-17)$$

Substituting in eq. (D-17) for T_{ho} and ΔT_h from Table 5.2(b) and eq. (D-16) yields

$$T_{hi} = 29.1 + .6448 = 29.75 \,^\circ C$$

The average temperature of the hot fluid slab is calculated as follows:

$$\overline{T}_h = \frac{T_{hi} + T_{ho}}{2} \qquad\qquad (D-18)$$

Substituting in eq. (D-18) for T_{hi} and T_{ho} from Table 5.2(b) and eq. (D-17) yields

$$\overline{T}_h = \frac{29.1 + 29.75}{2} = 29.42 \,^\circ C$$

Water density and specific heat at $\overline{T}_h = 29.42^\circ C$ and ν, the kinematic viscosity at $T_{ho} = 29.1^\circ C$ are as follows [8]:

$$\rho = .9959 \; \frac{Kg}{\ell} \; , \quad C_p = 4179 \; \frac{J}{Kg - {}^{o}C} \; , \quad \nu = .8181 \; ctsk$$

Using the data in Table 5.2(b) and eq. (B-2), the average output frequency of the hot water turbine flow meter is calculated to be

$$\overline{F}_h = \frac{173.0 + 173.2 + 173.3 + 173.1 + 172.5 + 173.4}{6} = 173.1 \; Hz \quad (D-20)$$

Therefore, the scaled frequency can be calculated as follows:

$$\frac{\overline{F}_h}{\nu} = \frac{173.1}{.8181} = 211.6 \; \frac{Hz}{ctsk} \qquad (D-21)$$

From the calibration curve shown in Figure B.2 for turbine flow meter no. ME-3907, at $\dfrac{\overline{F}_h}{\nu} = 211.6 \; \dfrac{Hz}{ctsk}$ the K-factor is

$$K\text{-factor} = \frac{\overline{F}_h}{\dot{V}_h} = 2845 \; \frac{cycles}{\ell} \qquad (D-22)$$

Substituting for $\overline{F}_h$ from eq. (D-19) in eq. (D-22) yields

$$\dot{V}_h = \frac{\overline{F}_h}{K} = \frac{173.1}{2845} = .06084 \; \ell/S$$

Substituting for $\dot{V}_h$, ρ, C_p, ΔT_h in eq. (D-15) yields

$$\dot{Q}_h = (.06084 \; \ell/S)(.9959 \; \frac{Kg}{\ell})(4179 \; \frac{J}{Kg - {}^{o}C})(.6448^{o}C) = 163.2 \; W$$

D.1.4 _Heat-Meter Mean Temperature._ The mean temperature of the heat-meter is as follows:

$$\overline{T} = \frac{\overline{T}_c + \overline{T}_h}{2} \qquad (D-23)$$

Substituting for $\overline{T}_c$ and $\overline{T}_h$ from eqs. (D-11) and (D-18), respectively, yields

$$\overline{T} = \frac{16.27 + 29.42}{2} = 22.85^{o}C$$

D.2 _Sample Calculation of Error_

D.2.1 _Error in Net Power Input._ The relative error in measurement of the net power input to the hot fluid is given by

$$\lambda_{P_n} = \sqrt{\frac{e_{P1}^2 + e_{P2}^2 + e_{PP}^2 + e_{P3}^2 + e_{\ell}^2}{P_n}} \ (100) \ \% \ Rdg \qquad (D-24)$$

where e_{P1} and e_{P2} are the absolute errors in measurement of the power input to the fans in the calorimeter box and the connecting tunnel, e_{PP} is the absolute error in measurement of the power input to the hot water pump, e_{P3} is the absolute error in measurement of the power input to the heating element and e_{ℓ} is the absolute error in the heat loss to the ambient air.

i) Error in Power Input to the Fans

The power input to the fans in the calorimeter box and the connecting tunnel during heat-meter calibration tests was comparable in magnitude to the power input to the fans in the heat loss calibration tests. The error in measurement of power input to the fans during heat loss calibration tests had a typical value of ± .1% as shown in Table C.5 of Appendix C. However, referring to Section D.1.1, the total power input to the fans during heat-meter calibration tests was only about 2% of the net power input to the hot water. Therefore, the error in measurement of the net power input due to error in measurement of the power input to the fans would be ± .1% of 2% or only about .002% of the total power input. This is a very small contribution to the total error and is therefore neglected in the error analysis of P_n.

ii) Error in Measurement of the Heat Loss

From Table C.5 in Appendix C, the error in reading the heat loss value from the heat loss calibration curve is estimated to be about ± .2 W. Thus,

$$Q_{\ell} = 3.2 \pm .2 \ W \ (\pm 6.3\%) \qquad (D-25)$$

iii) Error in Power Input to the Heating Element

The error in measurement of the power input to the heating element is

$$\lambda_{P3} = \sqrt{(\lambda_{S3} + \lambda_{V3})^2 + (\lambda_{R3})^2} \qquad \text{(D-26)}$$

where λ_{P3} is the error in P_h, λ_{S3} is the error in V_{S3}, λ_{V3} is the error in V_e and λ_{R3} is the error in R_{S3}. Note that eq. (D-26) assumes dependent errors in V_{S3} and V_3 since both measurements were made using the same instrument. The error in measurement of V_3 and V_{S3} is due to instrument uncertainty and is calculated from the following equations:

$$\lambda_{V3} = \frac{(.2\% \text{ of } V_3 + .015\% \text{ of range})}{V_3} (100) \quad \% \text{ Rdg} \qquad \text{(D-27)}$$

Substituting for V_3 from Table 5.2(b) yields

$$\lambda_{V3} = \frac{(.2)(37.66) + (.015)(200)}{37.66} = .28\% \text{ Rdg}$$

and

$$\lambda_{S3} = \frac{(.2\% \text{ of } V_{S3} + .015\% \text{ of range})}{V_{S3}} (100) \quad \% \text{ Rdg} \qquad \text{(D-28)}$$

Substituting for V_{S3} from Table 5.2(b) yields

$$\lambda_{S3} = \frac{(.2)(.857) + (.015)(2)}{.857} = .24 \ \% \text{ Rdg}$$

Substituting in eq. (D-26) for λ_{S3}, λ_{V3} and λ_{R3} yields

$$\lambda_{P3} = \sqrt{(.28 + .24)^2 + (.27)^2} = .59 \ \% \text{ Rdg}$$

Therefore

$$P_h = 97.88 \pm .57 \text{ W } (\pm .59\%)$$

iv) Error in Measurement of the Power Input to the Pump

The components of the error in measurement of the power input to the pump are resolution errors and instrument uncertainty.

$$e_{PP} = \sqrt{e_{res}^2 + e_{inst}^2} \qquad \text{(D-29)}$$

The resolution error, e_{res}, is given by

$$e_{res} = \frac{1}{2} \text{ (smallest scale division)} = 1 \text{ W} \qquad \text{(D-30)}$$

The instrument uncertainty is

$$e_{inst} = .25\% \text{ (full scale)} = .625 \text{ W} \qquad \text{(D-31)}$$

Substituting for e_{res} and e_{inst}, from eqs. (D-30) and (D-31), into eq. (D-29) yields

$$e_{pp} = \sqrt{(1)^2 + (.625)^2} = 1.18 \text{ W}$$

Therefore

$$P_p = 78 \pm 1.18 \text{ W } (\pm 1.5\%)$$

Substituting for e_ℓ, e_{p3}, e_{pp} and P_n, from eqs. (D-25), (D-26), (D-29) and (D-7), into eq. (D-24) yields

$$\lambda_{pn} = \sqrt{\frac{(1.18)^2 + (.2)^2 + (.57)^2}{176.3}} \; (100) = .75\% \text{ Rdg}$$

Therefore

$$P_n = 176.3 \pm 1.3 \text{ W } (\pm .75\%)$$

D.2.2 <u>Error in Measurement of the Cold Water Heat Gain</u>. Calculation of the error in measurement of the cold water heat gain is identical to calculation of the error in measurement of the hot water heat loss. Therefore a sample calculation will be shown only for the error in measurement of the cold water heat gain.

In eq. (D-8), the heat gain by the cold water is expressed as follows:

$$\dot{Q}_c = \dot{V}_c \; \rho C_p(m) \left(\frac{\Delta V_5}{10}\right)$$

Then, the error in $\dot{Q}_c$ is calculated from the following equation

$$\lambda_c = \sqrt{\lambda_V^2 + \lambda_\rho^2 + \lambda_{cp}^2 + \lambda_5^2 + \lambda_{m1}} \qquad \text{(D-32)}$$

where λ_V is the error in measurement of the volumetric flow rate, λ_ρ is the

error in measurement of the water density, λ_{cp} is the error in measurement of the specific heat of water, λ_5 is the error in measurement of the output of the thermopile measuring the cold fluid temperature change and λ_{m1} is the error in slope of the copper-constantan thermocouple output versus temperature and is neglected in the error analysis.

i) Error in measurement of the specific heat and density

The error in measurement of the specific heat and density of water are due to error in measurement of the water temperature. The error in temperature measurement is calculated as follows:

$$\lambda_T = \sqrt{\lambda_1^2 + \lambda_2^2} \tag{D-33}$$

where λ_1 is instrument uncertainty and λ_2 is the thermocouple wire error.

λ_1 and λ_2, according to the manufacturers of the thermocouple wire and the instrument used, are calculated as follows:

$$\lambda_1 = \frac{\sqrt{(.3)^2 + (.5)^2 + (.02\% \ T + .1)^2}}{T} \ (100) \ \% \ Rdg \tag{D-34}$$

where T is the temperature reading of the instrument.
Also

$$\lambda_2 = .75\% \ Rdg \tag{D-35}$$

Substituting for the average cold water temperature from eq. (D-11) into eq. (D-34) yields

$$\lambda_1 = \frac{\sqrt{(.3)^2 + (.5)^2 + (.02\% \times 16.26 + .1)^2}}{16.26} \ (100) = 3.7\% \ Rdg$$

Substituting for λ_1 and λ_2 into eq. (D-33) yields

$$\lambda_T = \sqrt{(3.7)^2 + (.75)^2} = 3.8\% \ Rdg$$

Therefore

$$\overline{T}_c = 16.26 \pm .62\,^{\circ}C \ (\pm \ 3.8\%)$$

The error in measurement of density and specific heat of water due to the $\pm$ .62°C error in temperature measurement is on the order of $\pm$ .01% and is therefore neglected.

ii) Error in measurement of ΔV_5

The error in measurement of the output on the thermopile measuring the cold fluid temperature change is calculated from the following equation.

$$\lambda_5 = \sqrt{\lambda_2^2 + \lambda'^2_{inst}} \qquad\qquad (D-36)$$

where λ_2 is the thermocouple wire error and λ'_{inst} is the instrument uncertainty.

According to the manufacturers of the thermocouple wire and the instrument used, λ_2 and λ'_{inst}, respectively are calculated as follows:

$$\lambda_2 = .75\% \text{ Rdg} \qquad\qquad (D-37)$$

and

$$\lambda'_{inst} = \frac{(.03\% \ \Delta V_5 + 3 \text{ mv})}{\Delta V_5} (100) \ \% \text{ Rdg} \qquad\qquad (D-38)$$

Substituting for ΔV_5 from Table 5.2(b) into eq. (D-38) yields

$$\lambda'_{inst} = \frac{(.03 \times .2100 + .3)}{.2100} = 1.5\% \text{ Rdg}$$

Substituting for λ_2 and λ'_{inst} into eq. (D-36) yields

$$\lambda_5 = \sqrt{(1.5)^2 + (.75)^2} = 1.7\% \text{ Rdg}$$

Therefore

$$\Delta V_5 = .2100 \pm .0036 \text{ mv } (\pm 1.7\%)$$

iii) Error in measurement of the volumetric flow rate

In eq. (D-14), the volumetric flow rate is expressed as follows:

$$\dot{V} = \frac{\overline{F}_c}{K}$$

Therefore, the error in $\dot{V}$ is calculated from the following equation.

$$\lambda_{\dot{V}} = \sqrt{\lambda_K^2 + \lambda_F^2} \qquad (D-39)$$

where λ_K is error in the K-factor for the turbine flowmeter and λ_F is error in measurement of the frequency which was calculated to be .019% using the data in Table 5.2(b) and eq. (B-1) through (B-5).

After substituting for λ_K from Table B.2 of Appendix B and λ_F, eq. (D-39) yields

$$\lambda_{\dot{V}} = \sqrt{(.48)^2 + (.019)^2} = .48\% \text{ Rdg}$$

Substituting for $\lambda_{\dot{V}}$ and λ_5, from eqs. (D-39) and (D-36), into eq. (D-32) yields

$$\lambda_c = \sqrt{(.48)^2 + (1.7)^2} = 1.8\% \text{ Rdg}$$

Therefore

$$\dot{Q}_c = 138.5 \pm 2.5 \text{ W } (\pm 1.8\%)$$

D.2.3 <u>Error in the Heat-Meter Mean Temperature</u>. In eq. (D-23), the heat-meter mean temperature was defined as follows:

$$\overline{T} = \frac{\overline{T}_c + \overline{T}_h}{2}$$

where $\overline{T}_c$ and $\overline{T}_h$, as expressed in eqs. (D-11) and (D-18), respectively, are as follows:

$$\overline{T}_c = \frac{T_{ci} + T_{co}}{2} = \frac{2T_{ci} + \Delta T_c}{2}$$

and

$$\overline{T}_h = \frac{T_{hi} + T_{ho}}{2} = \frac{2T_{ho} + \Delta T_h}{2}$$

Referring to eqs. (D-9) and (D-16) and Table 5.2(b) for values of ΔT_c, ΔT_h, T_{ci} and T_{ho}, the error in both ΔT_h and ΔT_c is typically on the order of $\pm$ .75% of .60°C as compared to the previously estimated error of $\pm$ .62°C

for T_{ci} and T_{ho}. Therefore, the error in magnitude of the $\overline{T}$ is essentially that due to error in measurement of T_{ci} and T_{ho} and may be calculated as follows:

$$e_{\overline{T}} = \sqrt{(\frac{e_c}{2})^2 + (\frac{e_h}{2})^2} \qquad (D-40)$$

where e_c is error in measurement of T_{ci} and e_h is error in measurement of T_{ho}.

The error in measurement of T_{ci} and T_{ho} is due to instrument uncertainty and thermocouple wire error. Referring to eq. (D-33), the combined error equation for temperature measurement is

$$e_T = \sqrt{(.3)^2+(.5)^2+(.02\%\ Rdg+.1)^2+(.75\%\ Rdg)^2}\ {}^oC \qquad (D-41)$$

Substituting for T_{ci} and T_{ho} from Table 5.2(b) into eq. (D-41) yields

$$e_c = \sqrt{(.3)^2+(.5)^2+(.02\%x16+.1)^2+(.75\%x16)^2} = .60^oC$$

and

$$e_h = \sqrt{(.3)^2+(.5)^2+(.02\%x29.1+.1)^2+(.75\%x29.1)^2} = .63^oC$$

Substituting for e_c and e_h into eq. (D-40) yields

$$e_{\overline{T}} = \sqrt{(\frac{.60}{2})^2 + (\frac{.63}{2})^2} = .44^oC$$

Therefore

$$\overline{T} = 22.85 \pm .44^oC$$

D.2.4 <u>Error in the Heat-Meter Output</u>. The error in measurement of the heat-meter voltage output is due to instrument uncertainty and thermocouple wire error. The instrument uncertainty compared to ± .75% error in thermo-couple wire is negligible. Then, the error in measurement of the heat-meter output would be as follows:

$$\lambda_v = .75\%\ Rdg \qquad (D-42)$$

Therefore, from Table 5.2(b), ΔV_6 can be written as:

$$\Delta V_6 = 10.13 \pm .076 \text{ mv } (\pm .75\%)$$

D.2.5 <u>Error in the Heat-Meter Sensitivity</u>. The heat-meter sensitivity is calculated as follows:

$$\text{Heat-Meter Sensitivity} = \frac{P_n}{\Delta V_6} \qquad (D\text{-}43)$$

where P_n is the net power input to the hot fluid and ΔV_6 is the heat-meter output.

The error in $\frac{P_n}{\Delta V_6}$ is calculated as follows:

$$\lambda_{pv} = \lambda_v^2 + \lambda_{pn}^2 \qquad (D\text{-}44)$$

where λ_v is error in measurement of the heat-meter output and λ_{pn} is error in the net power input.

Substituting for λ_{pn} and λ_v, from eqs. (D-24) and (D-42), respectively, into eq. (D-44) yields

$$\lambda_{pv} = (.75)^2 + (.75)^2 = 1.1\% \text{ Rdg}$$

Therefore

$$\frac{P_n}{\Delta V_6} = 17.46 \pm .19 \, \frac{W}{mv} \, (\pm \, 1.1\%)$$

APPENDIX E

NOMENCLATURE

Symbol

A Area, m^2

c_p Specific heat at constant pressure, $J/kg-^oC$

D Hydraulic diameter, m

e Absolute error (limit of error, 95% confidence)

e_{inst} Instrument uncertainty

e_m Error in measurement of mass, g

e_f Error in measurement of frequency, Hz

e_k Error in turbine flowmeter K-factor, cycles/1

$e_{F/\nu}$ Error in scaled frequency, cycles/ctsk

e_ρ Error in measurement of density, kg/m^3

e_t Error in measurement of time, sec

e_T Error in measurement of temperature, ^oC

e_{res} Resolution error

e_{V1} Error in measurement of V_1, v

e_{V2} Error in measurement of V_2, v

e_{V3} Error in measurement of V_3, v

e_{S1} Error in measurement of R_{S1}, Ω

e_{S2} Error in measurement of R_{S2}, Ω

e_{S3} Error in measurement of R_{S3}, Ω

e_{p1} Error in measurement of P_c, W

e_{p2} Error in measurement of P_t, W

Symbol

e_p	Error in measurement of P_{total}, W
e_{pp}	Error in measurement of P_h, W
e_ν	Error in measurement of viscosity, ctsks
F	Frequency output of turbine flowmeter, Hz
$\overline{F}$	Average frequency, Hz
f	Fanning friction factor
h	Convective heat transfer coefficient, W/m^2-^oC
h'	Enthalpy per unit mass, J/g
I	Electrical current, A
k	Thermal conductivity, W/m-^oC
K	K-factor, cycles/l
L	Length, m
L_e	Equivalent length, m
m	Mass, g
$\dot{m}$	Mass flowrater, l/sec (GPM)
Nu_d	Local Nusselt number based on the hydraulic diameter
P	Perimeter of flow channels, m
P_c	Power input to calorimeter box fan circuit, W
P_h	Power input to heating element in calorimeter box, W
P_n	Net power input to hot fluid, W
P_p	Power input to hot water pump, W
P_t	Power input to connecting tunnel fan circuit, W
P_{total}	Total heat loss from calorimeter box and connecting tunnel, W
Pr	Prandtl number
ΔP	Pressure difference, KN/m^2 (psi)

Symbol

$\dot{Q}$ Heat transfer rate, W

$\dot{Q}_{a1}$ Heat transfer rate from hot fluid to channel "a", W

$\dot{Q}_{a2}$ Heat transfer rate from channel "a" to cold fluid, W

$\dot{Q}_{b1}$ Heat transfer rate from hot fluid to channel "b", W

$\dot{Q}_{b2}$ Heat transfer rate from channel "b" to cold fluid, W

R_{S1} Resistance of standard resistor for fan circuit in calorimeter box, Ω

R_{S2} Resistance of standard resistor for fan circuit in connecting tunnel, Ω

R_{S3} Resistance of standard resistor for heating element circuit, Ω

R_e Reynolds number

S_t Total shape factor, m

S_e Shape factor for edges, m

S_c Shape factor for corners, m

S_w Shape factor for walls, m

t Time, sec

T_1 Temperature of air inside calorimeter box, $^{\circ}$C

T_2 Temperature of air inside connecting tunnel, $^{\circ}$C

T_3 Ambient temperature, $^{\circ}$C

T_4 Temperature of outside surface of calorimeter box, $^{\circ}$C

T_5 Temperature of hot water leaving heat-meter, $^{\circ}$C

T_6 Temperature of cold water entering heat-meter, $^{\circ}$C

T_i Inlet fluid temperature, $^{\circ}$C

T_o Outlet fluid temperature, $^{\circ}$C

T_b Bulk fluid temperature, $^{\circ}$C

Symbol

$\overline{T}$	Mean temperature, $^{\circ}C$
Δt	Time interval, sec
ΔT	Temperature difference, $^{\circ}C$
ΔT_{HM}	Temperature difference across thickness of heat-meter semi-conductive plate, $^{\circ}C$
Vol	Volume, ml
$\dot{V}$	Volumetric flowrate, l/s
V_1	Voltage across points A and B of calorimeter box fan circuit, V
V_2	Voltage across points A and B of connecting tunnel fan circuit, V
V_3	Voltage across points C and D of heating element circuit, V
V_{S1}	Voltage across standard resistor of fan circuit in calorimeter box, V
V_{S2}	Voltage across standard resistor of fan circuit in connecting tunnel, V
V_{S3}	Voltage across standard resistor of heating element circuit, V
ΔV_1	Output of thermopile measuring temperature difference across walls of calorimeter box, mV
ΔV_2	Output of thermopile measuring temperature difference across walls of connecting tunnel, mV
ΔV_3	Output of thermopile measuring temperature difference across heat-meter insulation, mV
ΔV_4	Output of thermopile measuring hot water temperature change, mV
ΔV_5	Output of thermopile measuring cold water temperature change, mV
ΔV_6	Output of heat-meter thermopile, mV
$\overline{V}$	Average of calorimeter box and connecting tunnel thermopile outputs per thermocouple, mV

Greek Symbol

ρ	Density, kg/m^3
ν	Kinematic viscosity, centistokes
σ	Standard deviation (68% confidence interval)
λ	Limit of error (95% confidence), % Rdg
λ_k	Error in measurement of K-factor, % Rdg
$\lambda_{\bar{F}/}$	Error in measurement of scaled frequency, % Rdg
λ_m	Error in measurement of mass, % Rdg
λ_t	Error in measurement of time, % Rdg
λ_ν	Error in measurement of viscosity, % Rdg
λ_{p3}	Error in measurement of P_h, % Rdg
λ_{pn}	Error in measurement of P_n, % Rdg
λ_c	Error in measurement of cold water heat gain, % Rdg
λ_h	Error in measurement of hot water heat transfer, % Rdg
$\lambda_{\dot{v}}$	Error in measurement of volumetric flowrate, % Rdg
λ_{cp}	Error in measurement of specific heat, % Rdg

Subscripts

a	Flow channel "a"
b	Flow channel "b"
1	Hot fluid slab
2	Cold fluid slab
h	Hot fluid
c	Cold fluid
s	Heat-meter semi-conductive plate
o	Exit condition
i	Inlet condition

VITA

FARID H. MIANDOAB

Candidate for the Degree of

Master of Science

Thesis: Design, Construction and Performance Testing of a Fluid-to-Fluid Heat-Meter Prototype

Major Field: Mechanical Engineering

Biographical:

   Personal Data: Born in Tabriz, Azarbaijan, Iran, July 1, 1958; son of Bayuk H. Miandoab and Azadeh Yavari.

   Education: Graduated from Ferdowsi High School in 1976; received the Bachelor of Science degree in Mechanical Engineering, Kansas State University, May, 1981.

   Professional Organizations: American Society of Mechanical Engineers, American Society of Heating, Refrigerating and Air-Conditioning Engineers.

   Professional Experience: Graduate Research Assistant, Department of Mechanical Engineering, Kansas State University, June, 1982 through July, 1983; Graduate Teaching Assistant, Department of Mechanical Engineering, Kansas State University, January, 1982 through May, 1982; Student Teaching Assistant, Department of Mechanical Engineering, Kansas State University, January, 1981 through May, 1981.

DESIGN, CONSTRUCTION AND PERFORMANCE TESTING

OF A FLUID-TO-FLUID HEAT-METER PROTOTYPE

by

FARID H. MIANDOAB

B.S., Kansas State University, 1981

‎ ‎ ‎ ‎ ‎ ‎ ‎ ‎ ‎ ‎ ‎ ‎—————————————

AN ABSTRACT OF A MASTER'S THESIS

submitted in partial fulfillment of the

requirements for the degree

MASTER OF SCIENCE

Department of Mechanical Engineering

KANSAS STATE UNIVERSITY

Manhattan, Kansas

1983

ABSTRACT

This research project was concerned with the design, construction and performance testing of a special-purpose fluid-to-fluid heat-meter prototype. The device consists of a thermally semi-conductive plate sandwiched between two aluminum slabs in which flow channels are machined for fluid circulation. Its function is to provide a calibrated measure of the heat flow between the fluids, indicated by the output of a thermopile measuring the temperature difference across the semi-conductive plate.

A heat-meter prototype was designed and constructed to operate over the range of 0-1 KW. The initial phase of tests indicated the feasibility of the heat-meter concept. Additional test facilities were constructed to study the accuracy, repeatability, and effect of heat-meter mean temperature and coolant flow rates on the heat-meter performance. Results of such tests indicated that the heat-meter was repeatable and accurate to within ±1% of the net power input and further studying of the effect of the mean temperature and the coolant flow rates was necessary.